Ice formation at moderate supercooling in mixed-phase clouds and its link to precipitation

Inauguraldissertation

zur

Erlangung der Würde eines Doktors der Philosophie

vorgelegt der

Philosophisch-Naturwissenschaftlichen Fakultät

der Universität Basel

von

Claudia Mignani

Basel, 2022

Genehmigt von der Philosophisch-Naturwissenschaftlichen Fakultät
auf Antrag von:

Dr. Franz Conen und Prof. Dr. Christine Alewell (Erstbetreuer)

Prof. Dr. Markus Kalberer (Zweitbetreuer)

Dr. Paul J. DeMott (Externer Experte)

Basel, den 16. November 2021

Prof. Dr. Marcel Mayor (Dekan)

"Snowflakes are letters sent from heaven."

Ukichiro Nakaya, 1954

Preface

Back in 2017, I applied for this doctoral position in the Environmental Geosciences Group at the Department of Environmental Sciences at University of Basel, Switzerland. During the first winter of my project in early 2018, I studied the formation of ice crystals at Jungfraujoch, a mountain peak in the Swiss Alps, where I photographed and analysed planar ice crystals with six branches (dendrites).

The next winter, I changed my place of study to another Alpine peak, as colleagues from ETH Zurich offered me to conduct my research as part of a larger field campaign in the Davos region. In close collaboration with colleagues from ETH, I set out to collect as many samples as possible to study the abundance of aerosol particles (tiny particles suspended in the air) that can promote freezing, while a graduate student from University of Basel analysed numerous dendrites.

In addition to the work in the Alps, I initially aimed to investigate the Arctic sources of aerosol particles that can form ice in clouds. This part of the project took an unexpected change of direction. First, the Department of Environmental Sciences funded the purchase of an automatic snowflake camera, that allowed me to remotely study snowfall at an Arctic location. Further, due to the pandemic, it was no longer possible to repeat the aerosol sampling in the Arctic, which would have been necessary.

In parallel to the investigation of snowfall, it was safe to conduct local field measurements adapted to the circumstances of the pandemic. As such, within the framework of an undergraduate research project, aerosol samples were collected along weather fronts in Basel. The results of the measurements carried out in mid-2021 confirmed our earlier findings from the summit sampling in the Davos region.

Today I completed writing this dissertation, which summarises the results of the field measurements mentioned above. The cumulative dissertation includes two peer-reviewed publications and a submitted manuscript. Each of them is a result of a collaboration between several people. The contributions of each author are listed in a dedicated section of the publications and the manuscript. In addition, I have had the great chance to contribute to other scientific projects during my doctorate, which are briefly mentioned and referred to at appropriate places in this thesis.

C. Mignani, October 2021

Summary

Ice formation in the atmosphere is important for the generation of precipitation and the radiative properties of clouds. An integrated understanding of ice formation processes is still missing. This is especially true for ice formation at low to moderate supercooling. In this mixed-phase cloud temperature regime, primary ice is formed via heterogeneous ice nucleation, where ice-nucleating particles (INPs) promote freezing. Such INPs are mainly of biological origin and are present in relatively low concentration in the atmosphere. If the ice particle concentration is higher than the INP concentration, this indicates that secondary ice formation processes are active in addition to heterogeneous nucleation. Secondary ice formation processes can multiply the primary ice by up to several orders of magnitude. However, these processes are diverse and difficult to quantify. After ice formation, various other processes may occur before surface precipitation is observed. The complex chain of intertwined microphysical mechanisms that ultimately lead to precipitation can take different paths.

Here we applied different approaches to obtain information on primary and secondary ice formation at moderate supercooling. In particular, we present observations of INPs active at around $-15\,^{\circ}\mathrm{C}$ in more than 120 aerosol samples and 220 individual dendritic ice crystals that were collected and analysed at mountain stations in the Swiss Alps during winter months of 2018 and 2019. Aerosol particle concentrations, air mass origin and precipitation history were combined to parameterise INP concentrations measured at Weissfluhjoch (2671 m a.s.l.). Primary dendritic ice crystals were quantified at Jungfraujoch (3580 m a.s.l.) using an approach that makes use of their particular and narrow growth temperature range. In addition, precipitating snow particles captured at ground level and coinciding radiosonde ascents were

analysed to investigate whether mixed-phase clouds were relevant for snowfall at an Arctic site throughout a total of eight cold months in 2019 and 2020.

We found that it is more promising to parameterise atmospheric concentrations of INPs active at $-15\,^{\circ}\mathrm{C}$ measured at Weissfluhjoch using aerosol particle number concentrations of a size $> 2\,\mu\mathrm{m}$ as compared to smaller aerosol particles (Chapter 2). Differentiating between air masses that were precipitating, non-precipitating, and carrying Saharan dust and non-precipitating improved the prediction. The ratio of INP to aerosol particle $> 2\,\mu\mathrm{m}$ was larger in precipitating air masses than in non-precipitating air masses. Through freezing assays of individual dendritic ice crystals sampled within clouds at Jungfraujoch, we found that on average one out of eight dendrites contained an INP active at moderate supercooling (Chapter 3). Therefore, the multiplication factor for dendrites was on average only around one order of magnitude. At a site in Northern Finland, observations of often small, unrimed snow particles and the matching relative humidity profiles indicated that probably one quarter of the precipitating clouds were mixed-phase and the remainder were fully glaciated (Chapter 4).

The simultaneous investigation of different microphysical ice processes in clouds can provide information about intertwined processes. Field observations of heterogeneous ice nucleation, secondary ice formation and precipitation are limited in space and time. In this thesis, we have used experimental top-down approaches to determine quantities related to ice formation at moderate supercooling. These results can be incorporated into atmospheric models, which in turn can place the measurements in a larger perspective. Therefore, experimental research in cloud physics is critical for the development of models that can be used to understand and simulate the driving forces and effects of microphysical ice processes and their changes in future climates. This will require close collaboration between researchers working in situ and in silico.

Zusammenfassung

Die Eisbildung in der Atmosphäre ist wichtig für die Entstehung von Niederschlag und für die Strahlungsbilanz von Wolken. Ein integriertes Verständnis der Eisbildungsprozesse fehlt jedoch noch. Dies gilt insbesondere für die Eisbildung bei niedriger bis mässiger Unterkühlung. In diesem gemischtphasigen Wolkentemperaturbereich wird primäres Eis durch heterogene Eisnukleation gebildet, bei der Eiskeime (engl. ice-nucleating particles, INPs) das Gefrieren fördern. Solche INPs sind hauptsächlich biologischen Ursprungs und in relativ geringer Konzentration in der Atmosphäre vorhanden. Ist die Eispartikelkonzentration höher als die INP-Konzentration, deutet dies darauf hin, dass neben der heteogenen Keimbildung auch sekundäre Eisbildungsprozesse aktiv sind. Sekundäre Eisbildungsprozesse können das primäre Eis um bis zu mehrere Grössenordnungen vervielfachen. Diese Prozesse sind jedoch vielfältig und schwer zu quantifizieren. Nach der Eisbildung können verschiedene andere Prozesse ablaufen, bevor Niederschlag in Bodennähe beobachtet wird. Die komplexe Kette von miteinander verflochtenen mikrophysikalischen Mechanismen, die letztlich zu Niederschlag führen, kann unterschiedliche Wege nehmen.

Hier haben wir verschiedene Ansätze angewandt, um Informationen über die primäre und sekundäre Eisbildung bei moderater Unterkühlung zu erhalten. Insbesondere präsentieren wir Beobachtungen von INPs, die bei etwa $-15\,^{\circ}\mathrm{C}$ aktiv sind, in mehr als 120 Aerosolproben und 220 einzelnen dendritischen Eiskristallen, die während der Wintermonate 2018 und 2019 an Bergstationen in den Schweizer Alpen gesammelt und analysiert wurden. Aerosolpartikelkonzentrationen, Luftmassenherkunft und Niederschlagsgeschichte wurden kombiniert, um die am Weissfluhjoch (2671 m ü.M.) gemessenen INP-Konzentrationen zu parametrisieren. Primäre dendritische Eiskristalle wurden auf dem Jungfraujoch (3580 m ü.M.) mit Hilfe eines Ansatzes quantifiziert,

der ihren besonderen und engen Wachstumstemperaturbereich nutzt. Darüber hinaus wurden in Bodennähe erfasste Schneepartikel und zeitgleiche Radiosondenaufstiege analysiert, um zu untersuchen, ob Mischphasenwolken für den Schneefall an einem arktischen Standort während insgesamt acht kalten Monaten in den Jahren 2019 und 2020 relevant waren.

Wir haben festgestellt, dass es vielversprechender ist, die atmosphärischen Konzentrationen von INPs, die bei $-15\,^{\circ}\mathrm{C}$ aktiv sind und am Weissfluhjoch gemessen wurden, mit Hilfe von Aerosolpartikelzahlkonzentrationen einer Grösse von $> 2\,\mu\mathrm{m}$ zu parametrisieren als mit kleineren Aerosolpartikeln (Kapitel 2). Die Unterscheidung zwischen Luftmassen, die ausregnen, nicht-ausregnen, und Saharastaub enthielten und nicht ausregnen, verbesserte die Vorhersage. Das Verhältnis von INP zu Aerosolpartikeln $> 2\,\mu\mathrm{m}$ war in Luftmassen, die ausregneten, grösser als in nicht-ausregnenden Luftmassen. Durch Gefrierversuche an einzelnen dendritischen Eiskristallen, die innerhalb von Wolken am Jungfraujoch entnommen wurden, fanden wir heraus, dass im Durchschnitt einer von acht Dendriten ein INP, der bei mässiger Unterkühlung aktiv war, enthielt (Kapitel 3). Der Multiplikationsfaktor für Dendriten betrug also im Durchschnitt nur etwa eine Grössenordnung. An einem Standort in Nordfinnland ergaben die Beobachtungen von oft kleinen, unbereiften Schneepartikel und die dazugehörigen Profile der relativen Luftfeuchtigkeit, dass wahrscheinlich 30% der Niederschlagswolken gemischtphasig und die übrigen vollständig vereist waren (Kapitel 4).

Die gleichzeitige Untersuchung verschiedener mikrophysikalischer Eisprozesse in Wolken kann Informationen über miteinander verflochtene Prozesse liefern. Feldbeobachtungen von heterogener Eisnukleation, sekundärer Eisbildung und Niederschlag sind räumlich und zeitlich begrenzt. In dieser Arbeit haben wir experimentelle Top-Down-Ansätze verwendet, um Grössen zu bestimmen, die mit der Eisbildung bei moderater Unterkühlung zusammenhängen. Diese Ergebnisse können in atmosphärische Modelle einfliessen, die wiederum die Messungen in einen grösseren Zusammenhang stellen können. Daher ist die experimentelle Forschung in der Wolkenphysik von entscheidender Bedeutung für die Entwicklung von Modellen, die zum Verständnis

und zur Simulation der treibenden Kräfte und Auswirkungen mikrophysikalischer Eisprozesse und ihrer Veränderungen in künftigen Klimazonen verwendet werden können. Dies wird eine enge Zusammenarbeit zwischen den in situ und in silico arbeitenden Forschern erfordern.

Contents

Dendritic ice crystal
Photo: Claudia Mignani

Chapter 1

Introduction

Detailed sketches of ice crystals date back to the early modern period (e.g. Hooke, 1664, 2005; Martens, 1675)[1]. Today, we know that the presence of ice particles in clouds is a prerequisite for most precipitation events over continents (Mülmenstädt et al., 2015). Furthermore, it is known that clouds play a role in the Earth's radiation budget (Matus and L'Ecuyer, 2017) by reflecting incident solar radiation back to space and absorbing and emitting long-wave radiation from the Earth system. A large fraction of clouds is in a mixed-phase state (Hogan et al., 2006), i.e. consists of ice particles and supercooled cloud droplets (Pruppacher and Klett, 2010). Such clouds can exist at temperatures between 0 and −38 °C. In this mixed-phase temperature regime, mixed-phase clouds as well as supercooled liquid and ice clouds can be found (Costa et al., 2017). At temperatures above 0 °C, clouds can be assumed to contain only liquid droplets (since ice melts at 0 °C). Below −38 °C, clouds generally consist entirely of ice particles, because at these temperatures supercooled cloud droplets freeze homogeneously (i.e. without any foreign substance assisting the freezing; Murray et al., 2010; Vali et al., 2015). In most cases of mixed phases, the ice particles grow at the expense of the liquid droplets, which makes these clouds rather short-lived (Korolev, 2007). On rare occasions, there are also persistent mixed-phase clouds, as have been observed in the Arctic for example (e.g. Fridlind et al., 2012). Changing the ice content in mixed-phase clouds alters their radiative

[1]See scheme 8 and page number 151 in the documents available on the following websites, respectively: https://www.gutenberg.org/cache/epub/15491/images/scheme-08.png and https://ia600302.us.archive.org/14/items/friderichmartens00mart/friderichmartens00mart.pdf, last access: 16 October 2021.

and microphysical properties significantly. However, observations of the partitioning between ice particles and liquid water droplets are not in line with the results of global climate models (McCoy et al., 2016). The complex microphysical interactions between ice particles and supercooled liquid cloud droplets make the theoretical understanding of mixed-phase clouds particularly difficult and incomplete to date (Korolev et al., 2017).

1.1 Microphysical processes in mixed-phase clouds

Several mechanisms are involved in the microphysical processes of mixed-phase clouds (Fig. 1.1). As indicated above, atmospheric water molecules are very unlikely to become arranged in an ice-lattice and coalesce (i.e. combine) into an ice crystal at temperatures above $-38\,^{\circ}\mathrm{C}$. Therefore, the onset ice in mixed-phase clouds forms heterogeneously, i.e. with the presence of ice-nucleating particles (INPs) (e.g. DeMott et al., 2010; Kanji et al., 2017). It is suggested that heterogeneous nucleation occurs via several pathways (e.g. Murray et al., 2012; David et al., 2019). In mixed-phase clouds, the dominant heterogeneous nucleation pathway consists of the freezing of droplets in which INPs are immersed (i.e. immersion freezing; Westbrook and Illingworth, 2011). Therefore, first, aerosol particles act as cloud condensation nuclei (CCN) and form supercooled cloud droplets (Pruppacher and Klett, 2010). A small portion of these immersed aerosol particles then can act as INPs. Owing to the ability of INPs to promote freezing, primary ice crystals are formed. Incidentally, ice particles can also be introduced into a cloud from outside by being lifted from the Earth's surface by wind (i.e. hoar frost or blowing snow; Lloyd et al., 2015; Beck et al., 2018) or by natural cloud seeding (i.e. ice crystals falling from an upper precipitating cloud into a lower cloud; e.g. Proske et al., 2021). Once ice is present in a cloud, secondary ice can be produced by secondary ice formation processes (also known as ice multiplication processes, e.g. Hallett and Mossop, 1974; Field et al., 2017). Moreover, the ice particles can undergo other atmospheric microphysical processes in and below a cloud. For example, they can gain mass by colliding and combining with water vapour molecules, aerosol particles (Knutson et al., 1976), water droplets or other ice particles (Rogers and Yau, 1989). These processes are known as vapour deposition, scavenging, riming or aggregation, respectively. If the

ice particles, such as ice crystals, snowflakes, hailstones, or others, fall on the Earth's surface, they form solid precipitation. If they melt on their way down, this will be liquid precipitation.

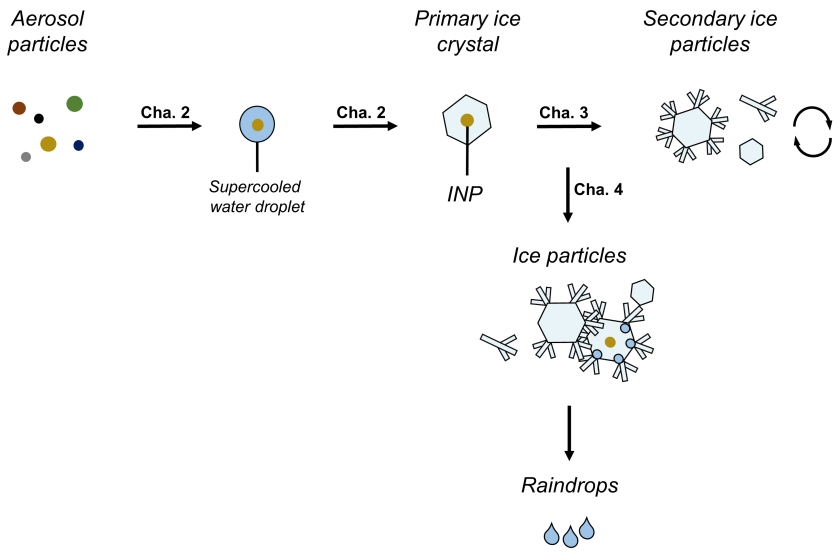

Figure 1.1: Schematic drawing of typical microphysical interactions under mixed-phase cloud conditions between aerosol particles, ice crystals and precipitation. Heterogeneous nucleation via immersion freezing is shown, which involves an aerosol particle immersed in a supercooled cloud water droplet that acts as an ice-nucleating particle (INP), forming a primary ice crystal. Secondary ice particles are generated through a process of secondary ice formation. Ice particles that are heavy enough to fall to the Earth's surface form solid precipitation. They may have grown by vapour deposition, be aggregated or rimed. As they melt on their way through the atmosphere, they become raindrops. The focus of each chapter of this thesis is indicated next to the corresponding arrow.

Each of the mechanisms mentioned above are dependent on atmospheric conditions, such as ambient relative humidity and temperature. For example, CCN activation depends on the ambient supersaturation (as defined by the Köhler theory) while the INP activation depends on the ambient temperature (Kanji et al., 2017). Ice crystal growth depends on a combination of relative humidity and temperature, resulting in different crystal shapes (Nakaya, 1954). Moreover, the microphysical mechanisms are intertwined. For instance, the collision efficiency of ice particles with supercooled cloud droplets, which result in rimed ice particles, depends on the cloud droplet size distribution (Mossop, 1978), which is linked to the CCN concentration (Borys et al., 2003). Riming (i.e. collision of ice crystals with supercooled water droplets

and subsequent freezing of the droplets on the ice surface), in turn, can produce small ice splinters, which can grow by vapour deposition into ice crystals (Hallett and Mossop, 1974). Finally, some processes can occur simultaneously in a cloud, such as the multiple secondary ice formation processes that happen at the same time (Rangno and Hobbs, 2001).

The process interactions in mixed-phase clouds have an impact on surface precipitation. Field case studies have provided evidence that an increase in CCN concentration reduces riming efficiency, and therefore the ice particle mass and precipitation amount (Lance et al., 2011; Saleeby et al., 2013). Furthermore, by using a general circulation model, Lohmann (2002) showed that an increase in INPs increases the number of ice particles, which leads to a global increase in precipitation on an annual scale. However, in mixed-phase clouds, the complex sequence of microphysical processes that ultimately result in precipitation is far from being understood. Ideally, we would have an integrated understanding of these processes, comprehending each underlying mechanism by itself as well as their interplay. This would require many observations in a variety of geographical locations and atmospheric conditions. Even if many mechanisms responsible for precipitation are not yet fully understood, fundamental knowledge has been gained in the last few decades. However, what topics have so far been studied to understand these mechanisms in mixed-phase clouds? And are microphysical processes in mixed-phase clouds that lead to precipitation as connected in research as they are in nature?

1.2 A scientometric analysis

To better understand how microphysical processes in mixed-phase clouds leading to precipitation are structured within research, a scientometric term co-occurrence analysis was performed (Mora-Valentín et al., 2018). Relevant articles were searched in the Web of Science bibliographic database in May 2021 (query: "("ice nucle*" OR "secondary ice" OR "snowflake*") AND "precipitati*""), which resulted in 879 publications ranging from 1971 to mid-2021. Incidentally, an average of 79 articles per year have been published over the last four years (2017−2020). Using the VOSviewer software, the co-occurrence of terms extracted from titles and abstracts was analysed

(van Eck and Waltman, 2010). By counting terms binarily and by merging synonyms, the minimal relevant number of occurrences was set at 25. Terms with a lower occurrence were not included in the analysis. This resulted in 215 terms, which were ranked by their relevance. The 60% most relevant terms were selected to produce a network map (Fig. 1.2).

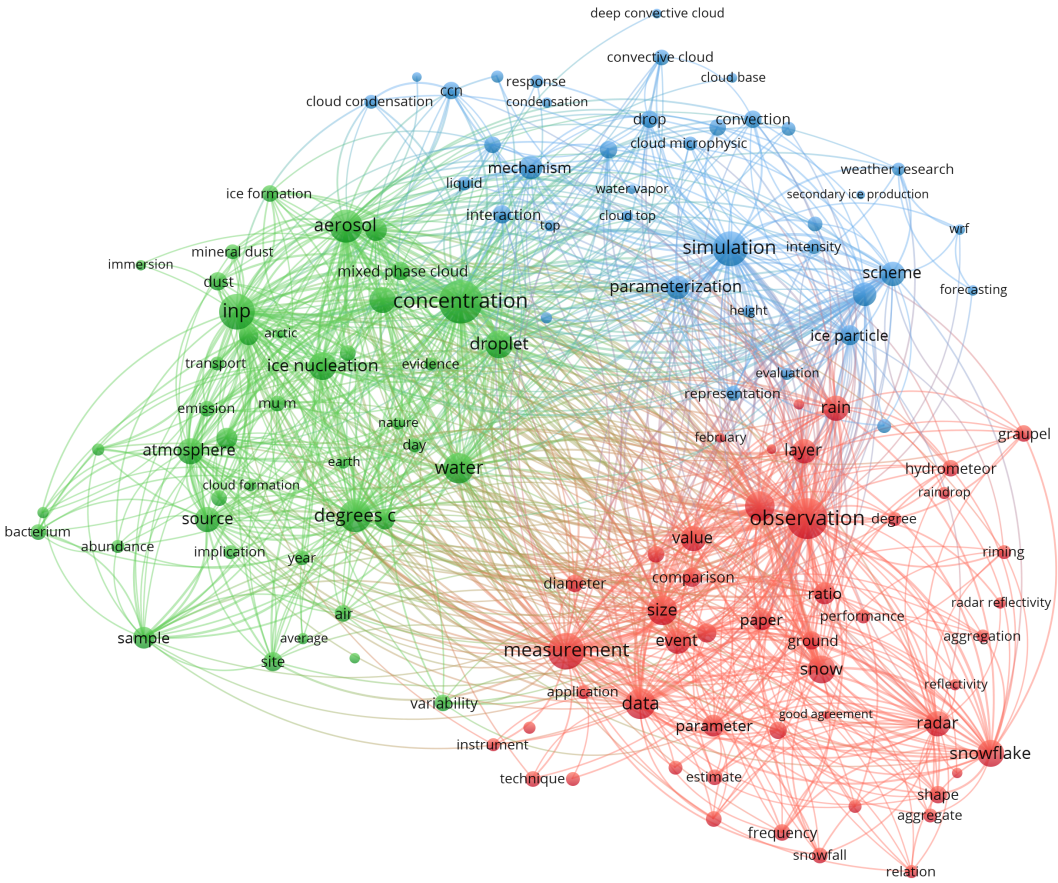

Figure 1.2: A term co-occurrence network map. The terms are represented by circles, the links between the terms by lines, and the clusters by the colour (Cluster A (left, green), Cluster B (top, blue), and Cluster C (right, red)). Default visualisation settings of VOSviewer were used. By default, the size of the circle and the label of each term are representative of its weight. The 1000 strongest links between terms are represented with lines. The distance between two terms gives some indication of the co-occurrence. Note that some labels are not displayed to avoid overlapping terms.

The terms of the scientometric analysis grouped into three clusters, which are displayed in the network map in Fig. 1.2. Cluster A focuses on the ice formation process itself, as derived from the occurrences of the terms “ice formation”, “ice nucleation” and “INP”. This research branch deals with the “concentration”, “abundance”, “emission” and “source” of INPs. Furthermore, the specific particle types

and activation temperatures play an important role in this cluster, as demonstrated by the terms "aerosol", "(mineral) dust", "bacterium" and "degrees C". Cluster C is situated separately from Cluster A, with a gap between terms and on the opposite side of the map. This research branch is closely linked to precipitation, as illustrated by the presence of the terms "snowfall" and "rain". Moreover, some terms are related to the habits of ice particles (e.g. "graupel", "aggregate", "shape"), which can be used to pinpoint microphysical processes (e.g. "riming", "aggregation"). Indicated by the co-occurrences of terms such as "measurement", "ground", "radar" and "(radar) reflectivity", this research branch mostly uses ground-based remote sensing measurement techniques. Cluster B connects the two previously described clusters and is primarily driven by model simulations. Words such as "forecasting", "scheme" and "parameterization" appear, along with the "Weather Research and Forecasting (WRF)" model, indicated by its abbreviation in Fig. 1.2. Moreover, the description of clouds plays a role (e.g. "convective cloud", "cloud top", "cloud base") and terms associated with the description of the liquid phase of clouds occur (e.g. "CCN", "cloud condensation", "liquid", "condensation").

In addition to the pure structure of the co-occurrences, the average normalised year of publication of the terms was superimposed on the network map (not shown). Cluster A seems to be the research branch, which has lately been of greatest interest, as it is the cluster with the most terms (e.g. "INP", "bacterium", "mineral dust", "mixed-phase cloud", "source", "abundance") occurring in recently published articles. Of note, the relevance of INP research was emphasised recently by Murray et al. (2021), who proposed "*that a concerted research effort is required to reduce substantial uncertainties related to the poorly understood sources, concentration, seasonal cycles and nature of [...] INPs*" to better represent clouds in climate models. Even if rare in terms of abundance in the atmosphere, INPs can initiate a sequence of succeeding processes that change the partitioning of ice particles and liquid droplets. Moreover, the INP concentration plays an important role in whether a cloud has a warming or a cooling effect on the Earth's radiation budget (DeMott et al., 2010).

Overall, the network map (Fig. 1.2) indicates that ice microphysical processes

are studied by focusing either on primary ice formation (Cluster A), secondary ice formation (Cluster B), or other microphysical processes, which occur after primary and secondary ice formation in a cloud (e.g. aggregation and riming; Cluster C). Cluster C is strongly linked to precipitation, while Cluster B, which connects Clusters A and C, is mostly associated with model simulations. Many microphysical processes can be simulated with models, which enables the investigation of their interactions and their relevance for precipitation formation (e.g. Sullivan et al., 2018b). However, in field studies, it is much more challenging to first observe multiple microphysical processes and precipitation and then second determine the relevance of each microphysical process on precipitation. This might explain why terms like "ice formation" (far left) and "snowfall" (bottom), which are closely linked in nature, are associated with different clusters and are therefore rather distant from each other on the map.

Besides identifying conceptual structures, the network map provides indications of shortcomings in knowledge or weak connections within the research field. One example, the term "secondary ice production", is placed in Cluster B. However, it has a lower frequency of occurrences compared to other terms and is not strongly connected (only the strongest 1000 connections are shown in the map). This indicates that secondary ice formation processes are mostly simulated (e.g. Sullivan et al., 2018b) and have not attracted as much attention from experimentalists as other topics. Secondary ice formation processes have only received more interest in the last few years (e.g. Korolev et al., 2020) in order to help explain the high number of ice particles observed in clouds that cannot be explained by INPs alone (e.g. Beck et al., 2018). Incidentally, the secondary ice formation processes most frequently discussed in the literature are rime-splintering (e.g. Hallett and Mossop, 1974) and droplet fragmentation (e.g. Takahashi and Yamashita, 1970) and ice–ice collision and breakup (e.g. Vardiman, 1978). Others have been less discussed (e.g. Korolev and Leisner, 2020) or only recently been discovered and described (e.g. James et al., 2021).

The microphysical processes in mixed-phase clouds leading to precipitation are intertwined in nature and seem to be partially connected in research. Drawing from two or more of the research branches shown on the map within an individual study

that goes beyond modelling could likely lead to further progress in better understanding cloud processes and precipitation. Of note, the terms at the extremities of the network map have fewer connections to the other clusters. However, some of them are closely linked in nature (like "ice formation" and "snowfall"). Hence, designing experiments that connect terms which are distant from each other on the map or belong to different clusters but are closely linked in nature might be particularly promising.

1.3 Microphysical ice processes at moderate supercooling

Temperature affects many microphysical ice processes in the atmosphere. At moderate supercooling (i.e. around $-15\,^{\circ}\mathrm{C}$), primary ice formation is often considered to be dominated by INPs of biological origin (DeMott and Prenni, 2010; Murray et al., 2012; Fröhlich-Nowoisky et al., 2016; Kanji et al., 2017; Huang et al., 2021). So-called biological INPs are associated with bacteria, fungi, plants, lichens, algae and microalgae (e.g. Pouleur et al., 1992; Ariya et al., 2009; Fröhlich-Nowoisky et al., 2015; Diehl et al., 2002; Christner, 2010; Tesson and Šantl-Temkiv, 2018). Emitted by the Earth's surface, they determine the atmospheric INP concentrations at temperatures $\geq -15\,^{\circ}\mathrm{C}$ (INPs_{-15}). Although INPs_{-15} tend to occur in low concentrations, i.e. in the range between 0.001 and 1 L^{-1} (Petters and Wright, 2015), they may initiate the formation of a crucial amount of ice crystals, which may be followed under suitable conditions by a cascade of microphysical cloud processes, including secondary ice formation processes. In general, the temperature of maximum secondary ice production rate is often around $-15\,^{\circ}\mathrm{C}$ or warmer, although the effect of temperature on secondary ice formation processes is yet uncertain (Korolev and Leisner, 2020). If the temperature ranges from $-12\,^{\circ}\mathrm{C}$ to $-17\,^{\circ}\mathrm{C}$ and water saturation is reached, ice crystals preferably grow into dendrites (e.g. Takahashi, 2014), which is one of the many ice crystal habits caused by the preferential arrangements of water molecules into an ice lattice (Libbrecht, 2017). Although dendrites indicate somewhat narrow growth conditions, the term "dendrite" does not occur in the network map (Fig. 1.2). However, terms related to ice particle classes, like "aggregate" or "graupel", are identified in the map (see Cluster C in Fig. 1.2). Generally, large and eventually rimed ice crystals form above water saturation, while small, compact and unrimed

crystals form below water saturation (Nakaya, 1954; Magono and Lee, 1966; Bailey and Hallett, 2009). Therefore, ice crystal habits can indicate the state of the cloud phase, i.e. either mixed-phase or ice-phase.

In response to global warming, precipitation patterns will change, including an intensification of precipitation extremes (O'Gorman, 2015). With rapid climate changes, the sources, fluxes and, consequently, the concentration of INPs might change rapidly too. If atmospheric INP concentrations change, the initiation of the ice phase in mixed-phase clouds can change (DeMott et al., 2010), possibly affecting the complex sequence of ice processes in clouds. This may drive feedback between production and emission of INPs, cloud properties and precipitation formation. Thus, there is a strong need to conduct research on the sources and drivers of atmospheric INPs (Murray et al., 2021) and secondary ice formation processes (Korolev and Leisner, 2020). Overall, clouds are expected to amplify future warming, although their impact on climate change remains uncertain (Boucher et al., 2013; Forster et al., 2021). The greater understanding of microphysical processes in clouds could improve weather and climate predictions, which could ultimately lead to climate change mitigation and adaptation strategies. Therefore, such an understanding would be beneficial for science, politicians, decision-makers and the public.

1.4 Objectives of this thesis

This thesis is motivated by the need to gain an integrated understanding of the microphysical ice processes that ultimately lead to precipitation. Therefore, information on ice formation at moderate supercooling and snowfall was collected. The main objectives of this thesis were:

1. to investigate the abundance of INPs at $\geq -15\,^{\circ}\mathrm{C}$ at cloud height. Aerosol samples were collected at Weissfluhjoch (2671 m a.s.l., Switzerland) during the winter of 2019. Work towards a parameterisation of atmospheric INPs at $-15\,^{\circ}\mathrm{C}$ based on aerosol particle concentration, air mass origin and precipitation history are presented (see Chapter 2).

2. to determine the fraction of primary versus secondary ice crystals in mixed-phase clouds. This includes an approach to evidence and quantify secondary ice crystals at around $-15\,^{\circ}\mathrm{C}$. Dendritic ice crystals were collected and analysed for their INP content using a custom-built cold-stage during fieldwork conducted at Jungfraujoch (3580 m a.s.l., Switzerland) in the winter of 2018 (see Chapter 3).

3. to explore whether mixed-phase clouds are the main source of solid precipitation at an Arctic continental site. Ice particles falling onto the Earth's surface were observed during two winter seasons (2019 and 2020) in Sondakylä, Finland (179 m a.s.l.) and coinciding radiosonde launches were analysed (see Chapter 4).

The thesis is organized as follows: In Chapter 2 to Chapter 4 the results of the studies conducted to achieve the objectives are presented; in Chapter 5 conclusions and suggestions for future research are given; and in Chapter 6 outlooks are provided. My further contributions and a personal note are added at the end.

View from the observatory at Weissfluhjoch
Photo: Claudia Mignani

Chapter 2

Towards parameterising atmospheric concentrations of ice-nucleating particles active at moderate supercooling

Claudia Mignani[1], Jörg Wieder[2], Michael A. Sprenger[2], Zamin A. Kanji[2], Jan Henneberger[2], Christine Alewell[1], Franz Conen[1]

[1]Department of Environmental Sciences, University of Basel, Bernoullistrasse 30, 4056 Basel, Switzerland

[2]Institute for Atmospheric and Climate Science, ETH Zurich, Universitätstrasse 16, 8092 Zurich, Switzerland

This chapter has been published as article in Atmospheric Chemistry and Physics.
DOI: 10.5194/acp-21-657-2021

Abstract

A small fraction of freezing cloud droplets probably initiates much of the precipitation above continents. Only a minute fraction of aerosol particles, so-called ice-nucleating particles (INPs), can trigger initial ice formation at −15 °C, at which cloud-top temperatures are frequently associated with snowfall. At a mountaintop site in the Swiss Alps, we found that concentrations of INPs active at −15 °C can be parameterised by different functions of coarse (> 2 µm) aerosol particle concentrations, depending on whether an air mass is (a) precipitating, (b) non-precipitating, or (c) carrying a substantial fraction of dust particles while non-precipitating. Consequently, we suggest that a parameterisation at moderate supercooling should consider coarse particles in combination with air mass differentiation.

2.1 Introduction

The presence of ice in clouds is important for precipitation initiation (Mülmenstädt et al., 2015; Heymsfield et al., 2020). Ice-nucleating particles (INPs) affect clouds and their development by generating primary ice at temperatures between 0 and −38 °C. The difficulty of understanding and thus predicting the atmospheric INP concentration ([INP]) originates from observational challenges related to field measurement techniques (Cziczo et al., 2017), the large variety of potential sources (Kanji et al., 2017), and the wide range in atmospheric abundances from 10^{-6} to $10^{3}\,\mathrm{L}^{-1}$ (Petters and Wright, 2015). The past decade has seen substantial efforts toward improving empirical parameterisations of [INP] (e.g. DeMott et al., 2010; Phillips et al., 2013; DeMott et al., 2015). A current empirical parameterisation established by DeMott et al. (2015), hereafter D15, predicts [INP] based on the nucleation temperature and number concentration of mineral dust particles with diameters > 0.5 µm ($[n_{0.5}]$) (DeMott et al., 2015). Although D15 may be applicable to temperatures below −20 °C, it is not expected to represent a multivariate INP population and remains *"weakly constrained at temperatures > −20° C, where much additional ambient and laboratory data are needed"* (DeMott et al., 2015).

The coldest part of a cloud – typically cloud tops and their temperature – de-

termines what fraction of the INP population will get activated and form ice crystals. Any INPs with colder activation temperatures will remain inactive. Cloud-top temperatures associated with winter snowfall have a primary temperature mode near $-15\,°C$, as derived from close to 10^5 parallel observations of cloud-top temperatures and falling solid precipitation throughout the United States (Hanna et al., 2008). The majority of these observations were for light snowfall. In contrast, cloud-top temperature distributions for moderate and heavy snowfall are bimodal, with a second minor mode around $-40\,°C$ (Hanna et al., 2008). This is consistent with observations in mountainous regions (Rauber, 1987). Of all snowfall observations with cloud tops above homogeneous freezing temperature (i.e. $> -38\,°C$), approximately 30 % are associated with cloud-top temperatures not colder than $-15\,°C$ (Hanna et al., 2008). Therefore, substantial fractions of initial ice crystals in snow-producing mixed-phase clouds may be caused by INPs that nucleate ice at temperatures $\geq -15\,°C$ ($INPs_{-15}$). This inference may extend to other midlatitude continental regions. Considering $-15\,°C$ to be a temperature that is important for snow formation also makes physical sense because maximum depositional growth of ice crystals is around $-15\,°C$ (Rogers and Yau, 1989). In this work, we therefore focus on INPs active at that temperature, although future studies would benefit from relating measurements to overall cloud thermal structures, which may at times include lower cloud-top temperatures.

Based on current understanding, atmospheric $INPs_{-15}$ are mostly biological aerosol particles (Murray et al., 2012). Although their number concentration is generally smaller compared to those $< -15\,°C$ (Petters and Wright, 2015), primary ice formed by $INPs_{-15}$ may get multiplied by an order of magnitude due to secondary ice formation (Mignani et al., 2019a). Findings from a sparse number of size-resolved measurements of atmospheric INPs show that $INPs_{-15}$ are mostly $> 2\,\mu m$ in diameter (Huffman et al., 2013; Mason et al., 2016; Creamean et al., 2018a). This particle size, however, is under-represented for instrumental reasons in the empirical data on which D15 and other parameterisations (e.g. DeMott et al., 2010; Phillips et al., 2013) are based. Furthermore, an increase in atmospheric abundance of INPs active at moderate supercooling has been observed during precipitation (Bigg and Miles, 1964; Huffman et al., 2013; Hara et al., 2016; Conen et al., 2017). This might be explained

by aerosolisation of INPs by rain itself, a mechanism similar to the generation of bioaerosol by raindrop impingement (Joung et al., 2017), which is probably dependent on various parameters like surface wetness or land cover.

To test whether the general approach of D15 (i.e. parameterising INPs as a function of particles larger than a certain size) can be reconciled with the findings of INPs$_{-15}$ being mostly larger than $> 2.0\,\mu m$ and increasing during precipitation, we collected and analysed aerosol samples from February to March 2019 on Weissfluhjoch, Switzerland, at an average local air temperature of -7.1 (standard deviation ± 4.3) °C during sampling intervals (Fig. A.1). The site, surrounding mountains, and nearby valleys were snow-covered, while most of the lower-lying plain and the foothill regions were not, and precipitation occurred in the form of rain in those regions during our study period.

2.2 Material and method

Between 11 February and 26 March 2019, we collected and analysed a total of 140 aerosol samples at Weissfluhjoch, Switzerland (46°49′58.670″ N, 9°48′23.309″ E; 2671 m a.s.l.), during the "Role of Aerosols and Clouds Enhanced by Topography on Snow (RACLETS)" campaign. Total aerosol was sampled through a heated inlet (heating element kept at +46 °C) similar to the one described in Weingartner et al. (1999), which was designed such that particles with diameters $< 40\,\mu m$ are sampled up to a wind speed of $20\,m\,s^{-1}$. The inlet extended through the eastern wall of the laboratory and was about 8 m above local ground. The aluminium inlet tubing had an inner diameter of 4.5 cm throughout its total length of 7 m. Particles entering the inlet travelled at a speed of about $3\,m\,s^{-1}$ first 2.5 m downward, then turned by 70° in a radius of 20 cm towards the inside of the laboratory and continued for another 4.5 m about 20° downslope before being trapped in the impinger, approximately 2.2 s after they had entered the inlet. Ice particles resuspended from surrounding surfaces (snow-covered throughout the campaign and with an average local wind speed of 7.1 (standard deviation ± 3.4) $m\,s^{-1}$ during sampling intervals) cannot be ruled out but are unlikely to contribute significant amounts to the total sampled particles. The airflow was maintained throughout the campaign at $300\,L\,min^{-1}$, during sampling by

a high-flow-rate impinger (Bertin Technologies, Coriolis®µ) and between sampling intervals by a makeup flow using an external blower. In addition, an aerodynamic particle sizer (APS; model 3321, TSI Corporation) sampled from the same inlet upstream of the impinger at $1\,\mathrm{L\,min^{-1}}$.

Aerosol samples were collected using the Coriolis®µ as was done in recent studies (Els et al., 2019; Tarn et al., 2020; Miller et al., 2021). Each sample consisted of aerosol particles collected throughout 20 min (i.e. from $6\,\mathrm{m^3}$ of air) into 15 mL of ultra-pure water (Sigma-Aldrich, W4502-1L). With increasing particle size the theoretical sampling efficiency of the Coriolis®µ increases from around 50 % for particles of 0.5 µm in size and 80 % for particles of 2.0 µm to close to 100 % for particles of 10 µm (personal communication with Bertin Technologies). Water losses due to evaporation were compensated for by replenishing the circulating water after 10 and 20 min. To avoid storage effects (Beall et al., 2020), samples were analysed immediately after collection in a drop-freezing assay with 52 droplets of 100 µL each, as previously described (Stopelli et al., 2014), and cumulative [INP] was calculated (Vali, 1971a). Sampling and analysis were designed in such a way that expected $[\mathrm{INP}_{-15}]$ of each sample would be well within the detection limits, meaning that several but not all droplets in the assay would be frozen. With our sampling and analysis design the detection range lies between 4.8×10^{-4} (i.e. first drop frozen) and $8.1 \times 10^{-2}\,\mathrm{L^{-1}}$ (i.e. second to last drop frozen). In 15 samples, all droplets were frozen and in one sample no droplet was frozen at $-15\,^{\circ}\mathrm{C}$. These samples were not considered because their $[\mathrm{INP}_{-15}]$ was outside the detection limits. For the other samples ($n = 124$) several, but not all, droplets froze. Background measurements ($n = 15$) following an identical procedure as with the samples, but without turning on the airflow of the impinger, were below the detection limit. Number concentrations of particles $[n]$ with aerodynamic diameters from 0.5 to 20 µm were measured with the APS (20 s scanning time) and were integrated (summed) from the particles sizes of interest onward, i.e. ≥ 0.542 µm for $[n_{0.5}]$ (51 bins) and ≥ 1.982 µm for $[n_{2.0}]$ (33 bins). The 20 s data were averaged over each time period (20 min) of the impinger-based aerosol samples taken. $[n_{0.5}]$, $[n_{2.0}]$, and $[\mathrm{INP}_{-15}]$ were adjusted to standard pressure conditions (std; $p_{\mathrm{ref}} = 1013.25$ hPa). $[\mathrm{INP}_{-15}]$ estimates based on D15 were calculated

as

$$\mathrm{INP}_T = \mathrm{CF} \cdot {n_{0.5}}^{\beta} \cdot e^{\gamma \cdot (-T) + \delta}, \tag{2.1}$$

where $\beta = 1.25$, $\gamma = 0.46$, $\delta = -11.6$, T is the temperature in degrees Celsius, INP_T the ice nucleation particle concentration (STP L^{-1}) at T, and $n_{0.5}$ the number concentration of aerosol predominantly consisting of mineral dust particles with a physical diameter $> 0.5\,\mu\mathrm{m}$ (STP cm^{-3}). A physical diameter of 0.5 µm is equivalent to an aerodynamic diameter of 0.9 µm, assuming a particle density of $2.6\,\mathrm{g\,cm}^{-2}$ and a shape factor of 1.3 (Raabe, 1976), which are typical values for mineral dust particles. Similar transformations for observations not dominated by mineral dust would require information about the densities and shapes of the main components of sampled particle populations, which were not available for our site and would require unsupported assumptions. Therefore, we chose to show for all our observations the directly measured particle concentrations in terms of aerodynamic diameter. To use the D15 parameterisation in our context, we corrected predicted [INP] for the difference between the aerodynamic diameter measured and the physical diameter used in Eq. (2.1) by multiplying $n_{0.5}$ in Eq. (2.1) by the ratio of particles with aerodynamic diameter $> 0.9\,\mu\mathrm{m}$ (equivalent to 0.5 µm physical diameter) to particles with aerodynamic diameters $> 0.5\,\mu\mathrm{m}$, which we observed in Saharan-dust-dominated air masses during our campaign. The average value of this ratio was 0.59. The calibration factor (CF) accounts for so-called instrument-specific calibration and is suggested to be 3 ($\mathrm{CF} = 3$) to predict maximum immersion-mode atmospheric [INP] (DeMott et al., 2015). Schrod et al. (2017), who collected samples with an unmanned aircraft system in the Mediterranean region with substantial Saharan dust influence, used it as a mathematical degree of freedom when fitting Eq. (2.1) to their observations.

The 5 d back trajectories were calculated using the Lagrangian analysis tool LAGRANTO (Sprenger and Wernli, 2015). For each sample, one trajectory was started at the full hour closest to the sampling time and from the exact sampling position. The driving wind fields were taken from the operational analysis of the Swiss National Weather Service (COSMO1; https://www.meteoswiss.admin.ch/home.html?tab=overview, last access: 7 January 2021) and the European Centre for Medium-Range

Weather Forecasts (ECMWF; https://www.ecmwf.int/, last access: 7 January 2021). Started in the COSMO domain, the trajectories were extended based on ECMWF data at the time and location where they leave this domain. Their position was saved every 10 min. Along the trajectories, total precipitation was traced amongst others (i.e. height, pressure, temperature, specific humidity, and surface height), enabling us to determine the total precipitation amount along the last 6 h prior to sampling (Fig. A.2).

2.3 Results and discussion

We found cumulative concentrations of atmospheric INPs active at −15 °C ($[INP_{-15}]$) that are lying within the lower half of values summarised in Petters and Wright (2015). From the total of 124 impinger-based aerosol samples with quantified $[INP_{-15}]$, about half (56) were collected from air masses that had precipitated at least 1.0 mm during the 6 h prior to sampling (defined as "precipitating"). About half of these air masses were also precipitating when sampled at Weissfluhjoch, as observed by a precipitation gauge. A similar number of samples (57) was from air masses with less or no prior precipitation ("non-precipitating"), and 11 were from air masses including a substantial fraction of Saharan dust (SD) and no prior precipitation. Air masses mainly reached the sampling position from the west (Fig. 2.1a). Precipitating air masses came on a rather direct path from the Atlantic, crossing the west of Europe with fewer detours than non-precipitating air masses, whereas air masses carrying dust came from the direction of the Sahara, passing the south of Europe. Considering 6 h before arriving at Weissfluhjoch, the trajectories crossed a mean distance of 242 (standard deviation ± 145) km and spent two-thirds of the time over Switzerland (Fig. 2.1b). Forested land (31 %), agricultural fields (17 %), pasture (12 %), and natural grasslands (12 %) were the most common land cover types they passed, as derived by the European Copernicus programme's Corine land cover map (https://land.copernicus.eu/pan-european/corine-land-cover/clc2018, last access: 13 October 2020).

Precipitating air masses had the lowest $[n_{0.5}]$ and the lowest concentration of aerosol particles with diameters > 2 µm ($[n_{2.0}]$) but similar ratios as non-precipitating air

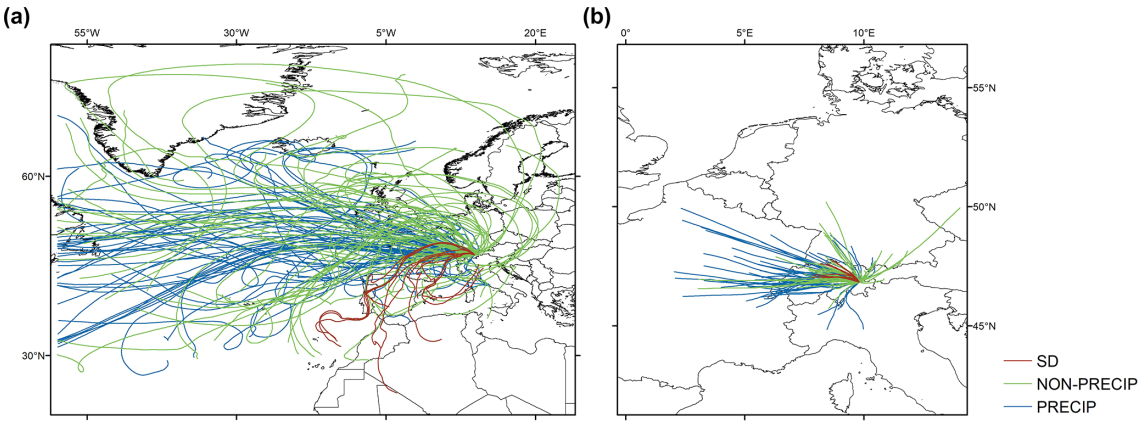

Figure 2.1: **(a)** 5 d and **(b)** 6 h back trajectories of air masses that were precipitating (PRECIP, blue), non-precipitating (NON-PRECIP, green), and carrying a substantial fraction of Saharan dust while non-precipitating (SD, red).

masses of $[n_{2.0}]$ to $[n_{0.5}]$ (Fig. 2.2a–b). The largest ratio of $[n_{2.0}]$ to $[n_{0.5}]$ was in SD air masses (Fig. 2.2c). Therefore, relative differences in measured $[\mathrm{INP}_{-15}]$ between precipitating and non-precipitating air masses would be affected very little if a substantial fraction of INPs_{-15} were of a size near 0.5 µm, which was sampled with a lower efficiency (50 %) than 2 µm (80 %). However, $[\mathrm{INP}_{-15}]$ in both of these air masses would have been underestimated relative to $[\mathrm{INP}_{-15}]$ in SD-affected air masses, which had the highest $[n_{2.0}]$ to $[n_{0.5}]$ ratio.

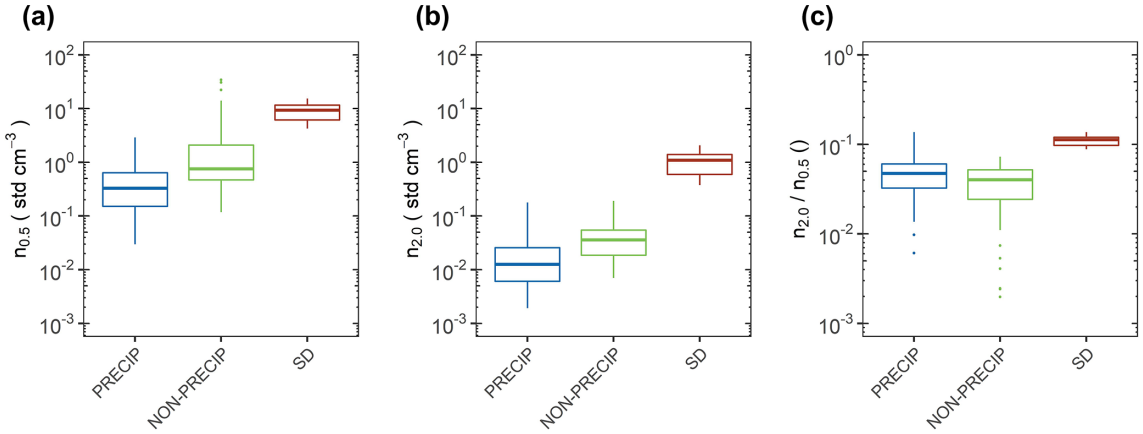

Figure 2.2: Number concentrations of aerosol particles with aerodynamic diameters **(a)** >0.5 µm $[n_{0.5}]$ and **(b)** >2.0 µm $[n_{2.0}]$ along with **(c)** their ratio for the aerosol populations of PRECIP, NON-PRECIP, and SD air masses.

In general, $[\mathrm{INP}_{-15}]$ in non-precipitating and precipitating (not dominated by mineral dust) air masses was higher than in mineral-dust-dominated air masses for the same $[n_{0.5}]$ (Fig. 2.3a). The observed slope for SD air masses was the same as that predicted

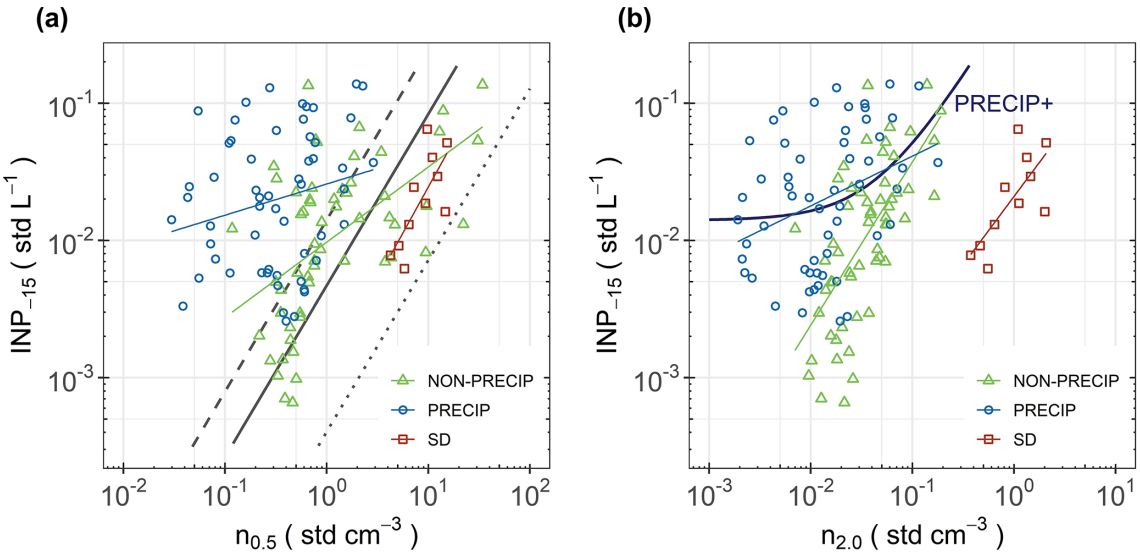

Figure 2.3: Cumulative concentrations of ice-nucleating particles active at −15 °C [INP$_{-15}$] **(a)** versus [$n_{0.5}$] and **(b)** versus [$n_{2.0}$] for PRECIP (blue circles), NON-PRECIP (green triangles), and SD (red squares) air masses. Power functions (solid lines) for each type of air mass based on [$n_{0.5}$] and [$n_{2.0}$] are shown. An additional preliminary parameterisation for precipitating air masses based on [$n_{2.0}$] is shown (PRECIP+, thick dark blue line). It is the same as for non-precipitating air masses but with an added constant equivalent to 0.014 INPs L^{-1}. The corresponding equations and R^2 values are shown in Table 2.1. The grey lines show the D15 parameterisation extrapolated to −15 °C and corrected for the difference between physical and aerodynamic diameters (see the "Material and method" section) with three different calibration factors (Eq. 2.1): CF = 3 (dashed), CF = 1 (continuous), and CF = 0.086 (dotted). The latter value was the best fit found by Schrod et al. (2017) for Saharan dust above Cyprus.

by the D15 parameterisation. The offset of the D15 curve depends on the calibration factor (see Eq. 2.1). Observed SD data were between the D15 curves with the CF set to 1 and to 0.086, respectively. The latter value is reported in Schrod et al. (2017), who sampled the Saharan dust layer above Cyprus with a drone up to 2850 m a.s.l.

Considering the fact that the observed size of INP$_{-15}$ is mostly larger than 2 µm (Huffman et al., 2013; Mason et al., 2016; Creamean et al., 2018a), we plot measured [INP$_{-15}$] against [$n_{2.0}$] instead of [$n_{0.5}$], resulting in a more distinct separation of the data to the different air masses (Fig. 2.3b). In each of the three categories of air masses, [INP$_{-15}$] can be described as a function of [$n_{2.0}$] that is valid for a range of [INP$_{-15}$] from 0.0006 to 0.14 std L^{-1} (Table 2.1). For data in SD and non-precipitating air masses, [INP$_{-15}$] can be described as power functions of [$n_{2.0}$], with similar linear slopes on a log–log plot but lower [INP$_{-15}$] per [$n_{2.0}$] for SD. This goes hand in hand with the earlier observations that air masses influenced by SD carry fewer INPs

Table 2.1: Equations of the functions shown in Fig. 2.3 (i.e. PRECIP, PRECIP+, NON-PRECIP, SD) predicting cumulative concentrations of ice-nucleating particles active at $-15\,°C$ [INP$_{-15}$] based on aerosol particles with aerodynamic diameters $>0.5\,\mu m$ [$n_{0.5}$] and $>2.0\,\mu m$ [$n_{2.0}$] along with their respective R^2 values. In addition, equations and R^2 values of power functions fitted to all data points irrespective of air mass classes are shown (ALL). The equations are listed based on the following formula: $y = b \cdot x^a + c$, with y equal to [INP$_{-15}$].

Air mass type	n	x	b	a	c	R^2
ALL	124	$[n_{0.5}]$	0.02	0.19	0	0.06
PRECIP	56	$[n_{0.5}]$	0.03	0.23	0	0.05
NON-PRECIP	57	$[n_{0.5}]$	0.01	0.55	0	0.29
SD	11	$[n_{0.5}]$	0.001	1.34	0	0.55
ALL	124	$[n_{2.0}]$	0.03	0.22	0	0.07
PRECIP	56	$[n_{2.0}]$	0.09	0.36	0	0.12
PRECIP+	56	$[n_{2.0}]$	0.58	1.19	0.014	0.14
NON-PRECIP	57	$[n_{2.0}]$	0.58	1.19	0	0.44
SD	11	$[n_{2.0}]$	0.02	0.99	0	0.55

active at moderate supercooling per unit mass of aerosol particles than European background air masses (Conen et al., 2015a). In precipitating air masses, the ratio between [INP$_{-15}$] and [$n_{2.0}$] was usually larger than in non-precipitating air masses. This reveals that the aerosol population was enriched with INPs active at moderate supercooling during precipitation, consistent with previous findings (Bigg and Miles, 1964; Huffman et al., 2013). Since additional INPs during precipitation might be due to aerosolisation of INPs by rain, which is likely independent of the background in [n], we describe [INP$_{-15}$] in precipitating air masses by adding a constant to the function fitted to the non-precipitating cases (Fig. 2.3b). The median difference between the function of non-precipitating air masses and measured [INP$_{-15}$] in precipitating air masses was $0.014\,\mathrm{std\,L^{-1}}$ (Fig. 2.4). The relationship between these differences and [$n_{2.0}$] was weakly positive and not significant, meaning that the absolute value of additional INPs in precipitating air masses was independent of [$n_{2.0}$]. This finding corroborates our assumption that additional INPs during precipitating air masses are independent of background [n]. A consequence of our finding is that for precipitating air masses with low [$n_{2.0}$], the addition of INPs aerosolised by precipitation makes a relatively large contribution to the overall [INP$_{-15}$]. The additional INPs during precipitation could be emitted through the impact of rain on snow-free lower-lying plain regions, a speculation which needs to be investigated in future.

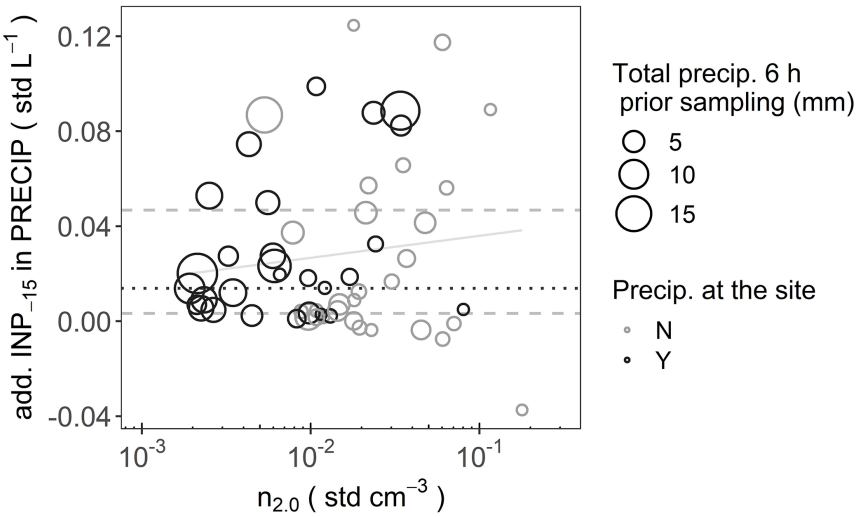

Figure 2.4: Difference between [INP$_{-15}$] in precipitating (PRECIP) air masses and the function fitted to the non-precipitating (NON-PRECIP) air masses (additional [INP$_{-15}$] in PRECIP) versus [$n_{2.0}$]. The median difference is $0.014\,\mathrm{std\,L^{-1}}$ (black dotted line), and the lower and upper quartiles are 0.003 and $0.047\,\mathrm{std\,L^{-1}}$, respectively (grey dashed lines). The linear fit (grey solid line) is weakly positive but not significant (Pearson correlation test, $R = 0.0027$, and $p = 0.98$). The circle area is proportional to the amount of precipitation along the last 6 h of the trajectory prior to sampling. Black circles are for samples precipitating at Weissfluhjoch.

Overall, for each air mass class, the correlation coefficient of the obtained functions is the same or higher with [$n_{2.0}$] as a predictor than with [$n_{0.5}$] (Table 2.1). This confirms that [$n_{2.0}$] is a more powerful predictor of INPs$_{-15}$ than [$n_{0.5}$] when combined with air mass differentiation (Fig. A.3). It underlines the importance of considering aerosol particles $> 2\,\mu\mathrm{m}$. To further develop a parameterisation valid for temperatures $> -20\,^{\circ}\mathrm{C}$, we suggest further investigating the presented functions because INPs active at other temperatures or at other locations and during different seasons may also be associated with other particle sizes or other INP concentrations. The addition of INPs in precipitating air masses, in particular, should be constrained with data from all over the globe.

2.4 Conclusion

In summary, it is possible to reconcile two fundamental aspects of INPs active at moderate supercooling – increased abundance during precipitation and size – with a widely used approach to parameterise INPs active at colder temperatures. Parameterisations based on the number concentration of aerosol particles are reasonable to

predict INPs at moderate supercooling. However, relating [INP$_{-15}$] to the number concentration of larger particles can further improve the predictions, which is not to say that INPs$_{-15}$ are always in such a size range. An even greater improvement in predictions is possible when we additionally distinguish between air masses that are precipitating, non-precipitating, or carrying a substantial fraction of Saharan dust. More of the variance of [INP] was explained by aerosol concentrations in air masses that were non-precipitating or carrying desert dust compared to air masses that were precipitating. The absolute value of additional INPs in precipitating air masses, versus non-precipitating air masses, seems to be independent of total aerosol concentrations.

To tackle predictions of INPs active at moderate supercooling, particular attention has to be devoted to sampling larger aerosol particles at mixed-phase cloud height, including air masses that have been precipitating, and adjusting procedures to reliably quantify [INP] at the targeted activation temperatures, as was done in this study. Although our proposed parameterisation has a generalisable structure, the parameters have so far only been constrained by data from one campaign. While a new parameterisation for a previously weakly constrained temperature is clearly beneficial, it complements rather than replaces previous parameterisations. In a changing climate with increasing temperatures and changing precipitation patterns, it is important to predict feedbacks between INPs and precipitation.

Data availability. The backward trajectories and the ice-nucleating particle concentrations plus complementary data are published on ENVIDAT (https://www.envidat.ch, last access: 7 January 2021) and are accessible via https://www.envidat.ch/dataset/raclets-backward-trajectories (last access: 7 January 2021, DOI: 10.16904/envidat.120, Sprenger, 2019) and https://www.envidat.ch/dataset/ice-nucleating-particle-concentrations-active-at-15-c-at-weissfluhjoch (last access: 7 January 2021, DOI: 10.16904/envidat.193, Mignani et al., 2020), respectively.

Author contributions. CM and FC conceived the study. CM and JW conducted the measurements. JW provided the aerosol data. MAS conducted the modelling. JH and ZAK hosted the entire measurement campaign. CM processed the data and prepared the figures for the paper. CM and FC interpreted the data and wrote the paper with contributions from JW, MAS, ZAK, JH, and CA.

Competing interests. The authors declare that they have no conflict of interest.

Acknowledgements. The authors would like to deeply thank Paul DeMott and the anonymous referee for their careful reviews. We are indebted to Martin Genter for logistical support, Carolin Rösch and Michael Rösch for technical support, Nora Els for borrowing the Coriolis®µ from the University of Innsbruck and sharing her experience, Lucie Roth and Mario Schär for helping with the measurements, and Pedro Batista for helping with preparing Fig. 2.1. We thank MeteoSwiss for weather data and providing access to the COSMO1 and ECMWF data and all the RACLETS members for fruitful discussions. We acknowledge funding from the Swiss National Science Foundation (SNSF).

Financial support. This research has been supported by the Swiss National Science Foundation (grant nos. 200021_169620, 200021_175824).

Review statement. This paper was edited by Ulrich Pöschl and reviewed by Paul DeMott and one anonymous referee.

Melting dendrite on cold-stage
Photo: Claudia Mignani

Chapter 3

New type of evidence for secondary ice formation at around -15 °C in mixed-phase clouds

Claudia Mignani[1], Jessie M. Creamean[2, 3, a], Lukas Zimmermann[1], Christine Alewell[1], Franz Conen[1]

[1] Institute of Environmental Geosciences, University of Basel, Basel, 4056, Switzerland

[2] Cooperative Institute for Research in Environmental Sciences, University of Colorado, Boulder, CO 80309, USA

[3] Physical Sciences Division, National Oceanic and Atmospheric Administration, Boulder, CO 80305, USA

[a] now at: Department of Atmospheric Science, Colorado State University, Fort Collins, CO 80521, USA

This chapter has been published as article in Atmospheric Chemistry and Physics.
DOI: 10.5194/acp-19-877-2019

Abstract

Ice crystal numbers can exceed the numbers of ice-nucleating particles (INPs) observed in mixed-phase clouds (MPCs) by several orders of magnitude, also at temperatures that are colder than −8 °C. This disparity provides circumstantial evidence of secondary ice formation, also other than via the Hallett–Mossop process. In a new approach, we made use of the fact that planar, branched ice crystals (e.g. dendrites) grow within a relatively narrow temperature range (i.e. −12 to −17 °C) and can be analysed individually for INPs using a field-deployable drop-freezing assay. The novelty of our approach lies in comparing the growth temperature encoded in the habit of an individual crystal with the activation temperature of the most efficient INP contained within the same crystal to tell whether it may be the result of primary ice formation. In February and March 2018, we analysed a total of 190 dendritic crystals (∼ 3 mm median size) deposited within MPCs at the high-altitude research station Jungfraujoch (3580 m a.s.l.). Overall, one in eight of the analysed crystals contained an INP active at −17 °C or warmer, while the remaining seven most likely resulted from secondary ice formation within the clouds. The ice multiplication factor we observed was small (8), but relatively stable throughout the course of documentation. These measurements show that secondary ice can be observed at temperatures around −15 °C and thus advance our understanding of the extent of secondary ice formation in MPCs, even where the multiplication factor is smaller than 10.

3.1 Introduction

Ice-nucleating particles (INPs) are required to catalyse primary ice formation in clouds at temperatures above −36 °C via heterogeneous freezing (e.g. Vali et al., 2015). In mixed-phase clouds (MPCs), heterogeneous freezing is expected to generate ice crystals, but secondary ice production mechanisms can also enhance the ice crystal number concentration (Cantrell and Heymsfield, 2005). The secondary production of ice particles requires the prior presence of other ice particles (Vali, 1985).

For example, secondary ice crystals can result from rime splinters that are re-

leased upon riming (i.e. supercooled cloud droplets that freeze upon contact with a solid hydrometeor) of ice crystals at temperatures between −3 and −8 °C (Hallett and Mossop, 1974; Jackson et al., 2018). Other than the well-known Hallett–Mossop process, mechanisms proposed for secondary ice production include ice–ice collisional break-up (e.g. Vardiman, 1978; Phillips et al., 2017), droplet shattering or fragmentation upon freezing (e.g. Takahashi and Yamashita, 1970; Lauber et al., 2018) and sublimation fragmentation (e.g. Bacon et al., 1998). These processes and indications of their occurrence in the atmosphere are summarised in Field et al. (2017). Sullivan et al. (2018b) have recently studied three of the above-mentioned secondary ice formation processes in terms of their thermodynamic and primary ice requirements in a parcel model. They showed that INP concentration can be as low as $2\,\mathrm{m}^{-3}$ ($0.002\,\mathrm{L}^{-1}$) to initiate ice multiplication by ice–ice collisional break-up. Furthermore, the number of INPs is less important with regard to cloud formation than a sufficiently warm cloud base temperature and modest vertical updraught velocity for frozen droplet shattering and rime splintering (Sullivan et al., 2018b). When droplet shattering and ice–ice collisional break-up were implemented into a large-scale weather model, secondary ice contributed as much to the ice crystal number concentration as did primary ice nucleation, even though high ice crystal numbers remain underestimated by the model (Sullivan et al., 2018a).

While modelling studies accounting for secondary ice production can to some extent explain the observed ice crystal numbers (e.g. Sullivan et al., 2018a), field measurements have not been conclusive as to the contribution of secondary ice production mechanisms until the present day. Kumai (1951, 1961) and Kumai and Francis (1962) found an insoluble particle of 0.5 to 8 µm in size in the centre of almost every one of about 1000 snow crystals they collected. The particles they found were clay and related minerals and were assumed to have initiated the formation of the crystals. Bigg (1996) suggested repeating the experiments by Kumai and Francis (1962) and looking at the ice nucleation properties of these particles. One reason it can be misleading to equate ice residuals with INPs is that MPC-generated ice crystals can contain cloud condensation nuclei (CCN) which have been collected upon riming but have not acted as INPs. One possibility of overcoming this issue

is to sample ice residuals of freshly formed, small ice crystals ($< 20\,\mu m$), which are assumed to have grown by the initial phase of vapour diffusional growth only (Mertes et al., 2007; Kupiszewski et al., 2015). On mountaintop stations, where such crystals can be collected in-cloud, however, hoar frost (cloud droplets frozen onto surfaces) can be a strong source of small (i.e. $< 100\,\mu m$) ice crystals (Lloyd et al., 2015; Farrington et al., 2016; Beck et al., 2018). Hoar frost grows in saturated conditions, breaks off when windy, and broken-off segments can become ingested into clouds and commonly mistaken for secondary ice (Rogers and Vali, 1987). Residuals in hoar frost particles are CCN that had not been activated as INPs. Only droplets freeze upon contact with an iced surface, while ice particles bounce off and remain in the airflow, a principle applied in counterflow virtual impactor inlets used to separate ice from liquid in MPCs (Mertes et al., 2007). Current ice selective inlets are not able to separate primary from secondary ice (Cziczo et al., 2017).

Another possibility of investigating secondary ice is by comparing the concentration of INPs with that of ice crystals in the same cloud. Most such studies report large discrepancies between measured INPs and ice crystal numbers (e.g. Hobbs and Rangno, 1985; Lasher-Trapp et al., 2016; Ladino et al., 2017; Beck et al., 2018), the latter being several orders of magnitude higher than the former. On the contrary, a good agreement between INPs and ice crystals was found by Eidhammer et al. (2010) in an orographic wave cloud. Furthermore, INP concentrations from bulk precipitation samples cannot be disentangled to the level of individual hydrometeors (Petters and Wright, 2015). Riming can affect the INP spectrum of a bulk precipitation sample by adding scavenged INPs immersed in supercooled cloud droplets, which have not been activated under in situ conditions (Creamean et al., 2019). Further, ice-nucleation active microbes can be scavenged by raindrops below cloud and alter the spectrum (Hanlon et al., 2017).

Another way to separate primary from secondary ice particles could be INP assays on individual hydrometeors collected within MPCs. The first experiment in which individual hydrometeors were analysed for INPs, and the only one to our knowledge, was conducted by Hoffer and Braham (1962). The hydrometeors they

had collected from aircraft were large, frozen water drops that had grown through riming ("snow pellets" or "ice pellets"; Braham, 1964) within summer clouds. Because they all ($n = 301$) refroze only at temperatures substantially lower than the estimated cloud top temperature, the authors presumed them to be of secondary origin. However, an ice multiplication factor (i.e. the number of all ice particles divided by the primary ice particles) could not be estimated because the number of primary ice particles was zero.

In this study, similarly to the one by Hoffer and Braham (1962), we collected in-cloud hydrometeors to obtain in situ evidence of secondary ice formation. We concentrated on secondary ice formation at around −15 °C for three reasons. First, the growth habit of ice crystals forming in supersaturated conditions between −12 and −17 °C is well and distinctively defined. These are single, planar, branched, sector-type or dendrite-type habits (Nakaya, 1954; Magono, 1962; Magono and Lee, 1966; Takahashi et al., 1991; Takahashi, 2014; Libbrecht, 2017) that grow by vapour diffusional growth into a diameter of several millimetres during a vertical fall of a few 100 m (Fukuta and Takahashi, 1999). Second, Westbrook and Illingworth (2013) observed a long-lived supercooled cloud layer with a cloud top temperature around −13.5 °C, which continued to precipitate ice crystals well beyond the expected exhaustion of its INP reservoir. Third, laboratory investigations revealed ice–ice collision to be most effective in producing secondary ice particles at around −16 °C (Takahashi et al., 1995) or in collisions involving dendritic crystals (Griggs and Choularton, 1986). Assuming that the growth temperature of a crystal is not much different from the temperature of its initial formation, these observations suggest that evidence for secondarily formed crystals might be obtained by collecting planar, branched snow crystals from supercooled clouds and testing them individually for the presence of INPs that might have nucleated their formation (i.e. INPs that were activated between −12 and −17 °C).

Table 3.1: Sampling periods including the date and the time span, numbers of analysed crystals (n), mean air temperature (T) (and standard deviation), mean wind velocity (u) (and standard deviation) and mean wind direction (dd) at Jungfraujoch; mean height of the station above cloud base (z_B) and estimated mean cloud base temperature (CBT).

Date dd/mm/yyyy	Time span UTC	n –	T °C	u m s^{-1}	dd –	z_B m	CBT °C
15/02/2018	07:30–21:50	38	−7.0 (0.8)	13.5 (2.1)	NW	944	0.1
16/02/2018	09:30–16:30	29	−8.7 (0.2)	9.0 (2.4)	NW	1239	0.6
17/02/2018	09:40–23:40	42	−8.6 (1.7)	5.8 (1.9)	NW	693	−3.3
23/02/2018	10:30–21:20	20	−14.8 (0.6)	11.9 (1.6)	SE	365	−12.1
06/03/2018	12:20–19:20	14	−13.1 (0.1)	5.5 (0.8)	NW	1284	−3.4
07/03/2018	08:00–16:40	23	−15.7 (0.8)	4.5 (2.6)	NW	1001	−8.2
10/03/2018	09:30–12:50	11	−6.8 (0.3)	5.1 (1.3)	E	196	−5.4
11/03/2018	15:40–17:00	6	−9.8 (0.1)	13.1 (1.4)	SE	1485	1.3
12/03/2018	09:10–11:10	12	−11.4 (0.1)	6.2 (0.7)	NW	878	−4.8
22/03/2018	15:50–22:30	34	−15.2 (1.2)	12.4 (1.5)	NW	1079	−7.1

3.2 Experiment

3.2.1 Location and meteorological conditions

Between 15 February and 22 March 2018, we collected and analysed a total of 229 planar, sector- and dendrite-type ice crystals (i.e. ice crystals of a size larger than 1.3 mm in diameter) during cloudy conditions at the high-altitude research station Jungfraujoch (3580 m a.s.l.) in the Swiss Alps. During the collection, cloud base height, measured by MeteoSwiss with a ceilometer located 5 km north-west of Jungfraujoch (Poltera et al., 2017), was on average 950 m below the station (z_B, Table 3.1). Based on air temperature measured by MeteoSwiss at Jungfraujoch, cloud base height and an assumed moist adiabatic lapse rate of 7.5 °C km^{-1} (plausible for approximately 650 hPa and −10 °C) we estimated that daily mean cloud base temperatures (CBTs) were between +1 and −12 °C. The mean air temperature at the station during the sampling periods was −11.0 °C (±3.6) and the mean wind velocity was 9.1 m s^{-1} (±3.9). On 3 days air masses arrived mainly from south-east (SE) or east (E), and on 7 days from the north-west (NW).

3.2.2 Single crystal selection and analysis

We collected snow crystals on a black aluminium plate (40 cm × 40 cm) at about 1 m above the floor of the main terrace of the Sphinx Observatory at Jungfraujoch and analysed the crystals inside a small, naturally cold (−1 to −7 °C) anteroom between the terrace and the laboratory. Among a usually wide variety of shapes and sizes precipitating onto the plate, we selected what we considered to be single, planar, branched or dendritic ice crystals (from here on "dendrites"), which can safely be assumed to have grown within MPCs at temperatures around −15 °C (Nakaya, 1954; Magono, 1962; Magono and Lee, 1966; Takahashi et al., 1991; Takahashi, 2014; Libbrecht, 2017). Generally, we exposed the plate for some seconds to the precipitating cloud until at least two dendritic snow crystals had deposited on it and then analysed those. Our selection criteria excluded small or irregular ice crystals, which are more typical for hoar frost particles which might have been generated by local surface sources around the station (Lloyd et al., 2015; Farrington et al., 2016; Beck et al., 2018). Rime on selected crystals is of little concern in our approach and was accounted for (see Sect. 3.2.3).

Selected crystals were documented by macro (1 : 1) photography (camera: OM-D E-M1 Mark II, pixel width: 3.3 µm; objective: M. Zuiko ED 60 mm f2.8; flash: SFT-8; all items from Olympus, Tokyo, Japan) stabilised by a focusing rack (Castel-L, Novoflex, Memmingen, Germany) propped up on the aluminium plate. The size of our crystals was determined by using ImageJ (Rueden et al., 2017; Schindelin et al., 2012). Images were later analysed visually and not by machine-learning methods, such as those developed by Praz et al. (2017), for the habit, including the degree of riming both categorised according to the latest ice crystal classification scheme, as presented by Kikuchi et al. (2013). The scheme catalogues solid precipitation particles into a total of 121 categories and provides for each category a representative image.

After selecting the crystals, we tested them for the most efficient insoluble INP they contained that can be activated through immersion freezing using a custom-built cold-stage (Fig. 3.1; more details in Supplement). A cold-stage is a drop-freezing

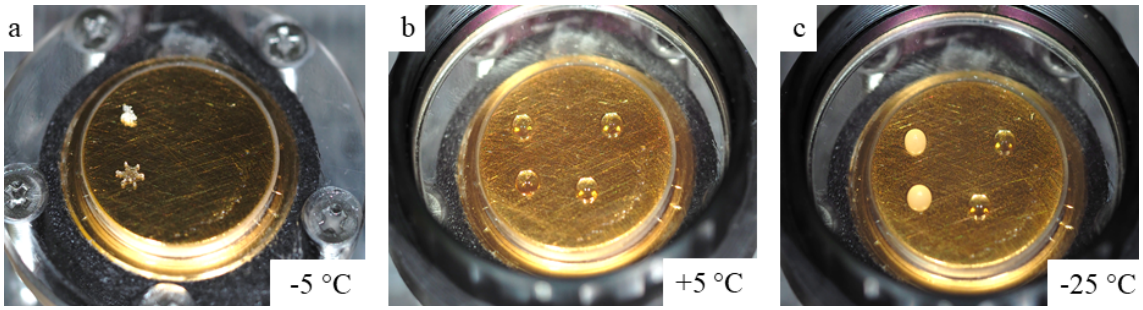

Figure 3.1: Illustration of one ice crystal droplet freezing experiment. Transparent droplets are liquid. **(a)** Two single crystals on the cold-stage (note: the cold-stage was set to below 0 °C for this image and the upper crystal is not a dendrite). **(b)** Melted ice crystals with addition of 3 µL ultrapure water to increase the detection volume (left) and two 3 µL control droplets of the same ultrapure water (right). **(c)** The frozen sample (left) and supercooled control (right) droplets after cooling to −25 °C.

apparatus, on which droplets are deposited onto a cooling surface and the temperature at which they freeze is observed (Vali, 1971b). This technique is commonly used today to assess the activation temperature of INPs immersed in droplets. Observations have shown that an overwhelming majority of ice particles originate from supercooled liquid clouds at temperatures $> -27\,^{\circ}\mathrm{C}$, which strongly suggests that the initial process of ice formation in MPCs $> -27\,^{\circ}\mathrm{C}$ occurs through immersion freezing (Westbrook and Illingworth, 2011). The cold-stage used in this study is meant to be taken into the field, can be set up within minutes and operated without additional infrastructure (i.e. no cooling water or lined power is required). It consists of a gold-plated copper disk with a surface diameter of 18 mm, which is large enough to easily accommodate simultaneously two dendrites and two control droplets (roughly 1 cm apart from each other).

With a fine brush, two crystals are transferred onto the cold-stage surface, thinly covered with Vaseline® petroleum jelly (Tobo, 2016; Polen et al., 2018), before being analysed within the next minutes (Fig. 3.1a). The manual application of Vaseline® requires precision and clean gloves in order to get as uniform and clean a cover as possible. At the transfer of the crystals, the surface of the stage was at a temperature between +1 and +5 °C, which is a common temperature range in which to store INPs in water for several hours before analysis (e.g. Wilson et al., 2015). Upon deposition onto the cold-stage, the crystals melted into liquid droplets. To aid visual detection of freezing, we increased the size of the melted crystal droplets by adding

3 µL of ultrapure water (Molecular Biology Reagent, Sigma-Aldrich) with a pipette (using a new tip for each measurement run). The melted crystal, containing all residuals and potentially the INP that had triggered its formation, has a rather small volume compared to the added water. For each crystal a control droplet (3 µL) of the same ultrapure water was placed next to the melted crystal droplet and served as control (blank) (Fig. 3.1b). Then we ramped the temperature of the cold-stage down to −25 °C. Shortly after the cold-stage temperature reached a value below the surrounding air temperature, we covered it with a transparent hood to minimise the chance of contamination from the environment surrounding the droplets and to prevent condensation on the cold-stage (Polen et al., 2018). From −12 °C and below we limited the cooling rate to 3 °C min^{-1}. The freezing of the droplet and thus the presence of the most efficient INP was detected visually, and the corresponding temperature was recorded manually (Fig. 3.1c). The presence of an INP active at −17 °C and warmer (INP_{-17}) was taken as evidence for the tested dendrite to have been generated through primary ice formation. Nevertheless, extending the drop-freeze assay down to −25 °C is useful for determining the fraction of rime associated with single crystals (see Sect. 3.2.3). In total, the procedure (i.e. collecting and analysing two samples) takes ∼ 15 min, a time interval which may allow for a reduction in particle surface area due to coagulation (Emersic et al., 2015). After a test was complete, we cleaned the cold-stage carefully with isopropanol.

3.2.3 Accounting for riming

A rimed ice crystal has collected liquid cloud droplets, each of them containing a CCN that may cause freezing of the droplet containing the residuals of this crystal. Such a CCN may be activated on the cold-stage as INP (from here on: scavenged INP), although it had not initiated the formation of the collected dendrite. The median concentration of INPs active at −25 °C or warmer (INP_{-25}) was determined for bulk rime samples collected on impactor plates ($conc_{rime}$) and used to estimate

the mass of rime associated with a single dendrite (m):

$$m = \frac{\ln\left((1 - \mathrm{FF}_{\mathrm{crystal}})^{-1}\right)}{\mathrm{conc}_{\mathrm{rime}}} \left[g\,\mathrm{rime\ crystal}^{-1} = \frac{\mathrm{INP}_{-25}\ \mathrm{crystal}^{-1}}{\mathrm{INP}_{-25}\ g^{-1}\,\mathrm{bulk\ rime}}\right], \tag{3.1}$$

with $\mathrm{FF}_{\mathrm{crystal}}$ being the frozen fraction of INP_{-25} in the analysed dendrites (after subtracting the control).

This step was necessary to estimate the contribution of scavenged INP_{-17} representing false positives of primary ice crystals in our results. They were estimated from the average mass of rime associated with a single dendrite (Eq. 3.1) and the concentration of INP_{-17} within the independent rime samples, as described next.

Independent rime samples were collected with a plexiglass impactor plate (Lacher et al., 2017) suspended on the railing of the terrace at Jungfraujoch for a few to several hours ($\sim$ 1–13 h). In total, 30 samples of aggregated rime droplets were collected between 15 February and 11 March. The freezing experiments of the rime samples were done with a drop-freezing assay similar to the set up described above, which was used for the single crystal analysis. However, rime samples were melted and portioned with a sterile syringe into 2.5 µL droplets and analysed with a drop-freezing cold plate following the description in (Creamean et al., 2018b). Of each sample 300 droplets were cooled until all droplets were frozen. The cumulative number of INPs active at a certain temperature (with a temperature interval of 0.5 °C) was calculated by taking into account the observed numbers of frozen droplets at a temperature, the total number of droplets and the analysed volume of sample (Vali, 1971a). The main reason for the use of a second cold-stage was to ensure that the custom-built one was always ready for single crystal analysis in case dendrites were precipitating. Other than that, the drop-freezing cold plate has a larger surface on which more droplets can be analysed at a time, making it more suitable for rime analysis. However, it also requires an external refrigerated circulation bath, lined power and it is relatively large, making it impossible to put it into the anteroom and to analyse single crystals.

3.3 Results and discussion

Of the 229 crystals analysed in the field, 39 had to be excluded retrospectively because a closer inspection of the enlarged photographs showed that they were either not planar or not branched. Most of the excluded crystals were spatial or radiating assemblages of plane-type crystals (P6 or P7, according to Kikuchi et al., 2013) and may hence have been initiated at temperatures $< -20\,^{\circ}\mathrm{C}$ (Bailey and Hallett, 2009). The remaining 190 crystals were confirmed as planar and branched, i.e. having a habit that typically forms between -12 and $-17\,^{\circ}\mathrm{C}$. They had been collected from a pathlength of 2368 km through a large number of MPCs from different wind directions (sum of sampling duration multiplied by average wind speed; see Table 3.1). A large fraction of them were rimed (31 %) or densely rimed (51 %) dendrites (R1c or R2c, according to Kikuchi et al., 2013; see Fig. B.3 in the Supplement for examples), while the remainder belonged to other categories (in order of decreasing frequency: graupel-like snow of hexagonal shape, hexagonal graupel, composite plane-type crystals, dendrite-type crystals, sector-type crystals or R3a, R4a, P4, P3, P2, respectively, according to Kikuchi et al., 2013). The greatest length in the a axis (outer diameter) of the 190 crystals ranged from 1.3 to 7.6 mm, with a median of 2.8 mm, a mean of 3.1 mm and a standard deviation of 1.1 mm.

We found no INP active above $-12\,^{\circ}\mathrm{C}$ present in the crystals. In 24 of the 190 crystals an INP active between -12 and $-17\,^{\circ}\mathrm{C}$ was present (Fig. 3.2). In the other 166 crystals no INP was found between -12 and $-17\,^{\circ}\mathrm{C}$. They either refroze below $-17\,^{\circ}\mathrm{C}$ (95) or stayed supercooled until $-25\,^{\circ}\mathrm{C}$ (71). The lack of INP_{-17} indicates that the formation of these crystals was most likely not triggered by heterogeneous freezing, but through a secondary ice formation process. It is highly unlikely that these crystals had grown from homogenously frozen cloud droplets. Homogenous freezing at a temperature well below $-20\,^{\circ}\mathrm{C}$ results in a polycrystalline initial ice crystal from which a polycrystalline snow crystal develops (Furukawa, 1982), and not a single crystal like a dendrite. Blanks that froze above $-17\,^{\circ}\mathrm{C}$ were limited to one count, occurring between -16 and $-17\,^{\circ}\mathrm{C}$ (not accounted for in further analysis). Between -17 and $-25\,^{\circ}\mathrm{C}$, 40 control droplets froze; the rest (149) stayed

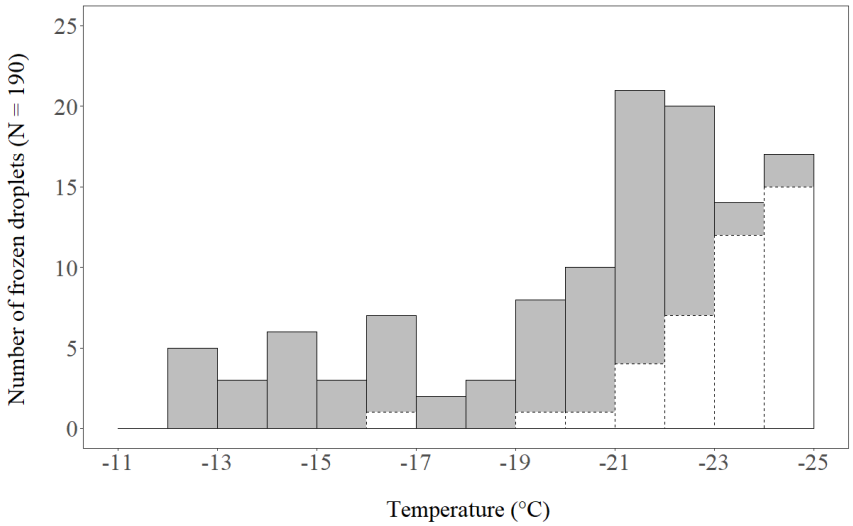

Figure 3.2: Number of planar, branched ice crystals that refroze on a cold-stage after having been molten (grey bars with solid contour), thereby confirming they contained an INP active within the respective 1 °C temperature step. Of 190 crystals analysed, 24 refroze at −17 °C or warmer (INP_{-17}). The white bars with dashed contour indicate the number of frozen control droplets. The total number of control droplets was 190 as well.

supercooled until −25 °C. A frozen fraction of 21 % of the control droplets at −25 °C is a rather low fraction compared to the results with pure water droplets (1 µL) on a Vaseline-coated substrate presented recently by Polen et al. (2018).

Throughout the observation period of 10 days the daily fraction of primarily nucleated ice was relatively stable (Fig. 3.3). From these results, we conclude that about one in eight of the analysed (24/190) planar, branched crystals resulted from primary ice formation. Seven out of eight were likely generated through a process of secondary ice formation given they did not refreeze above −17 °C. The uncertainty associated with the number of primary crystals in our observations is about 20 % ($\sqrt{24}/24$). Since we have randomly sampled crystals from many clouds over a prolonged period, we can extrapolate the found multiplication factor to dendrites in MPCs at Jungfraujoch during winter months in 2018 but we can not make detailed judgements about single clouds.

Our preliminary conclusion is based on the following four assumptions: the first assumption is that INPs embedded in natural ice crystals can be repeatedly activated at the same temperature. Second, that the analysed crystals did not grow from

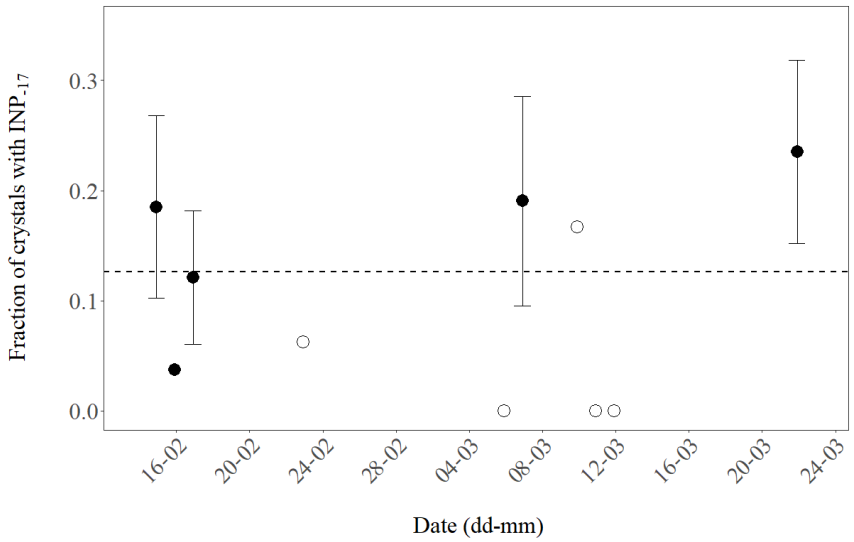

Figure 3.3: Daily fraction of ice crystals with INPs active at −17 °C or warmer (INP_{-17}) observed for 10 days during February and March 2018. The number of crystals analysed per day was between 21 and 34 (closed symbols) or less (3 to 16, open symbols). Error bars indicate an estimate of the standard deviation (proportional to $\sqrt{INP_{-17}}$) for days when at least four crystals with INP_{-17} were found. The dashed line shows the mean value of the pooled data (190 analysed crystals).

aerosolised parts of hoar frost growing on surrounding surfaces (Lloyd et al., 2015; Farrington et al., 2016; Beck et al., 2018). Third, that initial ice formation leading to the growth of the analysed crystals likely did not occur at a temperature colder than −17 °C. Fourth, that the detected INP_{-17} were not scavenged during riming of a secondarily formed crystal.

We are confident that the first condition (i.e. that INPs are stable over many refreezing cycles) for our preliminary conclusion is met. Although substantial fractions of bacterial INPs active above −7 °C are deactivated after a single freeze–thaw cycle, while those active below −7 °C are typically unaffected even after three freezing cycles (Polen et al., 2016). Further, experiments with INPs from soils show a remarkable stability of the ice nucleation temperature over tens of repeated melting and freezing cycles, with standard deviations of 0.2 °C (Vali, 2008). Furthermore, Wright et al. (2013) reported similar results for rainwater samples. Since we analysed the collected crystals within minutes of melting, we can also exclude changes due to storage (i.e. ageing), which has been observed with bulk snow samples over the course of days or weeks (Stopelli et al., 2014).

Surface frost can be a strong source of very small (i.e. $< 100\,\mu m$), secondary ice crystals at Jungfraujoch (Lloyd et al., 2015) and at other mountain stations (Beck et al., 2018). During 7 of 10 sampling events air masses approached from north-west. The terrain falls off steeply in this direction and reaches the average observed cloud base ($\sim 1000\,m$ below Jungfraujoch, Table 3.1) within a horizontal distance of about 2 km. At an average wind velocity of $8\,m\,s^{-1}$ from this direction the distance is covered within less than 5 min, which is too short for small, broken-off frost crystals to grow to the average size of the crystals we have analysed (average of 3.1 mm). Even in most favourable conditions a dendrite would not grow to 1 mm diameter within that time (Takahashi et al., 1991). Therefore, it seems unlikely that dendrites which were not associated with an INP_{-17} had grown from particles of hoar frost emitted by surfaces in the vicinity of Jungfraujoch.

The ice crystal habits encode information about the growth temperature of the crystals, not their formation temperature. The growth temperature from -20 to $-70\,°C$ is the so-called "polycrystalline regime" dominated by crystal shapes with a range of different angles between branches or plates extending in three dimensions (Bailey and Hallett, 2009). These crystals will continue to grow when falling into warmer layers of air, as long as these layers are supersaturated with respect to ice. Otherwise, the crystals will sublimate. The growth habit of the falling crystals may change depending on temperature and supersaturation, but it will remain polycrystalline and irregular (cf. Figs. 6 and 7 in Bailey and Hallett, 2009). Polycrystalline ice particles are highly unlikely to grow into the kind of crystals we have sampled, which had the same angle (60°) between all branches, and branches only extending in a single plane (i.e. dendrites; cf. Schwarzenboeck et al., 2009). The lowest temperature at which the formation of the collected crystals may have been initiated is very likely above $-20\,°C$ because crystals formed by homogeneous freezing or INPs activated at temperatures below $-20\,°C$ would have resulted in polycrystalline crystals (Bailey and Hallett, 2009), a different habit than that of the crystals we had collected. Furthermore, according to Fukuta and Takahashi (1999), a dendrite falls about 400 m while growing to a diameter of around 3 mm. Given a diabatic lapse rate of $7.5\,°C\,km^{-1}$ an initial ice crystal may have been generated in 3 °C colder

conditions than where its growth into a 3 mm dendrite was completed. However, as the deposition velocity of a tiny initial ice crystal is small, the initial ice formation will unlikely have occurred at much higher altitudes than where the main growth into dendrites occurred. Based on these findings, the information on growth temperature encoded in the habit of a crystal enables an assumption about the temperature range at which the crystal formed. For dendritic crystals, we can assume that the initial formation temperature is likely above −20 °C. Even if we consider all crystals which contained an INP active between −12 and −20 °C, a large fraction of them (81 %) remain to be considered the product of secondary ice formation.

The presence of INPs active at temperatures colder than −17 °C associated with the collected crystals might be explained by riming, i.e. the collection of cloud droplets containing such particles not activated as INP (i.e. scavenged INP) because ambient temperatures were not cold enough (Table 3.1). A majority of our crystals were rimed or densely rimed. The median concentration of INP_{-25} in the rime samples collected on an impactor plate at Jungfraujoch was about 1100 mL^{-1} during the period from 15 February to 12 March. Since 41 % (background subtracted) of our crystals contained an INP_{-25}, the average mass of rime associated with a single crystal (m) must have been about 4.9×10^{-4} g (see Eq. 3.1). This is about twice as much as the difference in mass ($\sim 2 \times 10^{-4}$ g) between rimed and unrimed dendrites of 3 mm diameter found at Mount Tokachi, Hokkaido (Nakaya and Terada, 1935). The median of INPs active at −17 °C or warmer in rime was 16 mL^{-1}. Therefore, less than 1 % of the crystals we have analysed might have scavenged an INP through riming that was active at −17 °C or warmer (16 [$INP_{-17}\,g^{-1}$ rime] $\times 4.9 \times 10^{-4}$ [g rime $crystal^{-1}$]).

3.4 Conclusion

The habit of a planar, branched ice crystal, growing exclusively between −12 and −17 °C, enables the verification of whether it derived from primary or secondary ice formation based on a number of reasonable assumptions. Although the required experimental procedure, including refreezing of dendrites using a drop-freezing assay, has a low throughput ($\sim$ 15 min for two ice crystals) it can provide an estimate for the ice multiplication factor around −15 °C, even when it is smaller than 10,

unlike previous in situ approaches. The low throughput only allows for averaging over prolonged sampling periods and not for investigating single clouds. The factor we observed was much smaller than the "several orders of magnitude" sometimes inferred from circumstantial evidence. Furthermore, we do not know whether the multiplication factor we found for dendrites is the same for other crystal habits found in the same MPCs. Because the estimated cloud base temperature was mostly below 0 °C during our observations, rime splintering and ice–ice collision break-up are more likely to have played a relevant role as secondary ice formation processes, compared to droplet shattering (Sullivan et al., 2018b). Whichever process was operating, it must have produced very small fragments, otherwise singular, regular, branched crystals (e.g. dendrites) would not have grown from them. To learn more about the occurrence of secondary ice formation in moderately supercooled clouds, we think it would be valuable to repeat these experiments in other meteorological conditions or in other locations, such as those where most crystals were previously found to contain an insoluble particle in their centre or where they are less rimed. Less riming is likely to generate a smaller number of fragments by ice–ice collision break-up of dendrites as parameterised by Phillips et al. (2017). Under such conditions we would expect to find a smaller ice multiplication factor. This study analyses the refreezing ability of single sampled crystals and has shown that growth temperature information contained in the habit of an ice crystal can be a starting point to quantify ice multiplication in clouds.

Data availability. The data are available from the authors upon request.

Author contributions. CM and FC conceived the field study. LZ designed, constructed and tested the custom-built cold stage. Field measurements and data analysis were done by CM, JMC and FC. CM, JMC, CA and FC interpreted the data. All authors contributed to writing the paper.

Competing interests. The authors declare that they have no conflict of interest.

Acknowledgements. The authors would like to thank Sylvia C. Sullivan and the two anonymous referees for their valuable suggestions and comments during the review process, which significantly improved this paper. We are grateful for the comments provided by Jann Schrod at Goethe University of Frankfurt on a draft of the paper. We also would like to thank the International Foundation high-altitude research stations, Jungfraujoch and Gornergrat (HFSJG), 3012 Bern, Switzerland, for providing the infrastructure and making it possible to work comfortably with mixed-phase clouds. Special thanks go to Joan and Martin Fischer, and Christine and Ruedi Käser, the custodians of the station, for their great support during the field campaign. Meteorological data at Jungfraujoch have been provided by MeteoSwiss, the Swiss Federal Office of Meteorology and Climatology. We are grateful to Maxime Hervo from MeteoSwiss for the provision of the ceilometer data collected at Kleine Scheidegg. We acknowledge Ulrike Lohmann's group, who allowed us to borrow their cloud droplet samplers and shared fruitful discussions. This study was financially supported by the Swiss National Science Foundation (SNF) through grant number 200021_169620. Participation of Jessie M. Creamean in the campaign on Jungfraujoch was made possible through the SNF Scientific Exchanges Programme, grant number IZSEZ0_179151.

Review statement. This paper was edited by Markus Petters and reviewed by Sylvia Sullivan and two anonymous referees.

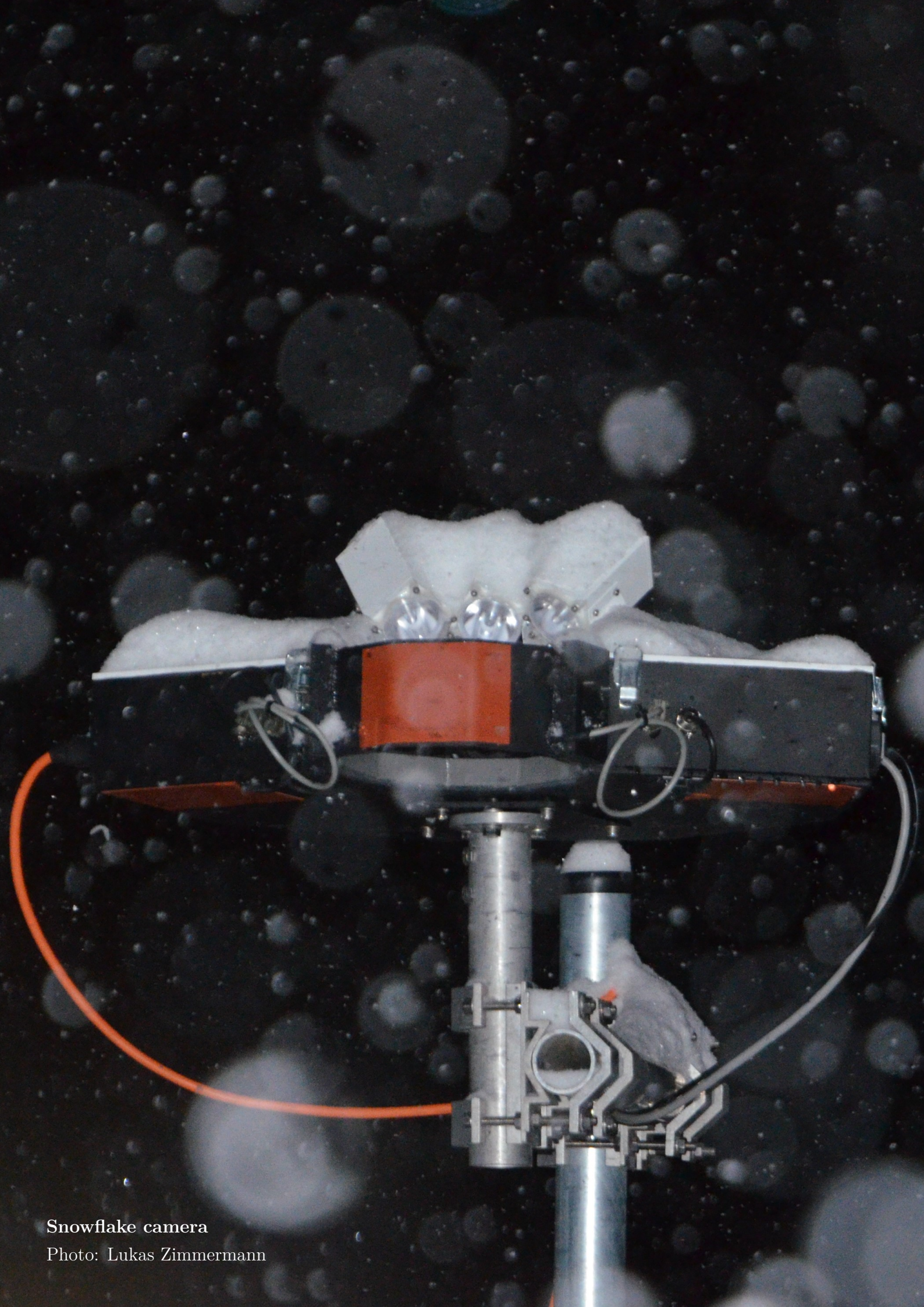

Snowflake camera
Photo: Lukas Zimmermann

Chapter 4

Snowfall in Northern Finland derives mostly from ice clouds

Claudia Mignani[1], Lukas Zimmermann[1], Rigel Kivi[2], Alexis Berne[3], Franz Conen[1]

[1]Department of Environmental Sciences, University of Basel, Bernoullistrasse 30, 4056 Basel, Switzerland

[2]Space and Earth Observation Centre, Finnish Meteorological Institute, 99600 Sodankylä, Finland

[3]Environmental Remote Sensing Laboratory, Swiss Federal Institute of Technology in Lausanne, 1015 Lausanne, Switzerland

This chapter has been submitted to Atmospheric Chemistry and Physics Discussions.

Abstract

Cloud properties play a critical role in the Arctic surface energy budget. We present ground-level observations of snowfall coinciding with radiosonde launches in Sodankylä (67.367 °N, 26.629 °E) through a period of eight cold months (October–April) in 2019 and 2020. They comprise 7401 depositing snow particles detected by a snowflake camera and 468 radiosonde profiles. Our results show that precipitating clouds were extending from ground to at least 2.7 km in altitude. Approximately one quarter of them were mixed-phase and the rest were likely fully glaciated. Estimations of the cloud top temperatures indicate that in roughly half of the snowfall events ice might have been initiated through heterogeneous freezing. For such cases, the predicted ice-nucleating particle concentrations active at cloud top temperatures could explain the analysed ice crystal particle concentrations observed near ground. In a warmer climate, the relative proportion of solid to liquid cloud particles will probably decrease, with implications on the Arctic radiation balance.

4.1 Introduction

Snowfall has a major impact on the hydrological cycle in the Arctic. It is a requirement for snow cover, which affects the freshwater supply (Barnett et al., 2005) and the albedo of the Earth's surface (Hall and Qu, 2006). Therefore, it is important to understand which atmospheric conditions are driving snowfall in that region. A prerequisite for snowfall is the atmospheric formation of ice crystals. Primary ice crystal formation can be initiated either by homogeneous or heterogeneous freezing, that is by cloud droplets freezing spontaneously below a temperature threshold of −38 °C (e.g. Murray et al., 2010) or by ice-nucleating particles (INPs) that promote freezing already at warmer temperatures (e.g. Kanji et al., 2017). Once primary ice crystals have formed, other atmospheric ice-related processes may occur, such as ice crystal growth by vapor deposition, riming, secondary ice formation and aggregation (Fukuta and Takahashi, 1999), followed by deposition and accumulation at the surface, if crystals do not vanish before through sublimation in drier air (Nelson and Baker, 1996). These processes depend on microphysical and dynamical conditions that can lead to fully glaciated clouds (Costa et al., 2017), i.e. ice clouds. Arctic

warming probably leads to a change from ice clouds to more liquid clouds, whose radiative properties (Shupe and Intrieri, 2004) further accelerate Arctic warming (Tan and Storelvmo, 2019). Clouds containing ice crystals and generating snowfall can be studied for example with space-borne remote sensing techniques (e.g. Liu, 2008; Mülmenstädt et al., 2015; Kikuchi et al., 2017; Casella et al., 2017), which may be combined with ground observations of precipitation (Hanna et al., 2008). Another approach is airborne or ground-based remote sensing (e.g. Delanoë et al., 2013; Kneifel and Moisseev, 2020), sometimes combined with radiosondes (e.g. Silber et al., 2021) and morphological investigation of ice crystals collected in-cloud (Morrison et al., 2011). Further, radiosondes have been combined with morphological investigations of ice particles collected at ground level in several studies (Power et al., 1964; Jiusto and Weickmann, 1973; Seo et al., 2015).

Pinpointing the origin of even very low-intensity snowfall requires sensitive snowfall detection at ground-level. The simultaneous capture of ice particle habits might enable to disentangle some of the microphysical and dynamical conditions, because ice particles encode atmospheric conditions and duration of growth they were exposed to. The shape, size, degree of riming, and eventually aggregation of ice particles encode the temperature and relative humidity with respect to ice and liquid water at which they grew (Nakaya, 1954). According to the current version of Nakaya's habit diagram (Nakaya, 1954; Magono and Lee, 1966; Bailey and Hallett, 2009), rather large and eventually rimed crystals (including needles, stellar plates, two or three dimensional dendritic crystals, and graupel) are the result of supersaturation with respect to (liquid) water. Below water saturation compact and unrimed ice particles are to be expected (such as plates, columns, radiating plates, or bullet rosettes), which grow very slowly (Kobayashi, 1961). Riming occurs if supercooled water droplets of certain sizes are present (Mossop, 1978) and aggregation of snow particles can be significant at $-17\,^{\circ}\mathrm{C}$ and warmer (Hobbs et al., 1974).

In the Arctic, observations of precipitating clouds were predominantly made at coastal or marine sites (e.g. Fridlind et al., 2012; Delanoë et al., 2013; Mioche et al., 2017; Gierens et al., 2020). Unlike coastal or marine sites, which are associated

with high moisture levels, continental regions, such as northern Eurasia, including Northern Finland, are drier and receive less snowfall. There, cloud conditions are likely different from those at coastal or marine sites. Here, we used the approach of combining observations of ice particles at the ground with concurrent radiosonde profiles to identify from what type of clouds, ice or mixed-phase, snowfall predominantly occurs in Northern Finland. Our focus is on identifying general patterns. Therefore, we analyse observations made throughout a total of eight months distributed over two cold seasons.

4.2 Methodology

The experimental setup was located at the Arctic Space Centre of the Finnish Meteorological Institute (FMI) in Sodankylä, in Northern Finland (67.367 °N, 26.629 °E; 179 m a.s.l.; Fig. 4.1).

4.2.1 Description of the site

The site is surrounded by a rural landscape consisting of coniferous forest and swamp (Hirsikko et al., 2014). It is situated just above the Arctic Circle. Due to the Gulf Stream, the climate and vegetation are subarctic, although the stratospheric meteorology is typically arctic (https://fmiarc.fmi.fi/, last access: 31 January 2022). The site is approximately 500 km from the Atlantic coast in the precipitation shadow of the mountain range along the north coast of Norway with a highest elevation around 1800 m.

In most Scandinavian countries the west coast regions receive more precipitation during the seven colder months (October–April), as compared to the mainland (Fig. 4.1). In large parts of Finland, including the location of our site, it does not exceed 300 mm. Within Europe, this is comparable to values in large parts of Northern Sweden, Western Russia, Eastern Europe and Eastern Spain.

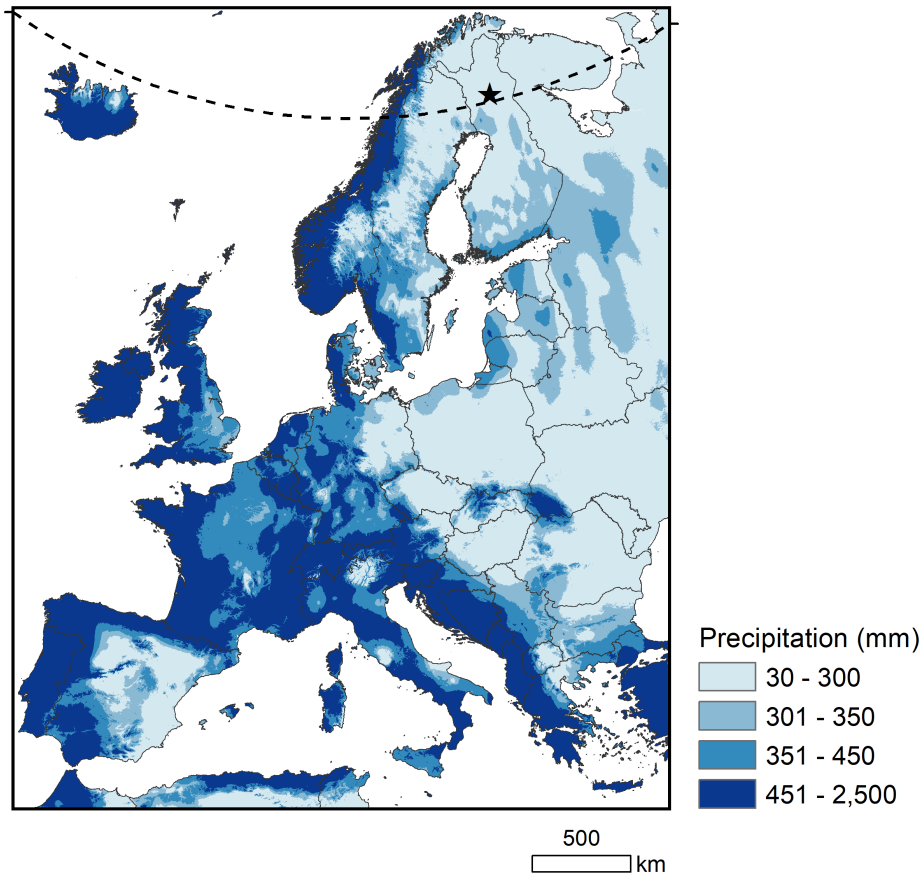

Figure 4.1: Overview of the geographical location of the experiment setup in Sodankylä, Finland (black star), located just above the Arctic Circle (dashed line). The average seven-month total precipitation (in mm) for the colder months per year (January-April and October-December) in the period 1970−2000 are shown in the map derived from the monthly climate data from WorldClim (Fick and Hijmans, 2017, see also https://www.worldclim.org/data/worldclim21.html, last access: 31 January 2022).

4.2.2 Snowfall measurements and ice particle image processing

A Multi-Angle Snowflake Camera (MASC, Particle Flux Analytics, USA; Garrett et al., 2012) took automatically photographs of precipitating ice particles from 28 February 2019 to 7 April 2020. During that time, the instrument was continuously in operation, excluding the summery months (May–September), when snowfall is very rare at the site (see monthly weather parameters in Fig. C.1) and during a short technical interruption between 11 and 25 October 2019. Of note, slight modifications to the original MASC instrument (e.g. new emitter box, exchanging external plugging

connectors and internal wiring, adding a box enclosing the isolating transformer and the computer) were performed before installation to make it run smoothly according to our needs. The instrument was installed at two meters above ground on the instrument field of the World Meteorological Organization (WMO) solid precipitation intercomparison experiment (SPICE; Nitu et al., 2018). Whenever an ice particle falls through the horizontal measurement cross-section of the instrument (roughly 10 cm^2), three flashlights and cameras (Unibrain Firewire-800 cameras, image resolution: 5 MP, chip size: 8.8 mm x 6.6 mm, focal length: 12.5 mm), which have a 36-deg angle to each other and an identical focal point, are triggered synchronously. Ice particles are captured against a black background. The images are 2448x2048 pixels, resulting in an optic resolution of ∼33 µm per pixel for particles in focus (Praz et al., 2017).

In the following, we only used images taken by the central camera. Generally, the ice particles that trigger the camera are captured in the middle of the resulting MASC images. MASC images on which the object or a part of it was outside the more or less central area of 1748x1430 pixels were rejected from further analysis. This selected area resulted from the original image by cropping 300 pixels from the top, 318 pixels from the bottom, and 350 pixels from both sides. Ice particles were automatically detected using a function provided by the Open Source Computer Vision library to identify the contours of bright (threshold at 20 out of 256 brightness values) continuous objects. We only considered objects with an area of least 500 continuous pixels, which is equivalent to a projected area of 0.54 mm^2, as ice particles suitable for further analysis. Smaller objects could generally not be classified according to criteria useful in the context of this study.

The area, position, maximal height, and maximal width of the projected objects larger than 0.54 mm^2 were retrieved from the image. A rectangle encompassing the ice particle was cut from the image and placed, while maintaining the optical size, in the center of a completely black background of a fixed size, i.e. the size of the largest object observed during the overall course of this study. This processing of images made later visual inspection of the large number of mostly small ice particles more convenient. To ensure fast processing of the data, the files of the MASC images and

the pre-defined selection images including extracted features were collected in an SQLite database.

Ice particle classification

Ice particle habits were visually classified. Such with an undefinable habit, such as broken off pieces, were classified as non-specific crystals. Single ice particles with unequivocal shape were divided into nine ice crystal classes (see Fig. 4.7a, i.e. needles, graupel, spatial dendrites, (planar) dendrites, stellar plates, plates, radiating plates, columns, rosettes). Aggregated ice particles were classified as aggregates composed of specific or non-specific single crystals. If aggregates were composed of a single crystal class, we classified them as such. Only aggregates composed of needles, spatial dendrites, dendrites, stellar plates, radiating plates, or rosettes were observed (see Fig. C.7). Each ice particle with an unequivocal shape was classified into rimed or unrimed. An ice particle classified as unrimed (rimed) corresponded to a riming degree of $0-1$ ($2-5$) according to Mosimann et al. (1994). Blurred or dark ice particle images were seen as invalid and classified as blurred or dark, respectively.

4.2.3 Vertical profiles and data processing

As part of the Global Climate Observing System Reference Upper-Air Network (GRUAN; WMO Integrated Global Observing System station identifier 0-20000-0-02836), vertical profiles of temperature, relative humidity with respect to liquid water, pressure, wind speed and direction were measured at the site with Vaisala RS41 radiosondes (Jensen et al., 2016). Radiosondes were launched daily at 11:30 and 23:30 UTC by an automated sonde system (Vaisala AS41 Autosonde system) (Madonna et al., 2020). The radiosondes were launched on balloons with an ascent velocity of approximately 6 m s^{-1} and data was recorded between ground level and an average of 28 km in altitude. According to the manufacturer, the humidity sensor of the radiosondes has a measurement uncertainty of 4% and a response time of < 0.3 s for $+20\,°C$ (< 10 s for $-40\,°C$), 6 m s^{-1}, and 1000 hPa. For temperature and pressure, the sensor measurement uncertainty above 100 hPa are $0.15\,°C$ (with a response time < 0.5 s) and 0.4 hPa (https://www.vaisala.com/sites/default/files/documents/RS41-SGP-Datasheet-B211444EN.pdf, last access: 31 January 2022).

We used the GRUAN data product, which provides validated data and meta-data. The vertical profiles of relative humidity with respect to ice (RH_{ice}) were calculated using the saturation vapor pressure ITS90 formulation by B. Hardy (https://www.decatur.de/javascript/dew/resources/its90formulas.pdf, last access: 31 January 2022) and averaged with a vertical resolution of 100 m.

4.2.4 Ground-based weather parameters

A ground-based weather station provided weather parameters in 10-min time intervals, including temperature, relative humidity with respect to water, wind measurements (at 22 m above ground), air pressure, snow depth, cloudiness, visibility, cloud base height, present weather, and precipitation determined by different instruments operated by the FMI (https://litdb.fmi.fi/luo0015_data.php, last access: 31 January 2022). The values for wind speed and direction were average values over 10-minute intervals. The values for the other parameters were instantaneous values. In the WMO SPICE field, precipitation was measured optically with a Parsivel^2 (OTT HydroMet, UK), which has a measurement accuracy of ± 20% for solid precipitation between 0.001 mm h^{-1} and 1200 mm h^{-1} (https://www.ott.com/products/meteorological-sensors-26/ott-parsivel2-laser-weather-sensor-2392/, last access: 31 January 2022), and by weight with a Pluvio^2 (OTT HydroMet, UK), a weighing gauge that has an absolute accuracy of ± 0.05 mm when averaged over 60 min (https://www.ott.com/products/accessories-109/ott-pluvio2-weighing-rain-gauge-963/, last access: 31 January 2022). As a note, both precipitation instruments obtained a reasonable agreement after reprocessing Parsivel^2 raw data (Boudala et al., 2014).

During the period of measurements (i.e. from 28 February 2019 to 7 April 2020, excluding May to September), local air temperature at the site was on average −5.8 °C, with minimum and maximum values of −34.4 °C and +16.2 °C, respectively. Average relatively humid was 87% and the average wind speed at 22 m above ground (i.e. above tree top) was 2.7 ms^{-1}, with a mean direction from Southwest–WestSouthwest (235 °). Moreover, the ground was covered with snow with a mean snow depth of 70 cm and the total precipitation during the eight months was 295 or 376 mm, depending on the measurement method (optical or by weight, respectively). This amount is

not unusual when compared to the local climatology of the period 1970−2020, as shown in Fig 4.1. The average locally-measured height of the lowest cloud base (i.e. vertical visibility) was roughly 1.2 km, and the total cloudiness was determined to be on average 5 oktas. Details of the local monthly weather parameters from February 2019 to April 2020 can be found in Fig. C.1.

4.3 Results and discussion

4.3.1 Snowfall events and coinciding vertical atmospheric profiles

We analysed a total of 468 radiosonde profiles that coincided with the MASC instrument being operational (i.e. eight months of two winter seasons). Radiosondes were launched at 11:30 and 23:30 UTC. Ice particles captured by the camera and recorded within the 15 minutes prior to each radiosonde launch were considered as coincident, although the path of the radiosondes is not exactly the same as that of the recorded ice particles. The time span of 15 minutes was chosen for practical reasons so that even during low precipitation intensity several ice particles were recorded. Three coinciding observations were not included in our analysis, as it was either raining (10 Feb 2020 at 11:30 and 23:30 UTC) or snow was likely blowing off the ground during unusually strong winds (30 Mar 2019 at 11:30 UTC). A minimum of 10 images with ice particles of ≥ 0.54 mm^2 in size within these 15-minute intervals before each radiosonde launch is the criterion for what we consider a snowfall event. Instances with less than 10 such images are considered "no-snowfall".

A snowfall event therefore corresponds to a minimum precipitation intensity of about 0.01 mm h^{-1} (assuming spherical ice particles with 0.4 mm radius). The maximum and median number of images with objects larger than 0.54 mm^2 per snowfall event were 630 and 68, respectively (Fig. C.3). Consequently, the median concentration of such objects in the precipitating air column would have been around 76 m^{-3}, assuming an average fall speed of 1 m s^{-1} (i.e. Locatelli and Hobbs, 1974). A total of 7401 objects were detected on MASC images coinciding with the radiosonde profiles. More than half of these objects (57%) were blurred, dark, or not entirely

visible on the pre-defined image selection. The remaining (3156) were analysed for their size and visually for ice particle class, eventual riming, and aggregation. These analysed objects had mean and median projected areas of 1.8 mm^2 and 1.1 mm^2, respectively (Fig. 4.2).

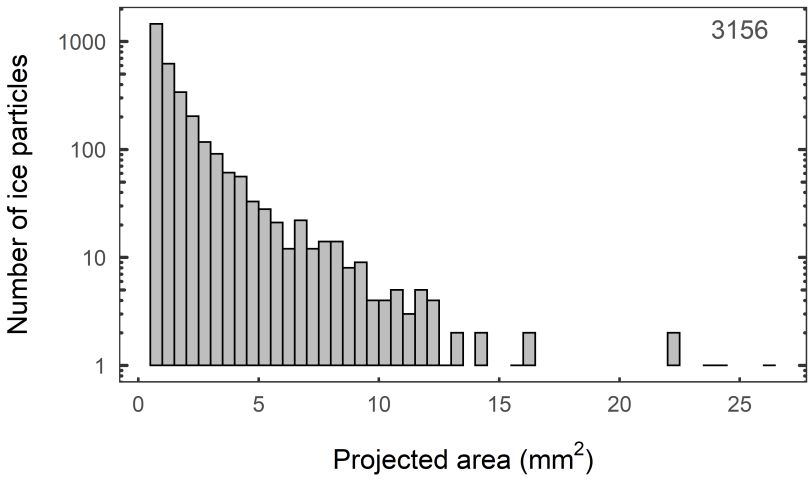

Figure 4.2: The number of analysed ice particles (n = 3156) by intervals of projected area (mm^2) roughly followed a power function. Analysed ice particles captured by the camera during the 15-min intervals prior to the radiosonde launches throughout the whole time span of interest (28 February 2019 to 7 April 2020) were considered.

Out of 468 radiosonde profiles coinciding with the MASC instrument being operational, 62 were classified as snowfall events and the rest were considered no-snowfall (Fig. C.3). For each 15-min event, meteorological parameters on ground were calculated from two weighed 10-min resolved data points and summarised (Fig. 4.3). During snowfall, the median and maximum wind speeds at 22 m above ground were 2.3 m s^{-1} and 4.2 m s^{-1}, respectively, and the median air temperature was −2.3 °C. This is consistent with the results of Kochendorfer et al. (2017) for precipitation periods in the winter seasons of the time period 2013−2015. Moreover, during snowfall events, the median wind at 22 m above ground was from the East (96 °) although at greater altitude (2.7 km) it was mostly from West to Southwest (Fig. C.2) and the median precipitation rate was relatively low with 0.15 mm h^{-1}, as determined optically with the Parsivel^2. Somewhat higher values were measured with the Pluvio^2 (0.24 mm h^{-1}). During snowfall, the visibility was on average 2020 m, the average base height of the lowest cloud was 213 m, the sky was fully cloud covered (cloud cover

= 8) and it was slightly snowing (code of "present weather" = 71). This suggests that snowfall was produced by stratiform clouds almost touching ground level. For events without snowfall, the median precipitation rate was zero, regardless of the measurement technique. The comparison of various other meteorological parameters between events with and without snowfall showed that some parameters differed in terms of range and median (i.e. relative humidity, pressure, wind direction, visibility, first cloud base height, cloudiness, and present weather). Other parameters were relatively similar during snowfall as during no-snowfall events (i.e. air temperature, snow depths, and wind speed).

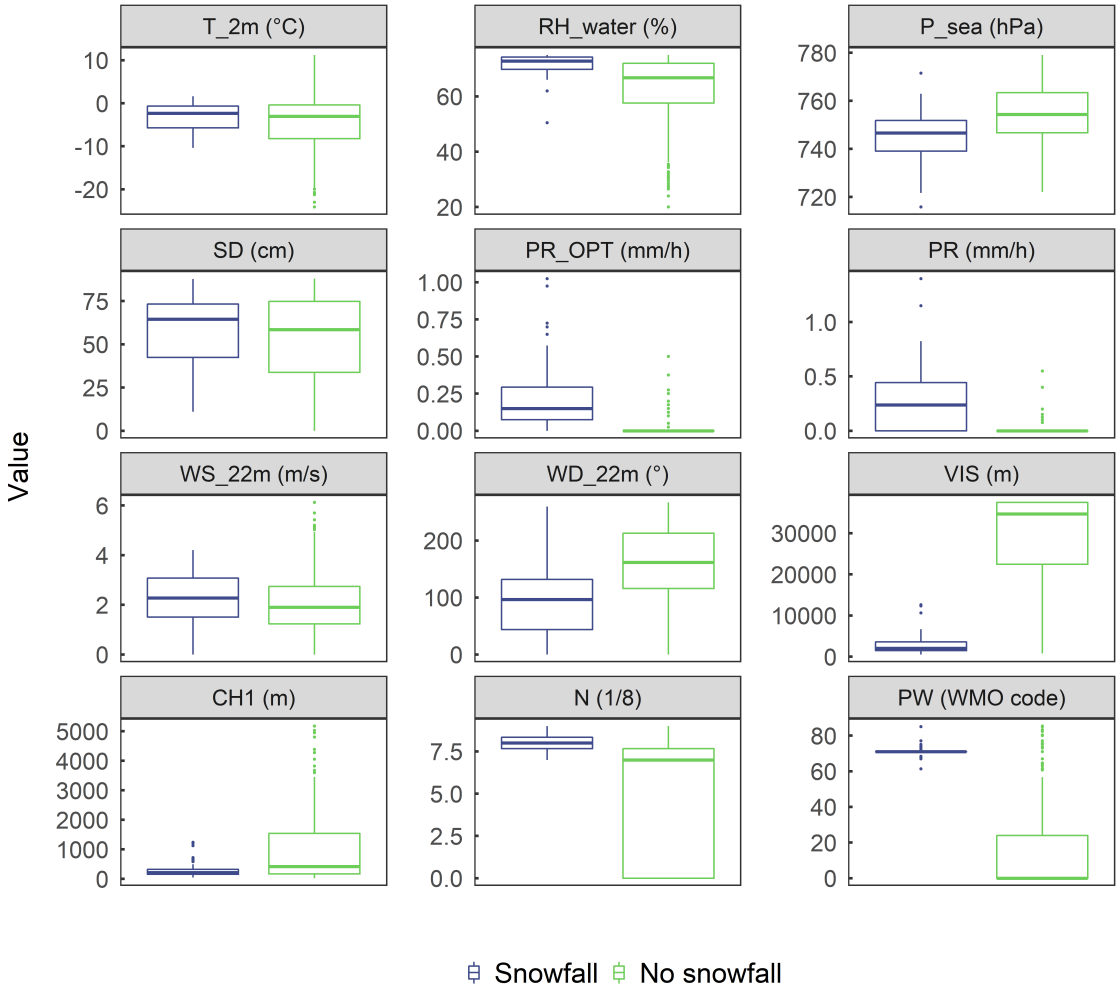

Figure 4.3: Boxplots (i.e. median (thick line), interquartile range (box), minima and maxima (whiskers), outliers (dots)) of weather parameters measured at the site coinciding with radiosonde profiles during events considered as snowfall (n = 62, blue) and as no-snowfall (n = 406, green). The following parameters are shown from the upper left to the bottom right: ambient air temperature at 2 m above ground (T_2m in °C), the relative humidity with respect to water (RH_water in %), the pressure at sea level (P_sea in hPa), the snow depth (SD in cm), the precipitation rate measured optically (PR_OPT in mm h^{-1}) and by weight (PR mm h^{-1}), the wind speed at 22 m above ground (WS_22m in m s^{-1}), the wind direction at 22 m above ground (WD_22m in °), the visibility (VIS in m), the height of the lowest cloud base (CH1 in m), the total cloudiness (N, a number between 1 (cloud free) and 8 (cloud covered)), and the present weather (PW using the WMO Code 4680).

The relative humidity with respect to ice (RH_{ice}) of the profiles during snowfall showed a consistent pattern (Fig. 4.4a). RH_{ice} was close to saturation at ground, increased slightly within the first few hundred metres, and remained above and close to 100% RH_{ice} in the lower troposphere up to roughly 3 km. Above this altitude, RH_{ice} values were more scattered among the profiles, with some profiles showing supersaturation with respect to ice up to 10 km. Consistently during snowfall, the relative humidity profiles with respect to water (RH_{water}) showed values close to 100% from ground to a few hundreds of meters, followed by a slight decrease with increasing altitude up to 3 km, and a stronger variation above this altitude (Fig. C.4a). RH_{ice} and RH_{water} of the profiles not associated with solid precipitation showed no such consistent pattern (Fig. 4.4b and Fig. C.4b).

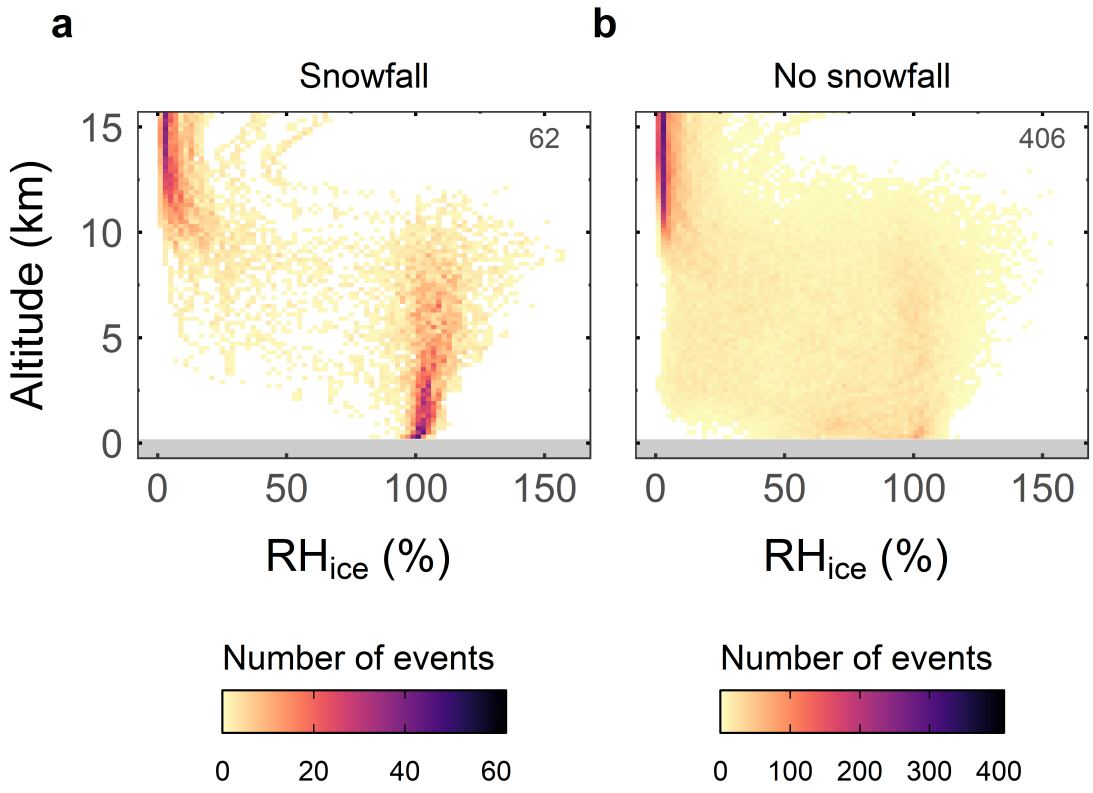

Figure 4.4: Relative humidity with respect to ice (RH_{ice}) within intervals of 200 m height and 2% RH_{ice} retrieved from the radiosonde profiles during (**a**) snowfall and (**b**) no-snowfall events. The total number of events for each group is provided in the upper right corner of each panel.

4.3.2 Necessary or sufficient RH_{ice} conditions for snowfall

To test whether RH_{ice} close to saturation throughout the lower $\sim$ 3 km of the atmosphere is a necessary or sufficient condition for snowfall at the site, we evaluated a range of RH_{ice} values and altitude ranges using different metrics, including accuracy (ACC), critical success index (CSI), and Heidke skill score (HSS), as shown in Fig. 4.5. An overview of the indices can be found in the Appendix (Table C.1). All three indices have an optimal value of 1, favour hits, and penalise both misses and false alarms. Based on the results of three indices, the best scores were obtained for the following combination of values (from hereon: criterion): running mean RH_{ice} $\geq$ 97% throughout the lower 2.7 km of the atmosphere. Choosing different values for running mean RH_{ice} and altitude reduced the overall accuracy of the prediction of snowfall events, although a running mean $RH_{ice} \geq 96\%$ throughout the lower 2.7 km of the atmosphere also yielded a very good score.

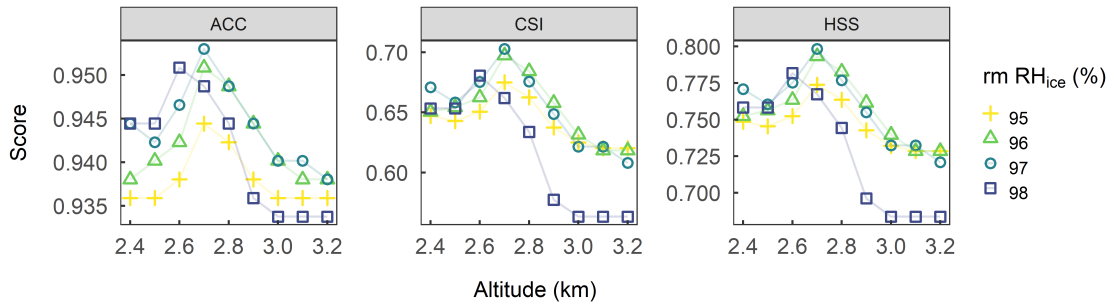

Figure 4.5: Scores to assess the prediction of snowfall using the running mean RH_{ice} values and altitude ranges were best for running mean $RH_{ice} \geq 97\%$ throughout the lower 2.7 km above ground. A set of different lower threshold values was investigated ranging for a running mean RH_{ice} from $\geq 95\%$ to $\geq 98\%$ throughout altitude ranges from ground level to between 2.4 km and 3.2 km above ground. Running means in RH_{ice} were calculated of five consecutive 100 m layers and the running mean was allocated to the lowest of the five layers. The following scores are shown: accuracy (ACC), critical success index (CSI), and Heidke skill score (HSS). See Table C.1 for more information on the metrics.

Of the total of 468 radiosonde profiles, 64 met the criterion of a running mean RH_{ice} $\geq$ 97% throughout the lower 2.7 km (Fig. 4.6). In 81% of them (52 of 64) snowfall was observed (*hits*). In 10 cases the criterion was not met but snowfall was observed (*misses*). In 12 cases the criterion was met but no snowfall was observed (*false alarms*) and in 394 cases the criterion was not met and no snowfall was observed (*correct negatives*). In other words, these specific thresholds of RH_{ice} and altitude correctly

predicted 84% (52 of 62) and 97% (394 of 406) of the cases with and without snowfall, respectively. Although the criterion of a running mean $RH_{ice} \geq 97\%$ throughout the lower 2.7 km was neither absolutely necessary nor sufficient for snowfall to occur, it still separates the majority of snowfall events from no-snowfall events and vice versa.

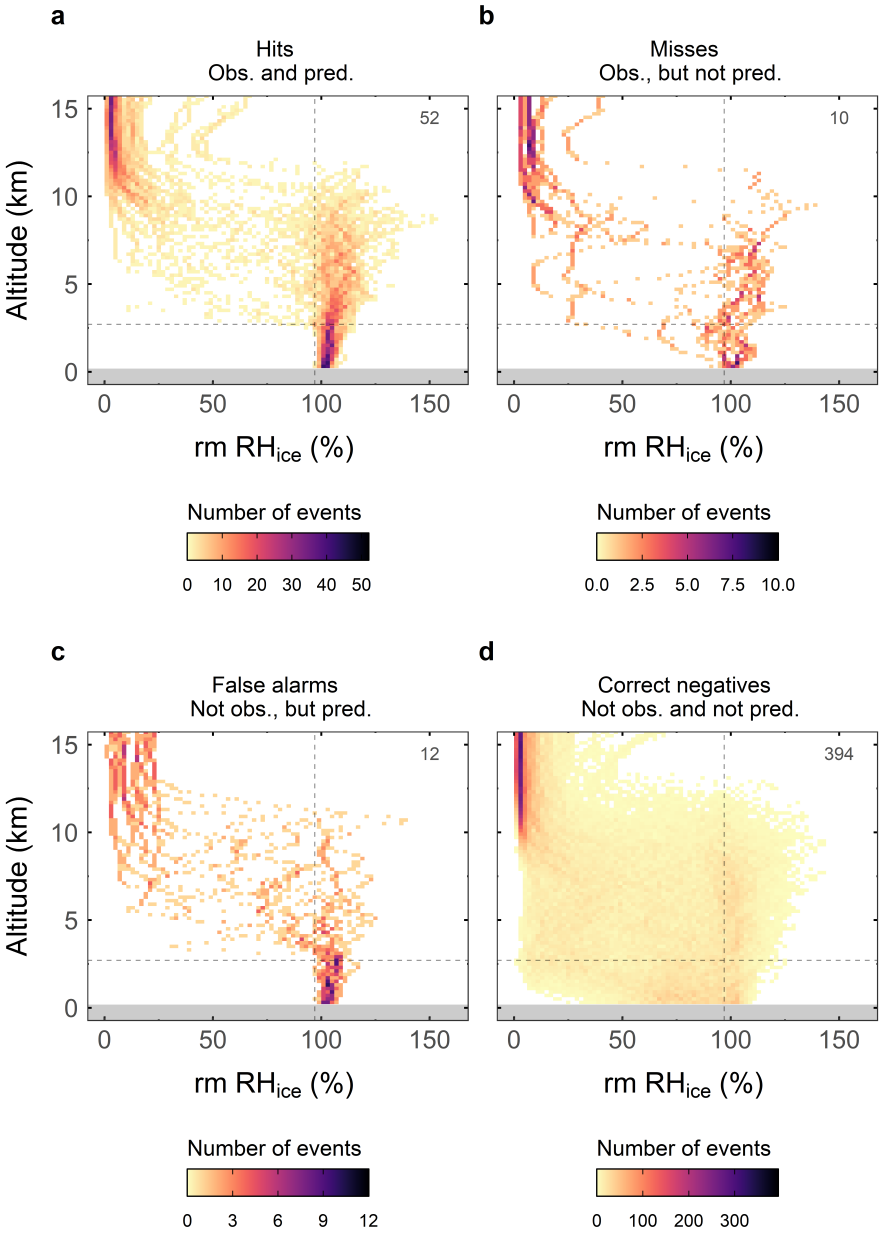

Figure 4.6: Observed values of running mean RH_{ice} binned in 200 m intervals and 2% steps of RH_{ice} for (**a**) *hits*, (**b**) *misses*, (**c**) *false alarms*, and (**d**) *correct negatives*. Snowfall was predicted for cases when running mean RH_{ice} measured along the radiosonde profile was $\geq 97\%$ (vertical dashed line) throughout the lower 2.7 km (horizontal dashed line) of the atmosphere. The total number of events per group is shown in the upper right corner of each panel.

4.3.3 Snowfall rate and type

In this section we will focus on the 52 snowfall events coinciding with a running mean $RH_{ice} \geq 97\%$ throughout the lower 2.7 km (i.e. *hits*, Fig. 4.6a), which seem to represent the predominant condition in which snowfall occurs in Northern Finland. These events were associated with optically measured median and maximum snowfall rates of 0.18 mm h^{-1} and 1.03 mm h^{-1}, respectively, as derived from the Parsivel^2 precipitation measurements. Only four of them were associated with snowfall rates <0.05 mm h^{-1} (Fig. C.6a). In general, the snowfall rates for the 52 snowfall events we now consider were significantly higher than for the other cases (i.e. *misses*, *false alarms* and *correct negatives* (see Fig. 4.6b-d), as shown in Fig. C.6.

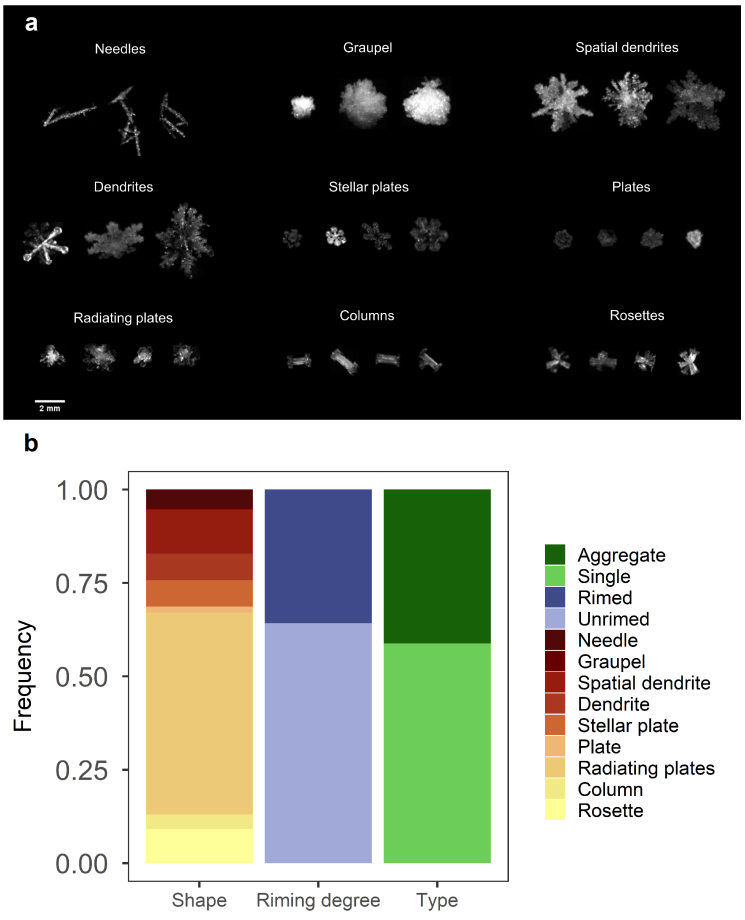

Figure 4.7: (**a**) Some examples of single, specifiable ice particles captured by the MASC and their shape. Of note, needles were only captured as aggregates. (**b**) Analysis of (827) unequivocal ice particles that were captured during the 52 snowfall events coinciding with a running mean $RH_{ice} \geq 97\%$ throughout the lower 2.7 km. Frequency with respect to shape (i.e. as shown in a), riming degree (i.e. unrimed or rimed) and type (i.e. single or aggregate) are shown.

Excluding the invalid objects (i.e. blurred or dark), a total of 2853 analysed ice particles were captured during these 52 snowfall events. They had a median projected area of around 1.1 mm^2 (not shown) and a very similar size distribution to that of all events, which are shown in Fig. 4.2. Many of these objects on the visually inspected images had undefinable habits. Only 29% of them (827 of 2835) could unequivocally be classified by their habit. Nine different unequivocal crystal habits were observed (Fig. 4.7a). The majority of them were single ice crystals and unrimed (Fig. 4.7b). Most ice crystals had habits that form below liquid water saturation (i.e. single plates, columns, radiating plates, rosettes, or their aggregates). Notably, the shapes that grow below the liquid water saturation were often unrimed (not shown). The most common habit of the classifiable ice particles was radiating plates, with a share of 54% (447 of 827).

4.3.4 Properties of ice crystals and air masses related to maximum RH_{water} along the profile

We grouped the 52 snowfall events under consideration according to their maximum running mean RH_{water} along the radiosonde profiles into three similarly large sub-groups: $< 98\%$ (n = 18), $\geq 98\%$ and $< 99\%$ (n = 20), and $\geq 99\%$ (n = 14), as shown in Fig. 4.8a-c. For each sub-group, we determined the corresponding ice particle size distribution and ice particle classes (Fig. 4.8d-i). Overall, 14 of 52 events (27%) reached a maximum running mean RH_{water} along the profile between 99% and 100% (Fig. 4.8c). These events coincided with ice particles that were (1) larger (Fig. 4.8f), (2) more often rimed and aggregated, and (3) more often associated with habits that grow above the water saturation line (i.e. needles, graupel, spatial dendrites, dendrites, and stellar plates; Fig. 4.8i) as compared to those events (38 of 52) that did not reach a maximum running mean RH_{water} of 99% (Fig. 4.8a,b,d,e,g,h). Hence, only around one quarter of all precipitating clouds seem to have been mixed-phase and the rest were probably fully glaciated. The lowest proportion of riming and aggregation was found for events for which the maximum running mean RH_{water} did not exceed 98% (Fig. 4.8a,d,g). These results suggest that the humidity measurements by the radiosondes during our measurement campaign and in the lower 3 km of the atmosphere were more accurate near saturation with respect to water than

the 4% promised by the manufacturer, at least when averaged over 500 m.

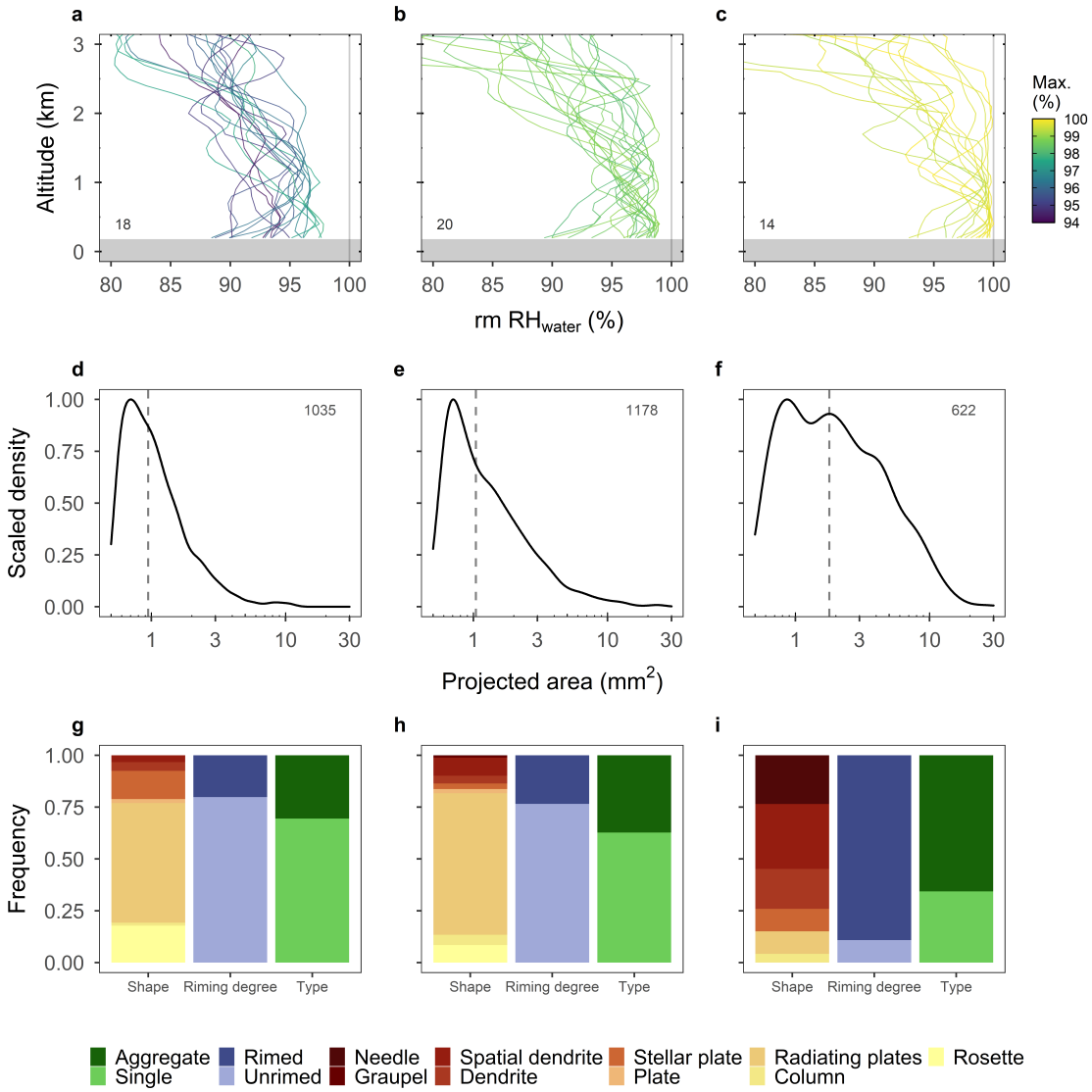

Figure 4.8: (**a, b, c**) Running mean RH_{water} profiles coinciding with snowfall and running mean $RH_{ice} \geq 97\%$ throughout the lower 2.7 km (52 events) grouped by the maximum running mean RH_{water}. The maximum running mean RH_{water} along the altitude profile is shown in colour. (**a**) Profiles with a maximum running mean $RH_{water} < 98\%$. (**b**) Profiles with a maximum running mean $RH_{water} \geq 98\%$ and $< 99\%$. (**c**) Profiles with a maximum running mean $RH_{water} \geq 99\%$. For each panel, the number of profiles is indicated in the left bottom corner. (**d, e, f**) The scaled density of ice particles by projected area (mm^2). All the analysed ice particles of the profiles in the above lying panel were considered. The dashed vertical line indicates the median area. The number of analysed ice particles is indicated by the number provided in the upper right corner. During the 52 snowfall events, a total of 2835 ice particles were analysed. (**g, h, i**) Same as Fig. 4.7b, but considering only the specifiable ice particles coinciding with the events of the above lying panels.

Most air masses associated with the 52 snowfall events tended to come from a southerly to westerly direction and crossed marine areas shortly before arriving at the site (Fig. 4.9 and Fig. C.2b), which suggests that the Baltic Sea, the Norwegian Sea and the North Sea were the major sources of moisture for snowfall in the observed cases. The few air masses that did not pass over marine areas recently, but crossed Russia and Eastern Europe, were associated with maximum running mean RH_{water} below 99%.

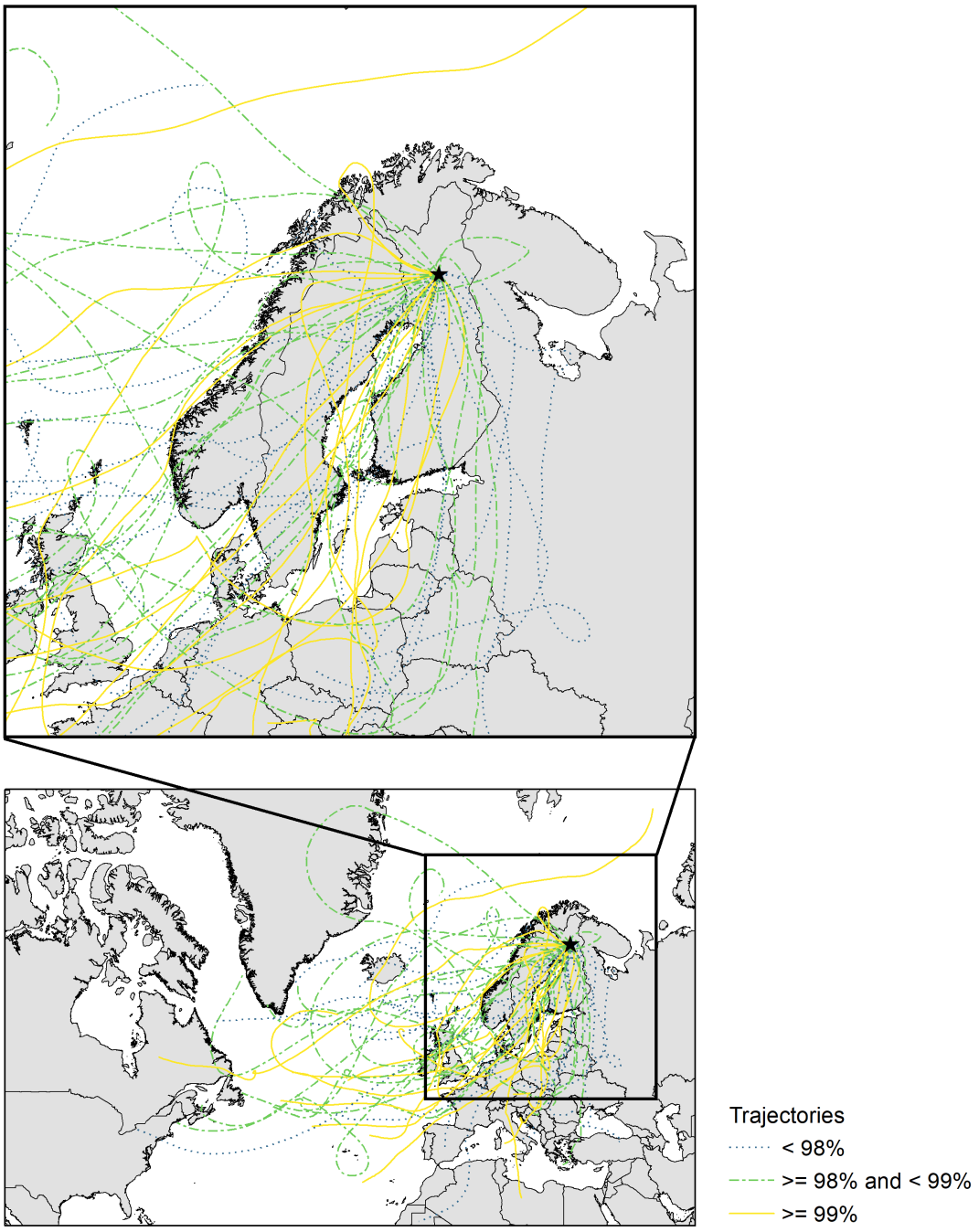

Figure 4.9: Five-day backward trajectories (lines) arriving at the measurement site in Sodankylä, Finland (black star) at 2.7 km above ground at full hour (i.e. 11 or 23 UTC) for each of the 52 snowfall events. The group of maximum running mean RH_{water} (as in Fig. 4.8) is shown in colour ($< 98\%$, dotted blue; $\geq 98\%$ and $< 99\%$, dashed green; $< 99\%$ continuous yellow). An inset map is shown in the upper panel. The trajectories were calculated using the NOAA's Hybrid Single-Particle Lagrangian Integrated Trajectory (HYSPLIT) model. One trajectory per event was computed using the GDAS one-degree meteorology dataset and the "model vertical velocity" vertical motion method.

4.3.5 Likely underlying ice formation processes

To determine whether heterogeneous or homogeneous freezing might have triggered the initial ice formation during the considered 52 snowfall events (coinciding with running mean $RH_{ice} \geq 97\%$ throughout the lower 2.7 km), we extracted from the radiosonde profiles the likely cloud top temperature, which is the temperature at which initial ice might have formed. Since a higher level cloud could seed a lower level cloud (e.g. Vassel et al., 2019; Ramelli et al., 2021; Proske et al., 2021), we determined the cloud top of the highest possible seeding cloud by assuming differently-sized gaps that ice crystals could potentially pass without complete sublimation. Depending on the assumed width of the gap between potential seeder and feeder clouds (i.e. ≤ 0.2 km, ≤ 0.5 km, or ≤ 1 km), between 30% and 75% of the cloud tops were colder than $-38\,°C$ (Fig. 4.10a). Here, freezing would have been initiated via homogeneous freezing (Murray et al., 2010). However, between 25% and 60% of the cloud tops may have had temperatures warmer than $-38\,°C$. In these cases, ice formation would have been initiated via heterogeneous freezing. Since RH_{ice} and RH_{water} along the profiles were often $< 130\%$ and $< 100\%$, respectively (i.e. Figs. 4.4a and 4.8a-c), it could be that initial ice formed via pore condensation and freezing onto mineral dust, biogenic particles or other ice-nucleating particles (INPs) (Kanji and Abbatt, 2006; David et al., 2019).

We may estimate whether enough INPs were present to explain the number of ice particles observed by using the empirical parameterisation by Schneider et al. (2021):

$$INP\,(T) = 0.1 \cdot exp\,(a1 \cdot T_{amb} + a2) \cdot exp\,(b1 \cdot T + b2)\; stdL^{-1} \tag{4.1}$$

where $INP(T)$ is the number concentration of INPs (in $stdL^{-1}$) active at temperature T (in K), T_{amb} is the ambient air temperature at ground level (in K), and $a1$, $a2$, $b1$, and $b2$ are empirically fitted parameters ($a1 = 0.074$ K^{-1}, $a2 = -18$, $b1 = -0.504$ K^{-1}, $b2 = 127$). For each event we used daily averaged local temperatures for T_{amb} to calculate the INP number concentration active at cloud top temperatures. Median INP concentrations were 19 m^{-3}, 79 m^{-3}, and 5054 m^{-3}, respectively, depending on the assumed gap-width between potential seeder and feeder clouds (Fig. 4.10b). Such INP

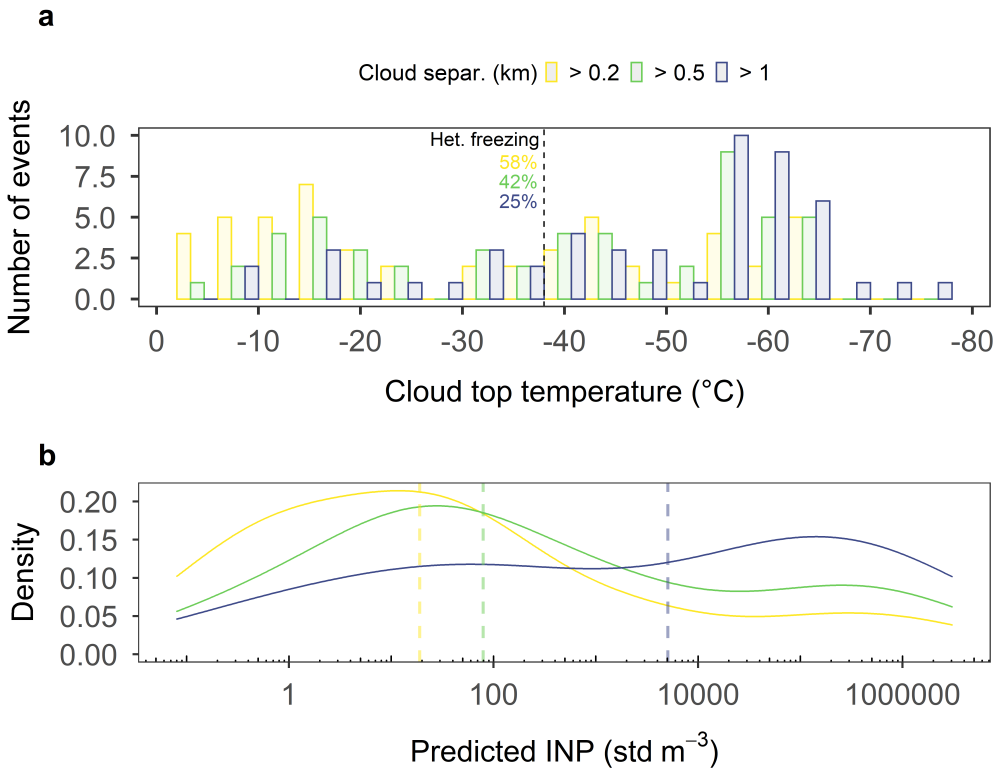

Figure 4.10: (**a**) Likely cloud top temperatures in 4 °C intervals of the 52 events coinciding with running mean $RH_{ice} \geq 97\%$ throughout the lower 2.7 km. The cloud top height was derived from the running mean RH_{ice}. The altitude at which the running mean RH_{ice} fell below 100% for > 0.2 km (yellow), > 0.5 km (green), and > 1 km (blue) with increasing height was defined as cloud top height. The fraction of events with cloud top temperatures above −38 °C is given in percent next to the dashed line. This is an estimation of the fraction of events for which the first ice crystals were likely formed via heterogeneous freezing. (**b**) Density of the INP concentration for the fraction of events with cloud top temperatures above −38 °C, using the different cloud top height criteria (in color) as shown in panel a. The respective median concentrations are shown by the dashed lines.

concentrations are within the range of observed long-term median INP concentrations active between −20 °C (60 m^{-3}) and −30 °C (690 m^{-3}) in condensation mode (i.e. $RH_{water} = 101\%$) at an Arctic site in Svalbard (474 m a.s.l.; Schrod et al., 2020). For an assumed gap-width between potential seeder and feeder clouds of 0.5 km and 1 km the number of estimated INPs would have been sufficient to generate the observed ice particles. For a narrower gap-width (0.2 km), a multiplication factor of 3 would need to be invoked to explain the observations. Therefore, secondary ice formation processes were probably not of much relevance, although we saw some broken-off branches of dendrites, suggesting at least occasional ice–ice collision followed by breakup (i.e. Vardiman, 1978). This secondary ice mechanism was shown to be linked to the collision force and the riming degree, with a number of observed fragments

per collision below 1 for unrimed dendrites and below 8 for lightly rimed dendrites (Vardiman, 1978; Phillips et al., 2017). Other secondary ice mechanism, such as rime-splintering (e.g. Hallett and Mossop, 1974) and droplet fragmentation (e.g. Takahashi and Yamashita, 1970), would require the presence of liquid droplets, which seem to have been rare during our observations.

4.4 Conclusion

Overall, about 70% of all classifiable ice crystals observed during the 52 snowfall events (i.e. events that had a minimum of 10 images with ice particles of ≥ 0.54 mm^2 in size within 15-minute intervals) that were correctly predicted using our basic RH_{ice} criteria (i.e. running mean $RH_{ice} \geq 97\%$ throughout the lower 2.7 km) in Northern Finland had habits that form below the water saturation. In a similar proportion of radiosonde profiles, the running mean RH_{water} did not reach values $\geq 99\%$. This suggests that snowfall in this region was derived from ice clouds in nearly three quarters of the cases. As ice particles grow very slowly in such conditions, the lower atmosphere can not be much below saturation with respect to ice for snowfall to occur. Otherwise, the small, often unrimed ice particles would not reach the surface before completely sublimating. These precipitating clouds are probably stratiform clouds that extend from close to the ground to at least 2.7 km altitude. At that altitude the air masses arrived mostly from West and Southwest. Probably, the Baltic Sea, the Norwegian Sea, and the North Sea were the major source of moisture generating snowfall in Northern Finland. Due to orographic lifting at the coastal mountain range, North Atlantic air masses might already have lost much of their initial moisture content when arriving in Northern Finland.

In a warmer climate, the partitioning of ice particles and liquid cloud droplets in Arctic clouds may shift in favour of liquid droplets. Therefore, a greater proportion of mixed-phase clouds than currently observed can be expected. Such microphysical changes depend on the availability of INPs, which are currently responsible for perhaps half of the initial ice formation and would affect cloud properties, such as radiation and precipitation. In the future, the effects of eventual changes in predominant cloud phase should be further investigated through measurements of

ice crystal habits, INPs, precipitation, and radiation properties to better understand potential feedback mechanisms between climate change and cloud properties.

Data availability. The RS41 GRUAN data products are available via https://www.gruan.org/instruments/radiosondes/sonde-models/vaisala-rs41 (last access: 31 January 2022). The ground-based weather parameters are accessible via https://litdb.fmi.fi/luo0015_data.php (last access: 31 January 2022). The MASC images and the code are available from the authors upon request.

Author contributions. CM and FC conceived the study. LZ modified, installed and maintained the MASC instrument with help from FC and know-how from AB. RK performed the radiosonde launches. LZ processed the MASC images and CM classified the ice particles. CM performed the analysis and prepared the figures. CM, LZ, RK, AB and FC interpreted the data. CM drafted the manuscript with contributions from all co-authors.

Competing interests. The authors declare that they have no conflict of interest.

Acknowledgements. The authors are grateful to the Finnish Meteorological Institute for providing the infrastructure as well as the ground-based weather parameters on site. We thank the team in Sodankylä for their support on site. Special thanks to Jaakko Siltakoski for providing images of the MASC instrument and helping during the installations in the SPICE field. We greatly appreciate the support of Antti Poikonen for establishing remote access to the MASC and Michael Sommer for his help in downloading the GRUAN data. We are grateful to Pedro Batista for his advice during coding in R and his help in creating the maps in GIS. We acknowledge the NOAA Air Resources Laboratory for providing access to the HYSPLIT model through the READY website (https://www.ready.noaa.gov/HYSPLIT.php, last access: 31 January 2022). We acknowledge financial support by the Swiss National Science Foundation as well as the Department of Environmental Sciences at University of Basel.

Financial support. This study has been supported by Swiss National Science Foundation (grant number 200021_169620) and the Department of Environmental Sciences, University of Basel.

Review statement. This study has not been peer-reviewed yet.

Snowflakes
Photo: Claudia Mignani

Chapter 5

Conclusions and suggestions for future research

In this thesis, I investigated primary and secondary ice in mixed-phase clouds, with a particular focus on moderate supercooling and explored whether mixed-phase clouds were the main source of solid precipitation using top-down approaches. The investigations were carried out during specific measurement campaigns conducted between 2018 and 2020 and mostly in the winter months. For each campaign, observations were collected over several weeks at an individual measurement site located in the Swiss Alps or the Arctic. Aerosol samples were collected and analysed at Weissflujoch (2671 m a.s.l., Switzerland) to study the abundance of atmospheric ice-nucleation particles (INPs). Backwards trajectories of sampled air parcels were simulated to determine the air mass origin and the precipitation history prior to sampling for each sample. Single falling dendritic ice crystals were collected, melted, and subsequently analysed to determine their INP content at Jungfraujoch (3580 m a.s.l., Switzerland) using the portable immersion freezing cold-stage to evidence and quantify primary versus secondary ice crystals. By thermocycling dendrites, this highly innovative approach connected ice nucleation to ice crystal growth. Moreover, ice particle images captured over several months in Sodankylä (179 m a.s.l., Finland), a continental Arctic site, were matched with radiosonde profiles to study the conditions under which solid precipitation occurs. The major conclusions in this thesis are the following (Fig. 5.1):

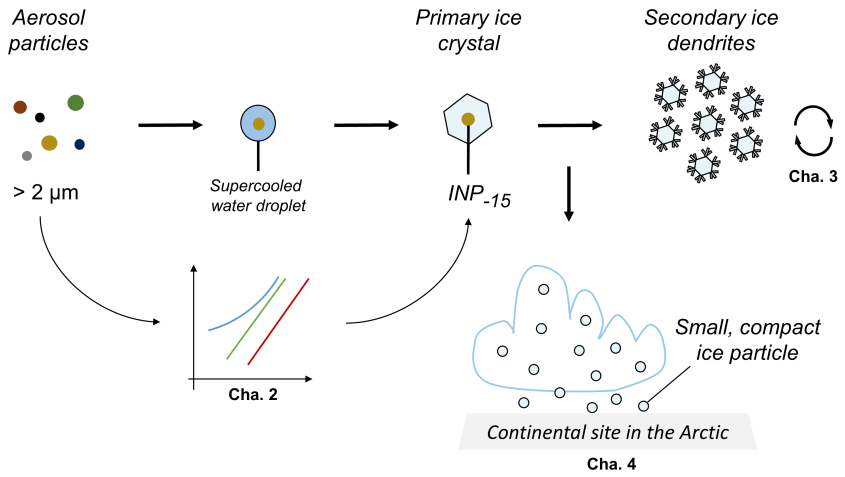

Figure 5.1: Schematic drawing of typical microphysical interactions under mixed-phase cloud conditions, similar to Fig. 1.1, but including an illustration of the main findings of this thesis. In Chapter 2, we found that atmospheric concentrations of INPs active at −15 °C (INP_{-15}), measured during February-March 2019 at Weissfluhjoch, can be parameterised using aerosol particle number concentrations of a certain size (> 2 µm). Differentiating between air mass origin and precipitation history improved the prediction. In Chapter 3, we found that one out of eight dendrites contain an INP active at moderate supercooling at Jungfraujoch in February-March 2018 and the rest (7 out of 8) were perhaps a result of secondary ice formation. In Chapter 4, we observed mainly small, often unrimed ice particles during eight months of snowfall during 2019−2020 at a continental site in the Arctic indicating that ice clouds were the main source of the solid precipitation at that site.

- It is more promising to parameterise the atmospheric concentrations of INPs active at −15 °C using aerosol particle number concentrations of a size > 2 µm as compared to smaller aerosol particles at Weissfluhjoch during February and March 2019 (Chap. 2). A novel insight of our work was that the predictions greatly improved when differentiating between air mass origins and precipitation histories. We found a higher INP to aerosol particle ratio in precipitating air masses, as compared to non-precipitating air masses. These findings suggest that rain on snow-free land surfaces may induce the emission of INPs that can be lifted to cloud heights.

- With an innovative approach, it is possible to gain a new type of evidence of secondary ice (Chap. 3). At Jungfraujoch in February and March 2018, one in eight dendritic ice crystals contained an INP. In other words, an ice multiplication factor

of eight was suggested based on the analysed dendrites. The secondary ice processes that might have been active were rime splintering and the collision of ice particles and subsequent break-up, which were assumed from the cloud base temperature, which was mostly below 0 °C (Sullivan et al., 2018b).

- Over a period of eight cold months snowfall emanating in three quarters of the cases from precipitating clouds that were fully glacitated at a site in Northern Finland (Chap. 4). We observed mainly small ice particles near the surface. About 70% of the ice particles with unequivocal shape have had habits that form below water saturation. The cloud often extended from the ground to at least 2.7 km and the estimated cloud top temperatures suggested that in about half of the cases initial ice crystals might have formed through heterogeneous freezing, for which sufficient INPs were probably available to generate the observed ice particle concentrations.

Compared to the results presented in Chapter 2, we recently found similar results for INPs active at $\geq -8\,^{\circ}\mathrm{C}$ derived from aerosol samples collected in Basel-Binningen, Switzerland, during two frontal passages (Einbock, 2021). Einbock (2021) found a higher INP to aerosol particle ratio (up to a factor of five) in air masses with recent rainfall than in air masses that had not precipitated recently. Moreover, surprisingly high temporal variability of INP concentrations was observed within short time spans (i.e. 20 min). To study ice formation at moderate supercooling, we should consider often rare but coarse INPs in cloud-relevant air volume and process-relevant time resolution. In other words, we should ideally pursue efforts to collect, measure and retrieve all sizes of aerosol particles at cloud heights on time scales that have a temporal resolution of a fraction of an hour. In addition, such results reveal that there is a need to study the sources, emissions and dispersion of INPs by rain. Considering local (e.g. at measurement location) precipitation alone is probably not sufficient to understand the effect of rainfall on INP concentrations in clouds. It would be better to consider the recent precipitation history of the sampled air mass. Since in situ measurements are non-lagrangian, lagrangian simulations that would complement observations would be ideal to determine the environmental parameters (e.g. precipitation, temperature, origin, vegetation cover) of the air experienced

prior to sampling. Likewise, I think there is great potential to consider precipitation history and its impact on INP concentrations in simulations by models that include INP parameterisations.

Similar to the measurements presented in Chapter 3, we had the opportunity to analyse dendrites at Weissfluhjoch in winter 2019 (Göldi, 2019). At this location, the fraction of secondary dendrites was about one order of magnitude higher than observed the year before at Jungfraujoch. A possible explanation for the difference in the multiplication factor could be explained by the topographic differences between both sites (Conen et al., 2019). While the Jungfraujoch is much more elevated than its surroundings, the Weissfluhjoch is surrounded by mountains of similar height. Hoar frost particles that were detached from surfaces at a similar altitude to the Weissfluhjoch and that travelled for several minutes before reaching the measurement site could be one reason for the larger apparent multiplication factor at Weissfluhjoch. The additional secondary dendrites found at Weissfluhjoch might therefore not have been formed by ice multiplication in the atmosphere, but by the entry of hoar frost particles from the ground surface into the mountain-skimming clouds (Vali et al., 2012). To test this hypothesis, as well as to constrain dendritic secondary ice fractions, more analyses of this kind are necessary. Accordingly, a few copies of the portable cold-stage have been built and are being made available to researchers interested in replicating such experiments (Conen et al., 2020). For future studies, I would suggest increasing the efficiency of our approach. For example, sample throughput could be increased by analysing multiple dendrites per droplet. However, caution is required for this, as the increase in ice crystals per droplet lowers the detection limit for the unknown fraction of primary ice. Furthermore, we demonstrated a new approach to investigate atmospheric ice multiplication by combining issues and techniques occurring in different clusters of the scientometric analysis shown at the beginning of the thesis (i.e. Fig. 1.2). One way of linking observations with processes is to choose the experimental conditions carefully and work in an interdisciplinary way. According to our findings, the multiplication factor of ice particles can sometimes be below 10, the need for primary ice estimates with uncertainties lower than one order of magnitude becomes clear. Also, the dependency of the multiplication factor on

ice crystal morphology can be further investigated, as ice crystal shape and riming degree probably influence the efficiency of secondary ice production. Moreover, such observations could be compared to modelling results as, for example, recently done by Georgakaki et al. (2021b).

The results in Chapter 4 illustrate the use of snow particle classes to pinpoint the cloud phase. Furthermore, the likely ice formation process during snowfall was determined by estimating the cloud top temperatures and predicting the INP concentrations using a parameterisation. In the future, it would be desirable to measure the INP concentrations in each studied case to improve the estimate of the underlying ice formation processes.

In this thesis, different research branches (here defined by the clusters from the scientometric network map shown in Fig. 1.2) were bridged to better understand intertwined ice formation and precipitation processes. The findings significantly increase the understanding of ice formation at moderate supercooling in mixed-phase clouds and its link to precipitation. Investigating multiple ice processes in mixed-phase clouds (as shown in Fig. 1.1), from the abundance of INPs to secondary ice production, and actual precipitation has been done mainly within the frame of large field campaigns (e.g. Fridlind et al., 2012; Ramelli et al., 2021). This thesis has reinforced that such investigations, even when they are undertaken with modest means, can shed light on a complex issue. In future studies, we should strive for further investigations that comprise several cloud microphysical processes at the same time. This implies the commitment to establish stronger links between research branches, which likely formed over the course of time. To meet this challenge, it would be beneficial to be able to draw on a broad range of skills and knowledge. This can be achieved through the collaboration of a diverse group of researchers consisting of theoretical, modelling, laboratory and field scientists, similar to what was done, for example, in Patade et al. (2021).

Mountain peaks rising out of a cloud layer
Photo: Claudia Mignani

Chapter 6

Outlooks

This work revealed ways for improving our understanding of primary and secondary ice formation at moderate supercooling in mixed-phase clouds, and its link to precipitation. Potential top-down studies that seemed relevant to me at the end of this thesis and that aim at further developments in mixed-phase clouds research are discussed in the following sections.

6.1 In quest of the sources of primary ice nucleation

Joint measurements of INP concentrations and aerosol particle distribution can enable INP parameterisations based on aerosol particle concentrations, which are often used in models to derive the effect of INP concentration on climate (e.g. DeMott et al., 2010). However, a link between the concentration of INPs active at a certain temperature and aerosol particles of a certain size alone does not indicate causality. Therefore, we should further improve our understanding of the physical, chemical and biological properties of INPs (e.g. size, shape, morphology, elemental and molecular composition) in aerosol, cloud water, or precipitation samples (e.g. Knopf et al., 2014). Over land surfaces in particular, where terrestrial sources contribute significantly to the INP concentrations (Mason et al., 2015; Si et al., 2018), many sources are considered for atmospheric INPs active at moderate supercooling. However, little is known about the nature of these INPs.

Collecting aerosol particles onto wafers in an electrostatic collector (Schrod et al., 2017), followed by the activation and analysis of individual atmospheric INPs, would allow their physical and chemical properties to be determined. An environmental scanning electron microscope (ESEM, i.e. with cloud chamber and electron microscopy functions) could be used to activate and analyse the INPs, similar to the approach used for feldspar by Kiselev et al. (2017). Comparable with the collection of aerosol samples, individual ice crystals could be collected on wafers in order to repeat the experiments by Kumai and Francis (1962). If the proportion of secondary ice is a factor of approximately 10 or less, such an analysis would be feasible without collecting thousands of crystals. In practice, the crystals can be transferred with a brush (as in Chapter 3) on wafers, followed by the sublimation of the ice crystal. Thereafter, the ice residuals can be activated and analysed using the ESEM chamber as described above. This could, for instance, be done with dendrites of an unrimed crystal population, which would exclude rime splintering as a source of secondary ice production.

We tested part of this approach by measuring the INPs of aerosol particles collected on silicon wafers using an isostatic diffusion chamber at the Goethe University of Frankfurt (FRIDGE, FRankfurt Ice nucleation Deposition freezinG Experiment Schrod et al., 2016) and analysing the INPs with a scanning electron microscope (SEM) at the Swiss Nano Institute in Basel (see Mignani et al., 2019b). To determine the position of the INPs, we superimposed images of initial ice crystal growth from the FRIDGE experiment and the SEM image using three reference crosses on the wafers. However, the tests were not continued because we were faced with a dilemma: either the volume of sampled air was too small to deposit a few INPs on the wafer, or it was too large, so that the density of the particles on the substrate was too high to clearly identify the INPs among the numerous aerosol particles within the determined area of initial ice growth.

Activating and analysing the aerosol particles in an ESEM, instead of the combination of a diffusion chamber and SEM, would open up many new possibilities. First and foremost, the often rare INPs in the aerosol could be clearly identified, an aim that is highly desired by scientists (e.g. Sanchez-Marroquin et al., 2021). This

would give further insights into the active sites of individual particles (e.g. Kiselev et al., 2017). If an INP is not a homogeneous particle but an aggregate (e.g. China et al., 2017), the INP entity could be determined. Further, initial ice crystal growth could be studied on atmospheric aerosol particles (e.g. Kiselev et al., 2017). The identification of the particle would allow for the effect of different treatments (e.g. heat, digestion with hydrogen peroxide or enzyme lysozyme; e.g. Hill et al., 2016) on the ice nucleation ability of specific types of atmospheric INPs to be studied. In addition to the individual INP analysis, one could measure the continuous atmospheric INP concentration, as well as the physical aerosol and ice crystal properties in real time, to shed further light on the sources of the primary ice crystals. For this, recent technical developments based on digital holography are very promising (e.g. Henneberger et al., 2013).

6.2 Determining whether rain aerosolises biological INPs

The discovery of the ice-nucleating properties of the bacterium *Pseudomonas syringae* led to the formulation of the bioprecipitation hypothesis a few decades ago (Sands et al., 1982). The general idea behind the bioprecipitation cycle is that biological INPs (BINPs) contribute to ice formation in clouds, which ultimately leads to precipitation. Rain, in turn, releases new BINPs into the atmosphere, which may be lifted to cloud heights where they again initiate rain (i.e. positive feedback loop: more rain enhances the amount of BINPs, which will lead to even more rain) (Sands et al., 1982; Morris et al., 2014). In the meantime, it was revealed that cultivatable *P. syringae* can only explain a minute fraction of the BINP in the atmosphere (Stopelli et al., 2017). Furthermore, many other bioaerosol particles have been discovered that can promote freezing (Huang et al., 2021). Moreover, there is increasing evidence that the atmosphere is enriched with bioaerosols and BINPs during and shortly after precipitation (Chapter 2; Huffman et al., 2013; Conen et al., 2017; Hara et al., 2016; Kita et al., 2020). This would enable the exploration of a more general conception of the bioprecipitation cycle. In Chapter 2, we hypothesised that these increases in INP_{-15} may be due to the release of BINPs by raindrops hitting snow-free land surfaces upwind. For bioaerosols in general, various aerosolisation mechanisms triggered by rain on terrestrial surfaces have been reported (e.g. Hassett et al., 2015;

Joung et al., 2017; Kim et al., 2019; Nath et al., 2019). However, a potential release mechanism by rain specific to BINPs has not yet been observed.

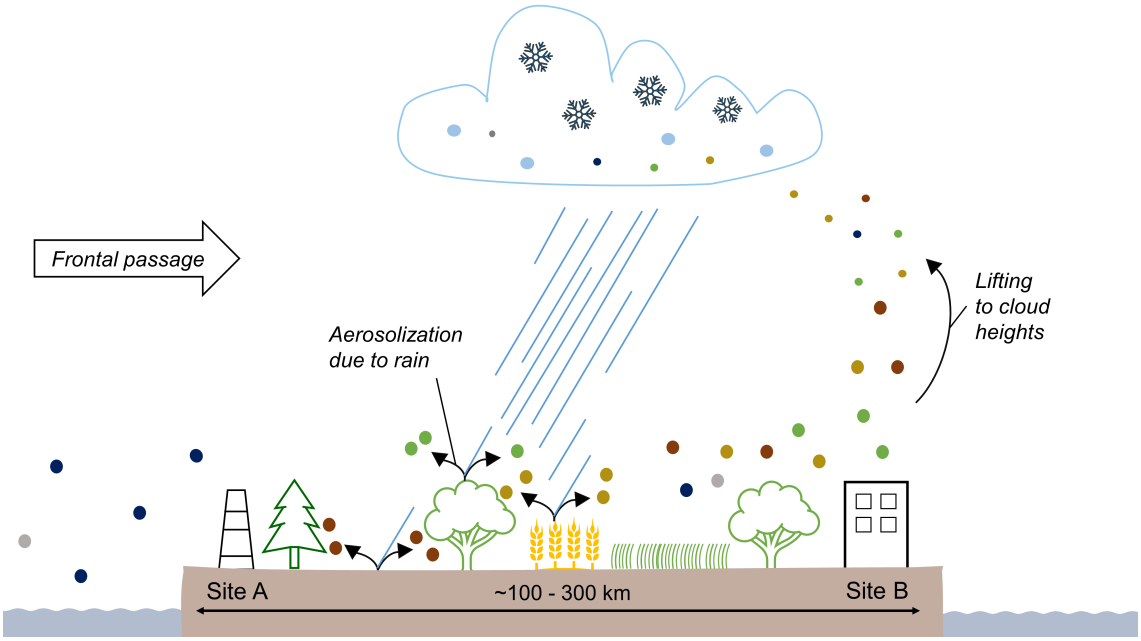

Figure 6.1: Schematic representation of a possible experiment with sampling during the passage of weather fronts. It shows a cross-section through a notional terrestrial landscape along a certain latitude with two coastal sites (Sites A and B) and a cold front passage. This shows the passage of a front and the associated rain that could trigger the release of various INPs that could be lifted to cloud height where they potentially alter the clouds and initiate precipitation.

Atmospheric INPs measured during the passage of weather fronts at two coastal sites on a peninsula could allow the quantification of BINP release resulting from rainfall (Fig. 6.1). Samples from two sites a few hundred kilometres apart (upwind and downwind of rainfall) could be paired by taking into account a time delay dependent on distance and the average wind speed. The resulting difference in BINP concentrations could lead to an estimate of the influence of the land surface and rain. To identify specific BINP characteristics, sample treatments (e.g. Hill et al., 2016) could be considered. Furthermore, known ice-nucleating active genes (Hill et al., 2014) or proteins (techniques apparently currently under development) could be quantified. In addition, the INP measurements could be supported by a set of auxiliary observations, such as spatial meteorological observations and size-dependent bioaerosol concentrations. Estimates of the height of the planetary boundary layer, quantification of marine versus terrestrial influence and properties of cloud or precip-

itation would be desirable and could be derived from lidar-radar measurements or atmospheric chemistry (e.g. radon, isotope ratios of precipitation, aerosol chemical composition). Furthermore, lagrangian backward air mass trajectories linked to land cover information could be useful for attempting to identify specific terrestrial sources. Terrestrial sources could be investigated with regard to the aerosolisation of INPs with splash droplets and the release of plant pathogens. A possible seasonal variability or the role of extreme precipitation events in the aerosolisation of INPs would be interesting to investigate as well. Finally, the already published BINP environmental data made available via a database or similar (e.g. the BACCHUS Ice Nucleation DataBase[2]) could be used to put the results into a wider spatial and temporal context.

6.3 Further quantification of secondary ice production

A promising approach to quantify secondary ice production seems to be the joint measurements of INP and ice particle concentrations in clouds. Such measurements were made, for instance, using aeroplanes (Eidhammer et al., 2010), at mountain stations (Beck et al., 2018), or with the help of above-ground systems, such as a tethered balloon (Ramelli et al., 2021) or a gondola (Lauber et al., 2021). However, such studies are often limited to specific cases, as the observations require a substantial amount of equipment, logistical effort and expertise. As online INP measurement techniques become more autonomous (e.g. Brunner and Kanji, 2021), such experiments could become more efficient to conduct over long time periods. The cloud top and bottom temperatures could limit the temperature range of INP measurements. In addition, the ice particle concentration could, for instance, be determined using holograms (e.g. Lauber et al., 2021). The ice particle habits derived from the holograms could also be used in relation to specific known secondary ice formation processes. For example, if half spherical frozen droplets were captured, droplet shattering (Lauber et al., 2018) as a secondary ice formation process could be assumed to be active. Once remote sensing instruments could reliably determine the concentrations of ice particles and INPs (as well as the prevailing habits of ice particles), such experiments would become even easier. A prerequisite, however, is that the results of the remote sens-

[2]https://www.bacchus-env.eu/in/ (last access: 16 October 2021)

ing retrievals have been validated with in situ measurements (e.g. Wieder et al., 2022).

To quantify secondary ice production, it is particularly important to determine whether external factors have an impact on the primary or secondary ice fraction in clouds. External factors include ice particles lifted from surfaces (e.g. hoar frost or blowing snow) and cloud seeding. Natural cloud seeding could be determined using a combination of radar measurements and radiosondes, as presented by Vassel et al. (2019). Furthermore, it may be possible to monitor human-induced cloud seeding, i.e. the introduction of INPs into the atmosphere by humans. With the increasing trend of weather modifications, human-induced seeding can no longer be completely ruled out in field measurements. For example, there is an ongoing pilot project in Switzerland, led by an insurance company, in which clouds associated with thunderstorms are seeded with artificial INPs (i.e. silver iodide (AgI) aerosol particles; e.g. DeMott, 1990) during the annual hail season to test whether this reduces the damage caused by hail.[3] For field experiments studying clouds and precipitation in general, it would be important to know where, when and how the clouds were seeded or otherwise affected.

6.4 Assessment of the impact of climate change on ice formation in mixed-phase clouds

Probably the most important outlook is the observation and assessment of changes in ice formation in mixed-phase clouds due to current and ongoing climate change. Climate change leads to a warmer climate. Since primary and secondary ice formation processes are linked to air temperature, they are also likely to change due to rising temperatures. However, how ice formation processes change due to ongoing climate change has, to my knowledge, only been investigated using model simulations (e.g. Murray et al., 2021) but has not yet been studied in the field. The simulated changes could be validated with field observations to better understand the way mixed-phase clouds respond to climate change.

[3] https://www.baloise.com/en/home/news-stories/news/media-releases/2020/baloise-cloud-seeder-positive-trend-in-2020-hailstorom-season.html (last access: 16 October 2021)

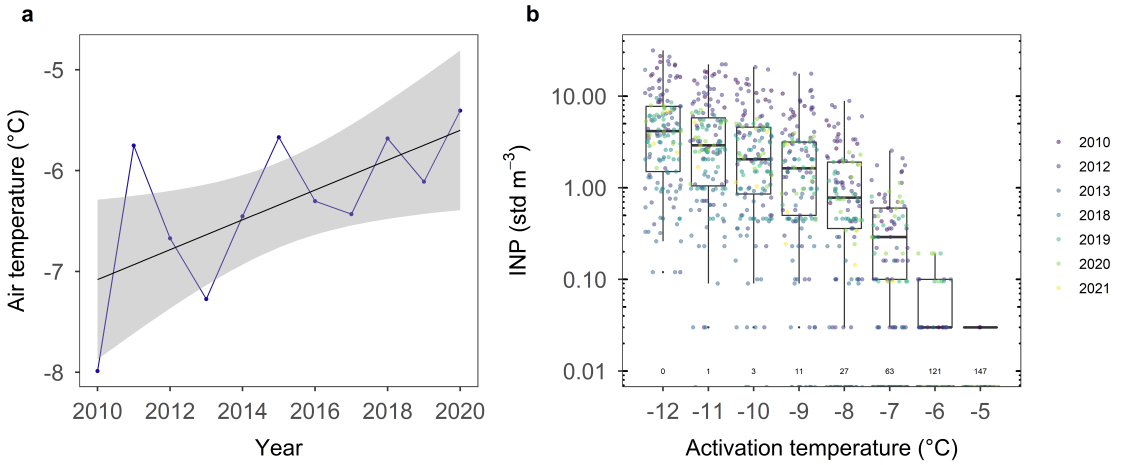

Figure 6.2: Annual mean air temperature (blue line and dots) and 10-year mean air temperature trend (black line) between 2010 and 2020 at Jungfraujoch **(a)**. Air temperature data were provided by the Swiss Federal Office of Meteorology and Climatology MeteoSwiss. Cumulative concentrations of ice-nucleating particles (INPs in std m^{-3}), active between $-5\,°C$ and $-12\,°C$, of 148 daily PM_{10} filter samples collected between 2010 and 2020 (colours of the dots showing the years) were analysed as described in Conen et al. (2012). Boxplots (i.e. median (thick line), interquartile range (box), minima and maxima (whiskers)) of the detected INP concentrations are shown. The number of data points below the detection limit are annotated. The INP data shown here have different references. The data from 2010 to 2013 have been published in Conen et al. (2012, 2015a), the data from 2018 are unpublished, and those from 2019 to 2021 will be reported in Conen et al. (2021).

Multiannual microphysical observations at a specific location would be helpful to determine actual changes in ice formation resulting from climate change. At Jungfraujoch (3580 m a.s.l.), the 10-year mean air temperature trend between 2010 and 2020 was $+1.5\,°C$, i.e. the average mean temperature increased from $-7.0\,°C$ to $-5.5\,°C$ (Fig. 6.2a). Assuming all other relevant factors remain constant, such a temperature increase would lead to a decrease of more than one order of magnitude in the number of INPs that could be activated around Jungfraujoch, as shown in Fig. 6.2b. This estimate was derived from the difference in atmospheric INP concentrations active at $-7.0\,°C$ and at $-6.0\,°C$ (Fig. 6.2b). Such large changes in atmospheric INP concentration could significantly alter the amount of ice in clouds, and therefore the cloud albedo and the hydrological cycle (Phillips et al., 2003). It should be noted that the minimum detectable INP concentration using the standard measurement technique of PM_{10} filters (Conen et al., 2012) does not allow a proper estimation of the INP concentrations active $\geq -6\,°C$, which shows the necessity of lowering the detection limit of such measurements in future studies. To overcome this limitation and detect often rare atmospheric INPs, a larger air volume (e.g. larger filter punches

per droplet for the particular measurement technique used in Fig. 6.2) needs to be analysed. Especially within the warm temperature regime of the INP concentration versus temperature, i.e between 0 °C and ~ -8 °C, the increase in INP concentration is extremely steep with decreasing temperature (Petters and Wright, 2015). Given the low number of INPs at such warm temperatures, the relationship between INP concentration and temperature remains uncertain.

Climate change does not only affect temperatures, but also the sources and fluxes of aerosol particles, which in turn have an influence on the concentration of INPs. As the INP concentration is undergoing seasonal variations (Conen et al., 2015b), it would be of advantage to continuously collect multi-year INP observations to estimate the long-term trend in INP concentrations. The observations shown in Fig. 6.2b were not collected evenly over each year, making it difficult to interpret the trend of INP concentration over that period of time. If climate change will lead to rapid changes in temperature and other parameters that have rapid feedbacks with clouds, it would be necessary to quickly start data collection and conduct cloud research where climate change alters such feedback processes.

Further contributions

In addition to the work presented above, I contributed to other scientific projects in my research area. In particular, I contributed as a co-author to peer-reviewed publications and manuscripts in preparation. These are briefly mentioned below. Moreover, I have co-supervised master's and bachelor's students working on related topics (Weber, 2018; Wyss, 2018; Göldi, 2019; Pasquier, 2021; Einbock, 2021). Where appropriate, I have referred to these contributions in the previous chapters.

- INP concentrations were measured in aerosol, rime, and cloud samples collected at Jungfraujoch during winter 2018 and the results were presented in Creamean et al. (2019).
- The secondary ice fractions amongst others were assessed during two selected cases in the region of Davos in winter 2019 during the "Role of Aerosols and CLouds Enhanced by Topography on Snow" (RACLETS) campaign (Lauber et al., 2021; Ramelli et al., 2021).
- A new drop freezing apparatus was developed and the results were compared to two precursor apparatuses including the one developed at the University of Basel (Miller et al., 2021).
- The variability of cloud droplet numbers was investigated in mixed-phase clouds (Georgakaki et al., 2021a).
- The atmospheric transport and mixing mechanisms of INPs in the Alps were investigated by samplings simultaneously in an elevated valley and at a mountaintop site in the Swiss Alps in late winter 2019 (Wieder et al., 2021).
- The concentrations of INPs $\geq -15\,^{\circ}\mathrm{C}$ in free tropospheric air at Jungfraujoch was determined on selected PM_{10} filters and are reported in Conen et al. (2021).
- Predicting the INP and secondary ice concentrations using remote sensing measurements are being validated by in situ observations (Wieder et al., 2022).

Aletsch Glacier in August 2016
Photo: Claudia Mignani

Personal note

Scientific consensus can change over time. A strong consensus, however, is that air temperatures are increasing due to anthropogenic greenhouse gas emissions. As this consensus has held true for many decades, it is very likely that scientists are correct about anthropogenic climate warming. On other issues, it is less easy to reach a consensus, as current scientific knowledge is subject to great uncertainties (e.g. estimating the impact of human-induced emissions on the anthropogenic forcing of aerosol-cloud-interactions). For yet other questions, consensus has only recently been reached. For instance, a rather recent consensus is that COVID-19 can be transmitted through the air.

I find it promising that since the beginning of the pandemic, I have witnessed that when many scientists work on a common topic, evidence can be found relatively quickly. In general, I am glad that – even if science is a human enterprise, including human ways of seeking credit, making mistakes and acting subjectively – there is still room for objectivity in science and therefore progress. Scientific consensus and progress are, however, not a guarantee for solving a global issue.

How humanity will face global crises such as a pandemic or climate change is ultimately in the hands of society. To solve such a global issue in a democratic society, it is probably necessary for most individuals of that society to develop an understanding of the issue and for politicians to make decisions based on scientific evidence, as well as to issue advice, measures, incentives, and likely also prohibitions. The pandemic is not quite over yet, but humanity is being increasingly confronted by the effects of climate change, a major and complex global issue that also needs to be solved. To limit further damage caused by climate change, we need to stop greenhouse gas emissions as soon as possible.

Stay safe. Stay cool.

Thank you for reading.

C. Mignani, October 2021

Appendix A

Supplement of: Towards parameterising atmospheric concentrations of ice-nucleating particles active at moderate supercooling

Claudia Mignani[1], Jörg Wieder[2], Michael A. Sprenger[2], Zamin A. Kanji[2], Jan Henneberger[2], Christine Alewell[1], Franz Conen[1]

[1]Department of Environmental Sciences, University of Basel, Bernoullistrasse 30, 4056 Basel, Switzerland

[2]Institute for Atmospheric and Climate Science, ETH Zurich, Universitätstrasse 16, 8092 Zurich, Switzerland

This chapter has been published as supplement in Atmospheric Chemistry and Physics.
DOI: 10.5194/acp-21-657-2021-supplement

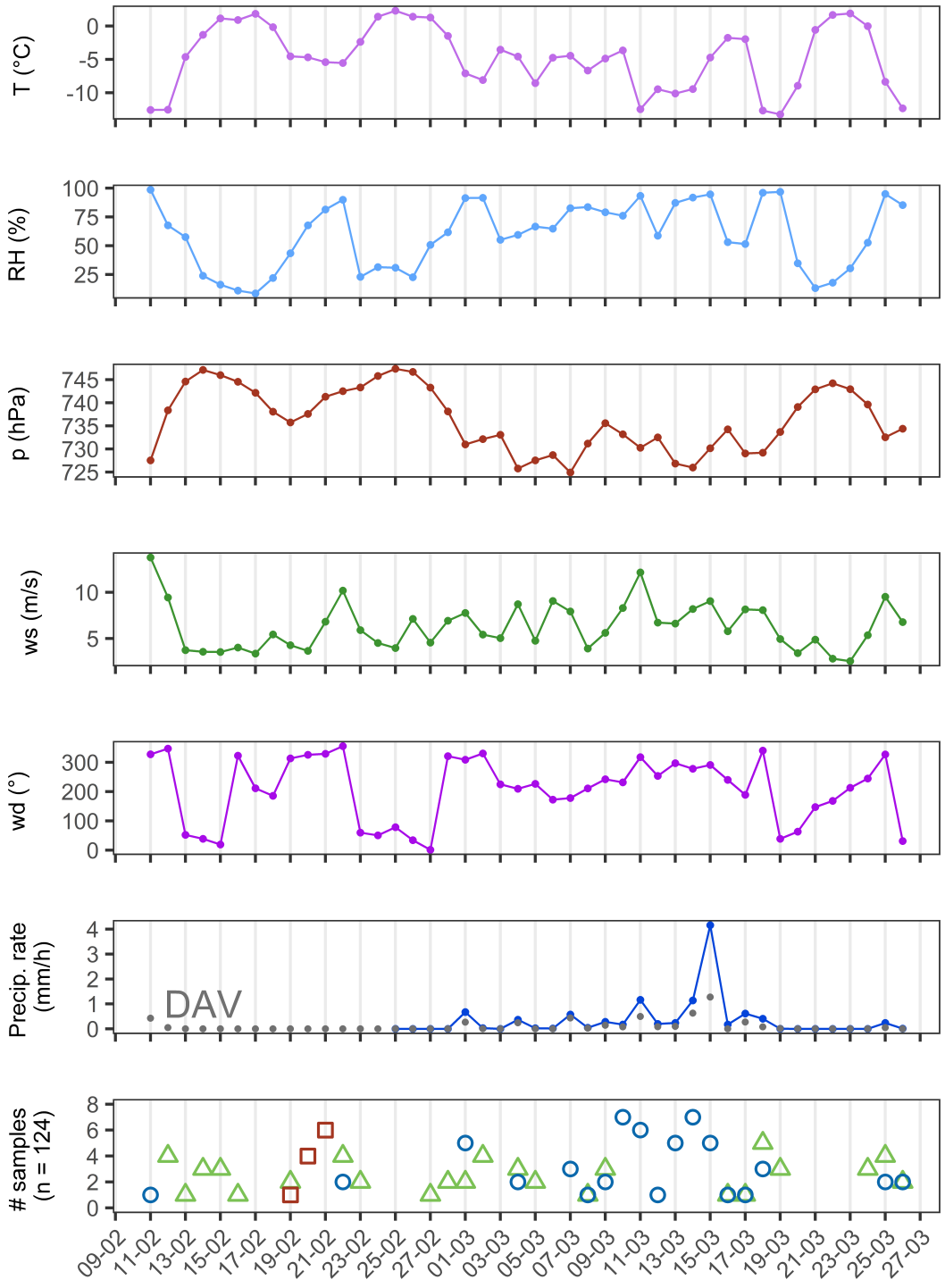

Figure A.1: Daily averaged meteorological data at Weissfluhjoch during "Role of Aerosols and Clouds Enhanced by Topography on Snow (RACLETS)" campaign, including air temperature (T, °C), relative humidity (RH, %), pressure (p, hPa), wind speed (ws, m s^{-1}), wind direction (wd, °), and precipitation rate (mm h^{-1}). Precipitation data were missing prior to 25 February, therefore those of the station in Davos (DAV) are shown as well (gray dots). Number of impinger-based aerosol samples with quantified [INP_{-15}] (n = 124) for air masses that were non-precipitating (green triangles, n = 57), precipitating (blue circles, n = 56), and carrying a substantial fraction of Saharan dust while non-precipitating (red squares, n = 11) are shown.

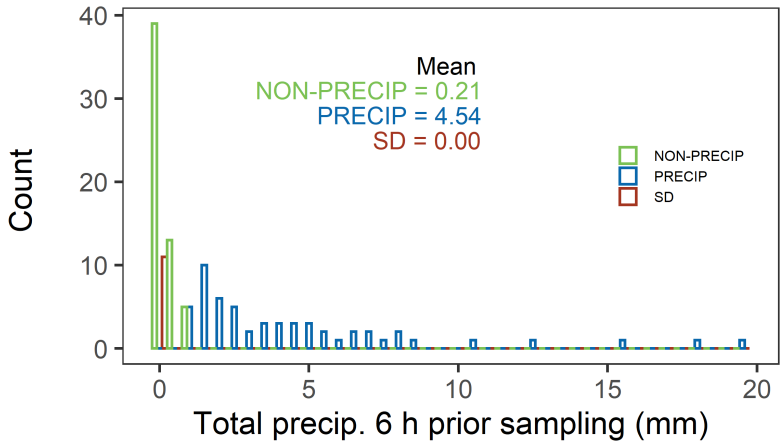

Figure A.2: Total precipitation along the last 6 hours (mm) of the trajectory prior to sampling of air masses that were precipitating (PRECIP, blue), non-precipitating (NON-PRECIP, green), and carrying a substantial fraction of Saharan dust while non-precipitating (SD, red). Histograms of 0.5 mm binned values are plotted (dodged). The mean of each category is denoted. The precipitation values were derived along the LAGRANTO backward trajectories.

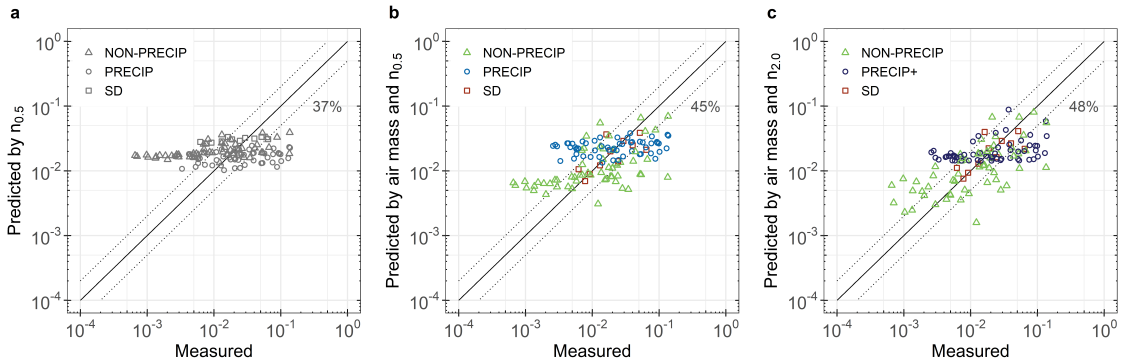

Figure A.3: Measured and predicted cumulative concentrations of ice nucleating particles active at −15 °C [INP_{-15}] (std L^{-1}) for (**a**) prediction based on a single trendline fitted through all data of aerosol particles with aerodynamic diameters > 0.5 µm [$n_{0.5}$], (**b**) predictions based on [$n_{0.5}$] and three different trendlines fitted through the data of PRECIP (blue circles), NON-PRECIP (green triangles), and SD (red squares) air masses, and (**c**) same as (**b**), but based on aerosol particles with aerodynamic diameters > 2.0 µm [$n_{2.0}$]. Shapes in (**a**) are consistent with those in (**b**). However, they are coloured in gray as the prediction is independent of air mass classes. A range of a factor of two (dotted lines) about the 1:1 line (solid line) as well as the percentage of values lying within that range are shown in all panels.

Appendix B

Supplement of: New type of evidence for secondary ice formation at around -15 °C in mixed-phase clouds

Claudia Mignani[1], Jessie M. Creamean[2, 3, a], Lukas Zimmermann[1], Christine Alewell[1], Franz Conen[1]

[1] Institute of Environmental Geosciences, University of Basel, Basel, 4056, Switzerland

[2] Cooperative Institute for Research in Environmental Sciences, University of Colorado, Boulder, CO 80309, USA

[3] Physical Sciences Division, National Oceanic and Atmospheric Administration, Boulder, CO 80305, USA

[a] now at: Department of Atmospheric Science, Colorado State University, Fort Collins, CO 80521, USA

This chapter has been published as supplement in Atmospheric Chemistry and Physics.
DOI: 10.5194/acp-19-877-2019-supplement

Further details of the custom-built stage

Cooling (and heating) of the cold stage is achieved with a Peltier element (13 mm x 12 mm x 2.75 mm, −40 °C to +80 °C; model TE-65-0.6-1.5P, TE Technology Inc., Traverse City, MI, USA). Temperature is measured with a thermistor (0.9 mm diameter, 5 kOhm at 25 °C; model MP-3176, TE Technology Inc., Traverse City, MI, USA) located in the centre of the cylinder just below the surface. Surface temperature can be adjusted within a range from +10 °C to −30 °C. It is set via a single-board microcontroller (Arduino, https://www.arduino.cc/, last access: 18 May 2021) with a touchpad and a LCD display (control unit). The display shows the actual temperature of the stage, the set-point temperature, cooling rate, and other instrumental parameters. The heat formed during cooling is discharged through a ventilated heat-sink (Fig. B.1). Power is supplied to the stage and the control unit from a 12 V, 4.5 Ah LiFePO4 battery (model V-LFP-12-5, Vision Group, Shenzhen, China) lasting about four hours at ambient temperatures a few degrees below 0 °C. The cold stage, control unit, and other items necessary for the analysis of single crystals fit onto a small area (approximately 30 cm x 30 cm; Fig. B.2). Together with the macro camera used to document the crystals, the equipment fits into case the size of a piece of hand luggage allowed inside an aircraft. Its total weight is roughly 10 kg.

We validated the temperature of the cold stage by detecting the melting point of ice. For that purpose, a thin frost layer was grown on the cold stage surface. We then increased the temperature of the cold stage in 0.1 °C steps, starting from −0.2 °C. Melting of the frost layer occurred between the temperature readings of 0.0 °C and 0.1 °C. In addition, we conducted a surface temperature test with a commercial thermometer (model RDXL4SD, sensor type K, Pt100 Ohm, Omega Engineering Inc., Norwalk, CT, USA) in the temperature range of interest from −12 °C to −25 °C with a cooling rate of 3 K min^{-1}. For this test we greased the sensor of the thermometer with petrol jelly and pressed it with Styrofoam onto the surface of the cold stage. When the control unit of the cold stage indicated −12 °C the thermometer indicated −12.1 °C. When the cold stage gave a reading of −17.0 °C the thermometer indicated −16.4 °C. At −25.0 °C the offset of the thermometer had increased to 0.9 °C. This difference might be due to an imperfect contact between

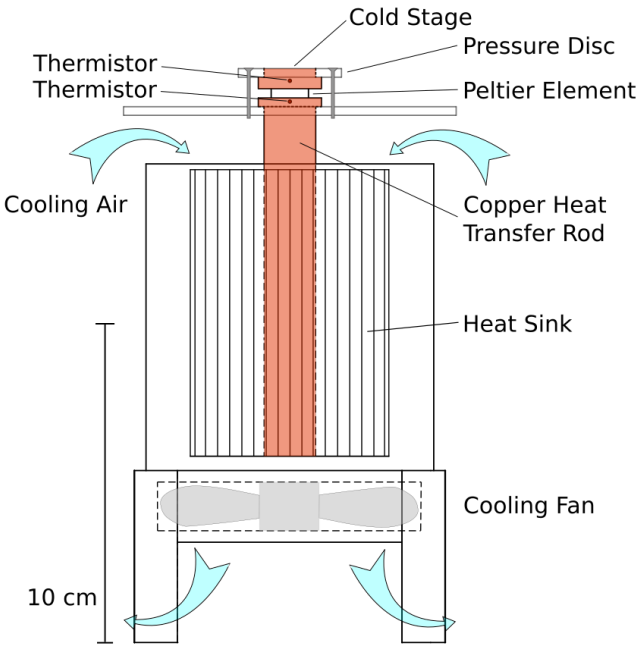

Figure B.1: Technical drawing of the cold stage apparatus.

sensor of the thermometer, which is a bead of about 1 mm diameter, and cold stage surface. Or, it could be due to heat diffusion through the wires of the temperature sensor. Overall, the difference is too small to matter in the context of our study.

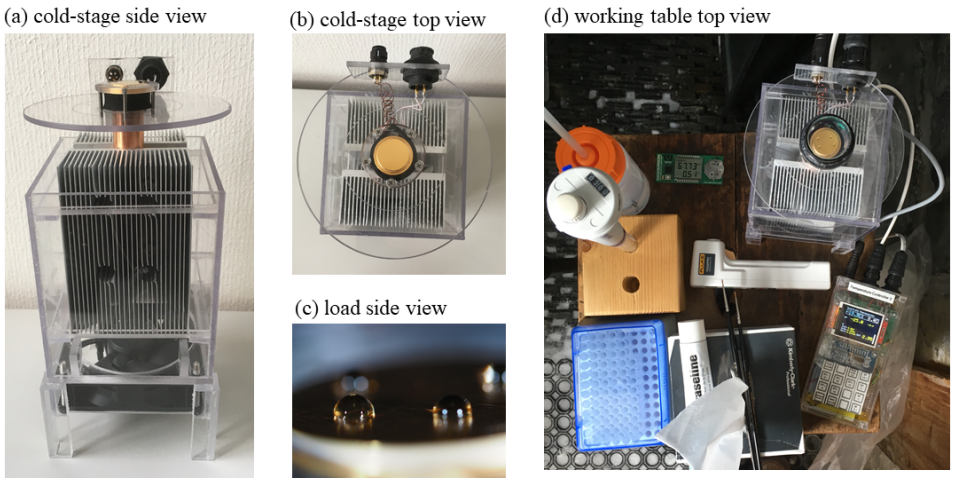

Figure B.2: Photographs of the cold-stage **(a)** from the side and; **(b)** from the top; **(c)** a close-up view of the stage loaded with droplets; **(d)** view from the top onto the working table during operations on Jungfraujoch.

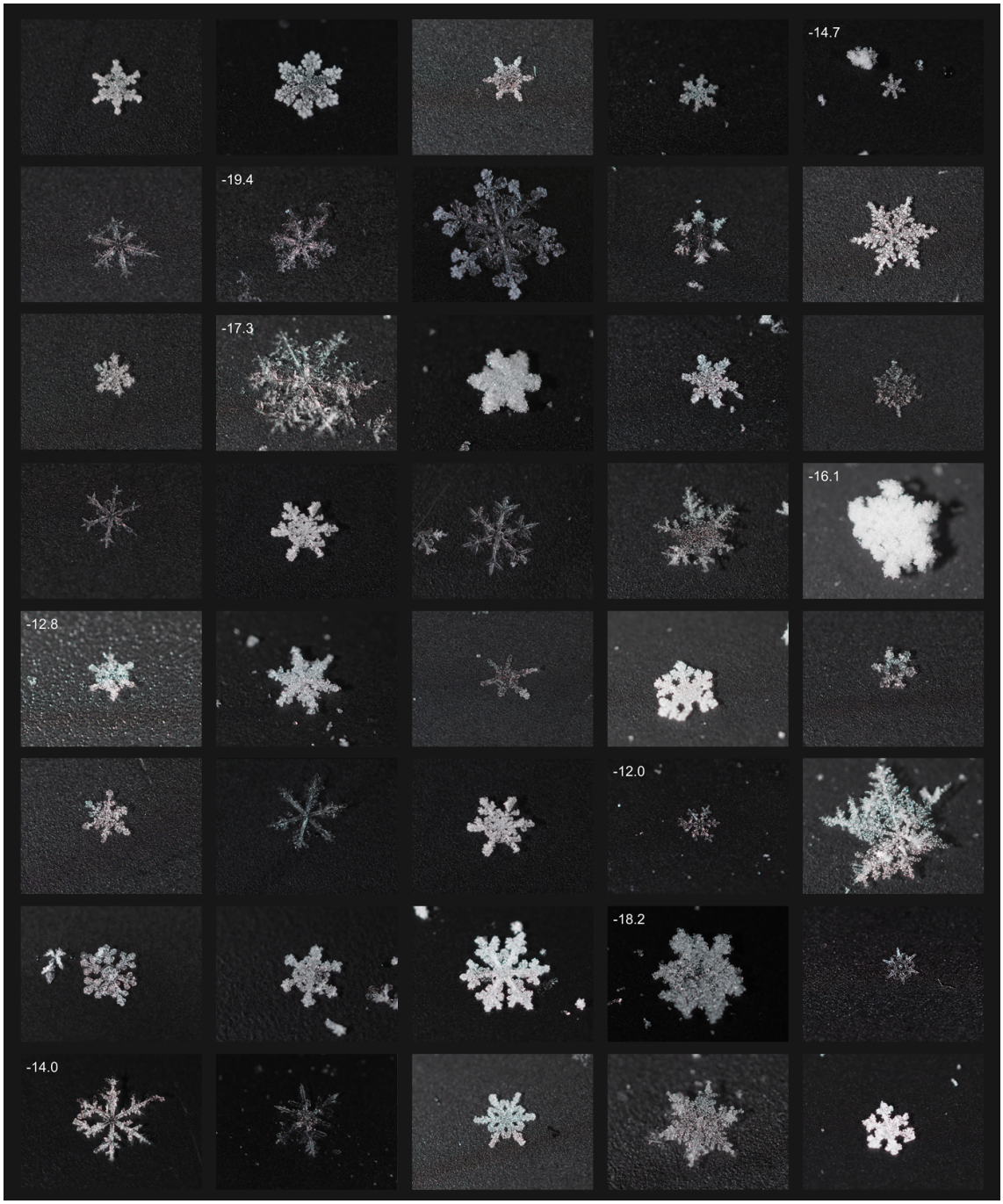

Figure B.3: Examples of images of the analysed dendrites taken by macro (1:1) photography. Crystals of which the residues immersed in a water droplet froze above −20 °C have the freezing temperature added in the upper left corner of their image. Each image shows an area of 8.6 mm x 6.4 mm on the black surface where the crystals had been collected.

Appendix C

Supplement of: Snowfall in Northern Finland derives mostly from ice clouds

Claudia Mignani[1], Lukas Zimmermann[1], Rigel Kivi[2], Alexis Berne[3], Franz Conen[1]

[1]Department of Environmental Sciences, University of Basel, Bernoullistrasse 30, 4056 Basel, Switzerland

[2]Space and Earth Observation Centre, Finnish Meteorological Institute, 99600 Sodankylä, Finland

[3]Environmental Remote Sensing Laboratory, Swiss Federal Institute of Technology in Lausanne, 1015 Lausanne, Switzerland

This chapter has been submitted as appendix to Atmospheric Chemistry and Physics Discussions.

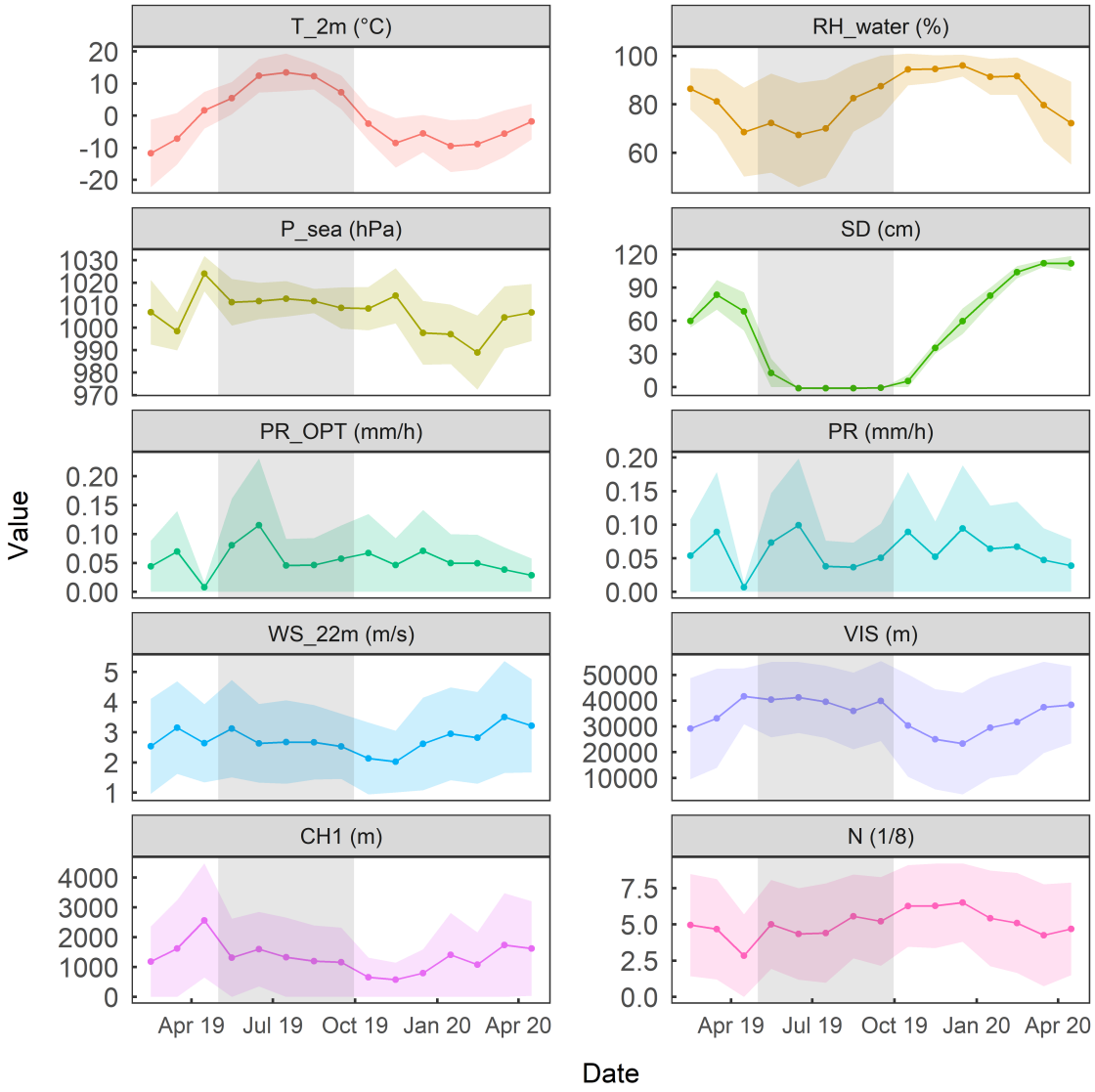

Figure C.1: Time series of monthly weather parameters (means (dots and connecting lines) and standard deviations (ribbons)) at the measurement site in Sodankylä from February 2019 to April 2020. The following variables are shown (from the upper left to the bottom right): ambient air temperature at 2 m above ground (T_2m in °C), relative humidity with respect to water (RH_water in %), the pressure at sea level (P_sea in hPa), snow depth (SD in cm), precipitation rate measured optically (PR_OPT in mm h^{-1}) and by weight (PR mm h^{-1}), wind speed (WS at 22 m above ground in m s^{-1}), visibility (VIS in m), height of the lowest cloud base (CH1 in m), and total cloudiness (N, a value between 1 and 8). The grey areas lowlight the months from May to September, that were excluded from our analysis.

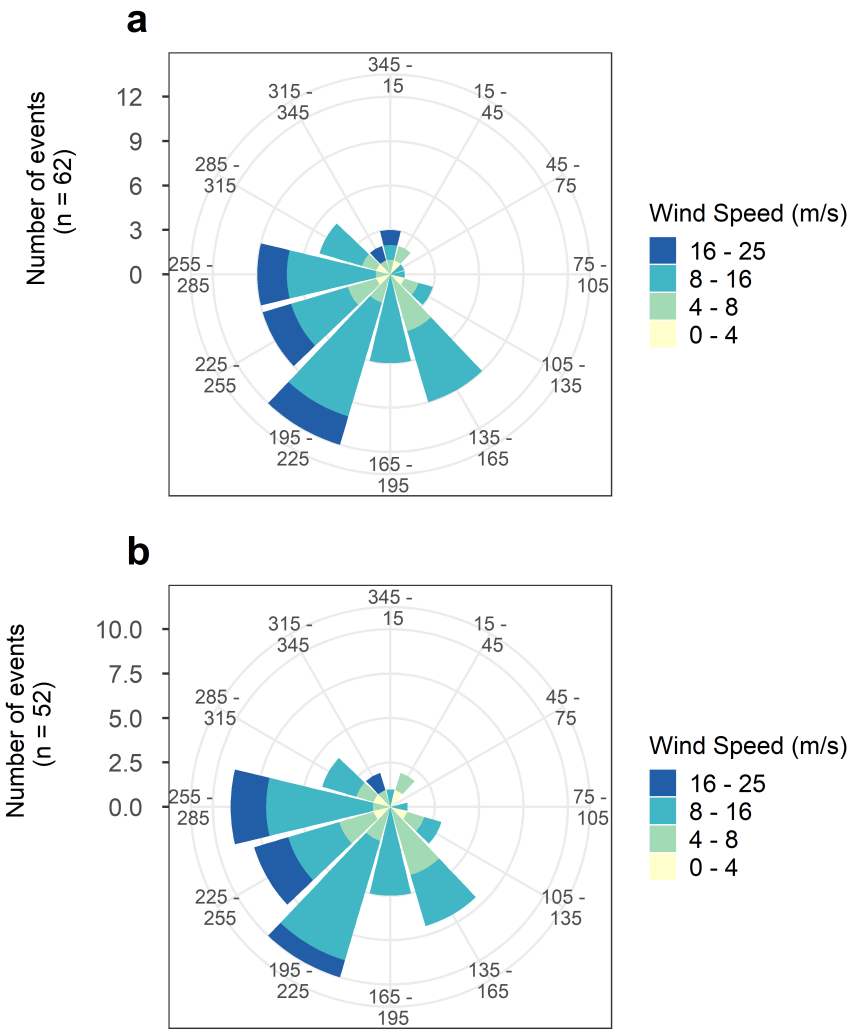

Figure C.2: Wind direction measured by the radiosondes at 2.7 km of (**a**) the 62 snowfall events and (**b**) the 52 snowfall events coinciding with running mean $\mathrm{RH_{ice}} \geq 97\%$ throughout the lower 2.7 km (see Sect. 4.3.2 for criterion).

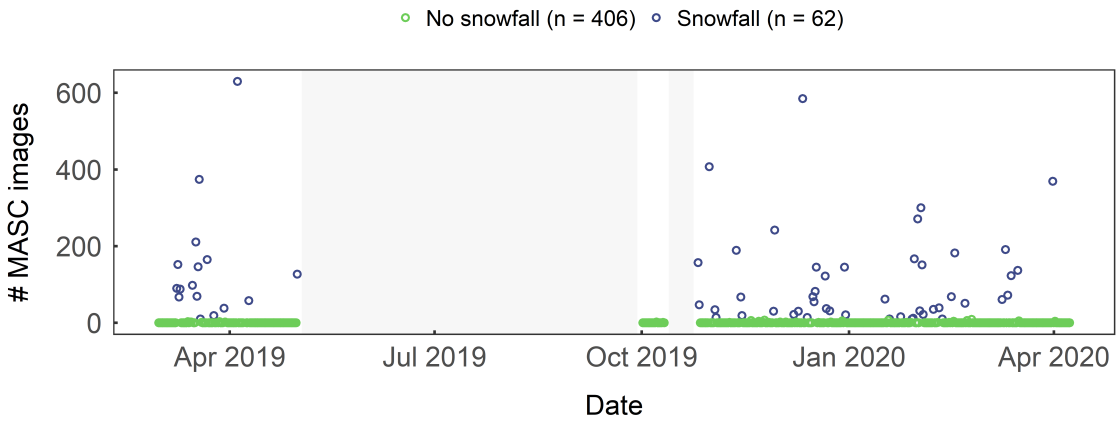

Figure C.3: The number of images with objects larger than 0.54 mm^2 captured by the operational MASC instrument during coinciding radiosonde profiles from 28 February 2019 to 7 April 2020. Radiosondes were launched twice a day, at 11:30 and 23:30 UTC. Images considered were captured within a time span of 15 minutes before each radiosonde launch. Cases (i.e. 15-min time intervals) with 10 or more of such images are classified as snowfall events (n = 62, blue dots). The others are classified as no-snowfall events (n = 406, green dots). No data (gray area) was collected in the summer months (May to September) and during a technical interruption between 11 and 25 October 2019.

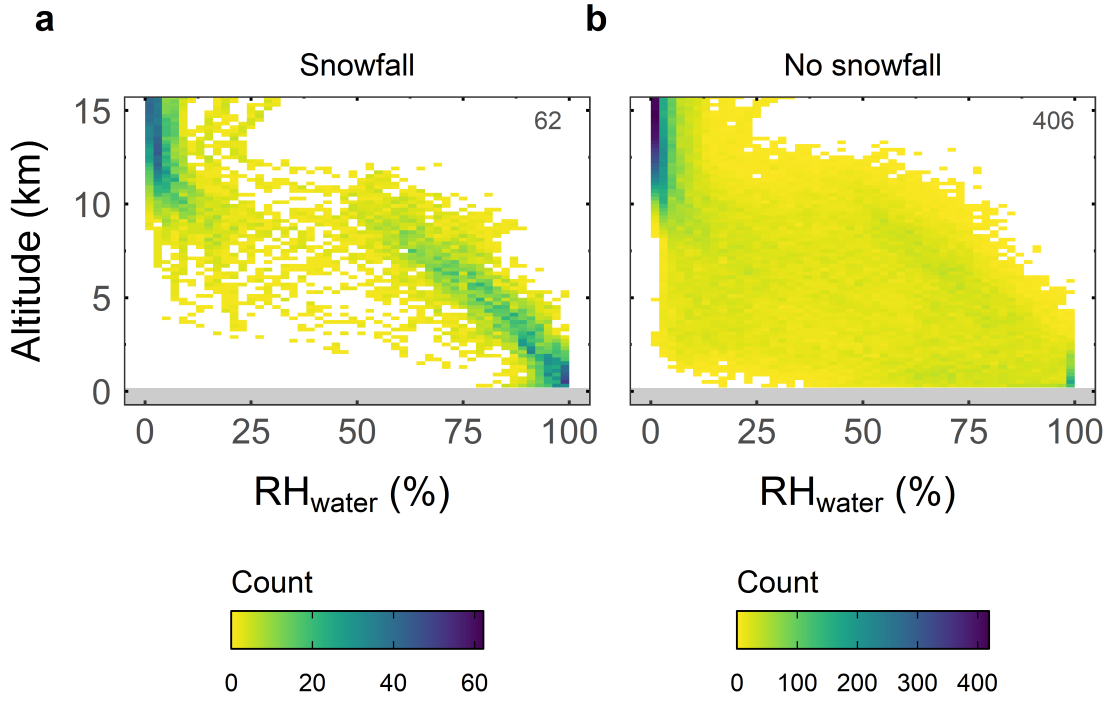

Figure C.4: Same plot as Fig. 4.4, but for RH_{water}.

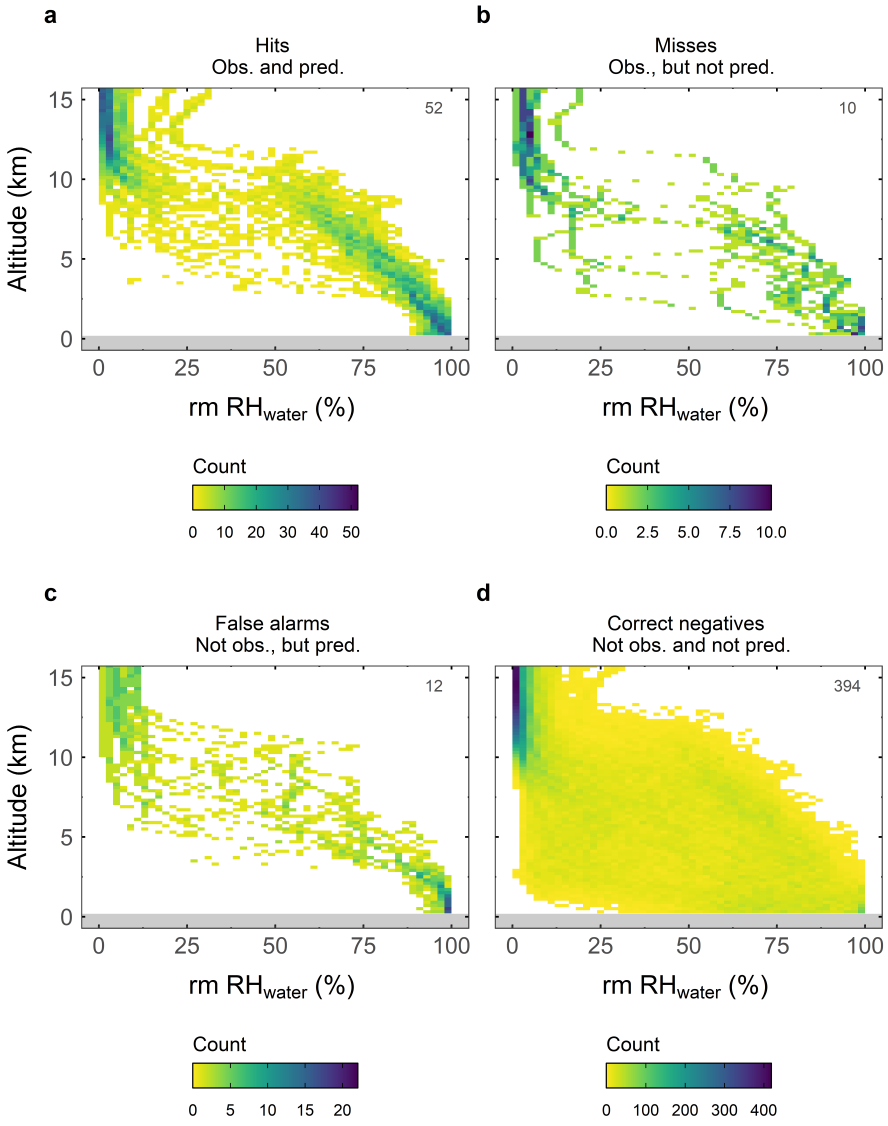

Figure C.5: Same plot as Fig. 4.6, but for RH_{water}.

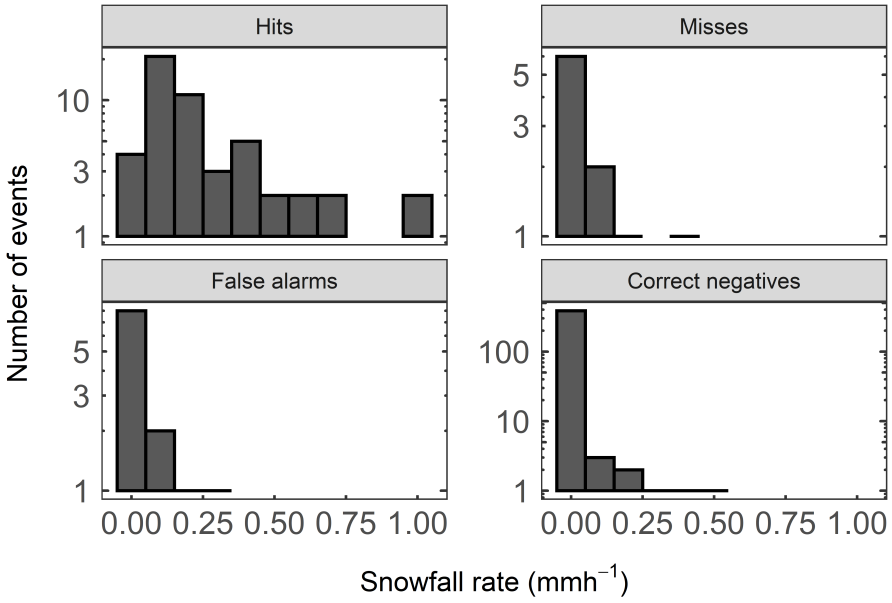

Figure C.6: Snowfall rate by intervals measured optically during the events grouped by *hits*, *misses*, *false alarms*, and *correct negatives* based on the criterion running mean RH_{ice} $\geq$ 97% throughout the lower 2.7 km to predict snowfall.

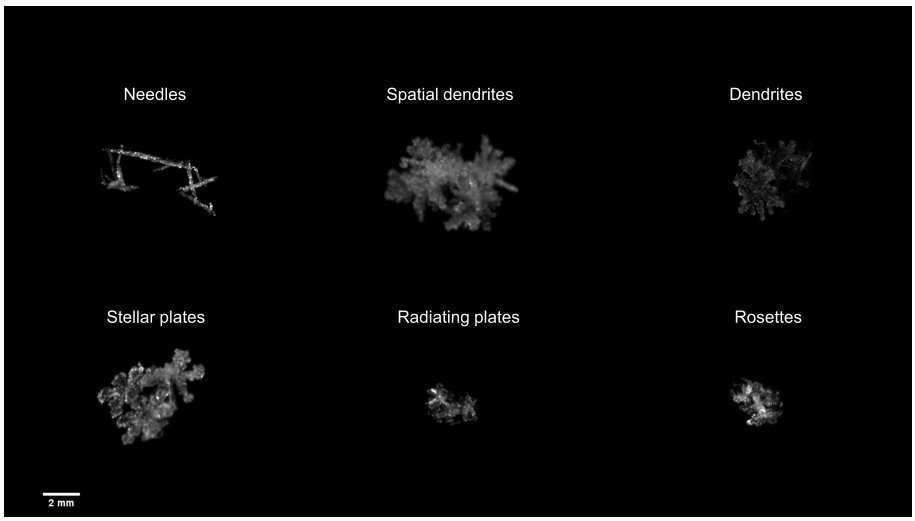

Figure C.7: Similar as Fig. 4.7a, but for aggregates.

Table C.1: Details of scores that compare observed versus predicted events. The scores are calculated with the help of hits (H), misses (M), false alarms (F), correct negatives (C), and the total number of events (Total).

Abbreviation	Name	Formula		Range	Ideal value	Reference
ACC	Accuracy	$\frac{H+C}{Total}$	(C.1)	(0, 1)	1	Bennett et al. (2013)
CSI	Critical success index	$\frac{H}{H+M+F}$	(C.2)	(0, 1)	1	Bennett et al. (2013)
HSS	Heidke skill score	$2\frac{H \cdot C - F \cdot M}{(H+M)(M+C)+(H+F)(F+C)}$	(C.3)	(0, 1)	1	Hyvärinen (2014)

List of symbols and abbreviations

$CH1$ ..... lowest cloud base

dd ..... wind direction

n ..... number

$[n_d]$ ..... number concentration of aerosol particles $\geq$ a diameter d

m ..... mass

N ..... total cloudiness

p ..... air pressure

PR ..... precipitation

PW ..... present weather

RH_{ice} ..... relative humidity with respect to ice

RH_{water} ..... relative humidity with respect to water

SD ..... snow depth

T ..... (air or nucleation) temperature

T_{amb} ..... ambient temperature

u ..... wind velocity

VIS ..... visibility

wd **or** WD ..... wind direction

ws **or** WS ..... wind speed

z_B ..... height of station above cloud base

ACC ..... accuracy

ALL ..... all data points

APS ..... aerodynamic particle sizer

CBT ..... cloud base temperature

CCN ..... cloud condensation nuclei

CF ..... calibration factor

COSMO ..... COnsortium for Small-scale MOdeling

CSI ..... critical success index

D15 ..... parameterisation established by DeMott et al. (2015)

DAV ..... Davos

E ..... east

ECMWF ..... European Centre for Medium-Range Weather Forecasts

ESEM ..... environmental scanning electron microscope

FF ..... frozen fraction

FMI ..... Finnish Meteorological Institute

FRIDGE ..... FRankfurt Ice nucleation Deposition freezinG Experiment

GRUAN ..... Global Climate Observing System Reference Upper-Air Network

HSS ..... Heidke skill score

INP ..... ice-nucleating particle

INP$_T$ ..... INP active at a certain temperature T and warmer

[**INP**] ..... cumulative ice-nucleating particle concentration

JFJ ..... Jungfraujoch

LAGRANTO ... Lagrangian analysis tool

LINDA ..... LED-based Ice Nucleation Detection Apparatus

MASC ..... Multi-Angle Snowflake Camera

MPC ..... mixed-phase cloud

NON-PRECIP . air masses that were non-precipitating

NW ..... north-west

P2 - P7 ..... specific ice crystal classes according to Kikuchi et al. 2013

PRECIP ..... air masses that were precipitating

PRECIP+ ..... additional parameterisation for precipitating air masses

R1c - R4a ..... specific ice crystal classes according to Kikuchi et al. 2013

RACLETS ..... Role of Aerosols and CLouds Enhanced by Topography on Snow

RH ..... relative humidity

SE ..... south-est

SEM ..... scanning electron microscope

SD ..... air masses carrying a substantial fraction of Saharan dust

SNSF ..... Swiss National Science Foundation

SPICE ..... solid precipitation intercomparison experiment

STP ..... standard temperature and pressure

std ..... standard

WMO ..... World Meteorological Organization

List of Tables

List of Figures

Bibliography

Ariya, P. A., Sun, J., Eltouny, N. A., Hudson, E. D., Hayes, C. T., and Kos, G.: Physical and chemical characterization of bioaerosols – Implications for nucleation processes, International Reviews in Physical Chemistry, 28, 1–32, https://doi.org/10.1080/01442350802597438, 2009.

Bacon, N. J., Swanson, B. D.and Baker, M. B., and Davis, E. J.: Breakup of levitated frost particles, J. Geophys. Res., 103, 13 763–13 775, https://doi.org/10.1029/98JD01162, 1998.

Bailey, M. P. and Hallett, J.: A comprehensive habit diagram for atmospheric ice crystals: confirmation from the laboratory, AIRS II, and other field studies, J. Atmos. Sci., 66, 2888–2899, https://doi.org/10.1175/2009JAS2883.1, 2009.

Barnett, T., Adam, J., and Lettenmaier, D.: Potential impacts of a warming climate on water availability in snow-dominated regions, Nature, 438, 303–309, https://doi.org/10.1038/nature04141, 2005.

Beall, C. M., Lucero, D., Hill, T. C., DeMott, P. J., Stokes, M. D., and Prather, K. A.: Best practices for precipitation sample storage for offline studies of ice nucleation, Atmos. Meas. Tech., 13, 6473–6486, https://doi.org/10.5194/amt-13-6473-2020, 2020.

Beck, A., Henneberger, J., Fugal, J. P., David, R. O., Lacher, L., and Lohmann, U.: Impact of surface and near-surface processes on ice crystal concentrations measured at mountain-top research stations, Atmos. Chem. Phys., 18, 8909–8927, https://doi.org/10.5194/acp-18-8909-2018, 2018.

Bennett, N. D., Croke, B. F., Guariso, G., Guillaume, J. H., Hamilton, S. H., Jakeman, A. J., Marsili-Libelli, S., Newham, L. T., Norton, J. P., Perrin, C., Pierce, S. A., Robson, B., Seppelt, R., Voinov, A. A., Fath, B. D., and Andreassian, V.: Characterising performance of environmental models, Environ. Modell. Softw., 40, 1–20, https://doi.org/10.1016/j.envsoft.2012.09.011, 2013.

Bigg, E. K.: Ice forming nuclei in the high Arctic, Tellus, 48B, 223–233, 1996.

Bigg, E. K. and Miles, G. T.: The results of large-scale measurements of natural ice nuclei, J. Atmos. Sci., 21, 396–403, https://doi.org/10.1175/1520-0469(1964)021⟨0396:TROLMO⟩2.0.CO;2, 1964.

Borys, R. D., Lowenthal, D. H., Cohn, S. A., and Brown, W. O. J.: Mountaintop and radar measurements of anthropogenic aerosol effects on snow growth and snowfall rate, Geophys. Res. Lett., 30, https://doi.org/10.1029/2002GL016855, 2003.

Boucher, O., Randall, D., Artaxo, P., Bretherton, C., Feingold, G., Forster, P., Kerminen, V.-M., Kondo, Y., Liao, H., Lohmann, U., Rasch, P., Satheesh, S., Sherwood, S., Stevens, B., and Zhang, X.: Clouds and Aerosols. Climate Change 2013: The Physical Science Basis. Contribution of Working Group I to the Fifth Assessment Report of the Intergovernmental Panel on Climate Change. [Stocker, T.F., D. Qin, G.-K. Plattner, M. Tignor, S.K. Allen, J. Boschung, A. Nauels, Y. Xia, V. Bex and P.M. Midgley (eds)], Cambridge University Press, Cambridge, United Kingdom and New York, NY, USA, pp. 571–658, https://doi.org/10.1017/CBO9781107415324.016, 2013.

Boudala, F. S., Isaac, G. A., Rasmussen, R., Cober, S. G., and Scott, B.: Comparisons of Snowfall Measurements in Complex Terrain Made During the 2010 Winter Olympics in Vancouver, Pure Appl. Geophys., 171, 113–127, https://doi.org/10.1007/s00024-012-0610-5, 2014.

Braham, R. R.: What is the role of ice in summer rain showers?, J. Atmos. Sci., 21, 640–645, 1964.

Brunner, C. and Kanji, Z. A.: Continuous online monitoring of ice-nucleating particles: development of the automated Horizontal Ice Nucleation Chamber (HINC-Auto), Atmos. Meas. Tech., 14, 269–293, https://doi.org/10.5194/amt-14-269-2021, 2021.

Cantrell, W. and Heymsfield, A.: Production of ice in tropospheric clouds: a review, B. Am. Meteorol. Soc., 86, 795–807, https://doi.org/10.1175/BAMS-86-6-795, 2005.

Casella, D., Panegrossi, G., Sanò, P., Marra, A. C., Dietrich, S., Johnson, B. T., and Kulie, M. S.: Evaluation of the GPM-DPR snowfall detection capability: Comparison with CloudSat-CPR, Atmospheric Research, 197, 64–75, https://doi.org/10.1016/j.atmosres.2017.06.018, 2017.

China, S., Alpert, P. A., Zhang, B., Schum, S., Dzepina, K., Wright, K., Owen, R. C., Fialho, P., Mazzoleni, L. R., Mazzoleni, C., and Knopf, D. A.: Ice cloud formation potential by free tropospheric particles from long-range transport over the Northern Atlantic Ocean, J. Geophys., 122, 3065–3079, https://doi.org/10.1002/2016JD025817, 2017.

Christner, B. C.: Bioprospecting for microbial products that affect ice crystal formation and growth, Applied Microbiology and Biotechnology, 85, 481–489, https://doi.org/10.1007/s00253-009-2291-2, 2010.

Conen, F., Henne, S., Morris, C. E., and Alewell, C.: Atmospheric ice nucleators active $> -12\,^{\circ}\mathrm{C}$ can be quantified on PM_{10} filters, Atmos. Meas. Tech., 5, 321–327, https://doi.org/10.5194/amt-5-321-2012, 2012.

Conen, F., Rodríguez, S., Hüglin, C., Henne, S., Herrmann, E., Bukowiecki, N., and Alewell, C.: Atmospheric ice nuclei at the high-altitude observatory Jungfraujoch, Switzerland, Tellus B, 67, https://doi.org/10.3402/tellusb.v67.25014, 2015a.

Conen, F., Rodríguez, S., Hülin, C., Henne, S., Herrmann, E., Bukowiecki, N., and Alewell, C.: Atmospheric ice nuclei at the high-altitude observatory Jungfraujoch, Switzerland, Tellus B: Chemical and Physical Meteorology, 67, 25 014, https://doi.org/10.3402/tellusb.v67.25014, 2015b.

Conen, F., Eckhardt, S., Gundersen, H., Stohl, A., and Yttri, K. E.: Rainfall drives atmospheric ice-nucleating particles in the coastal climate of southern Norway, Atmos. Chem. Phys., 17, 11 065–11 073, https://doi.org/10.5194/acp-17-11065-2017, 2017.

Conen, F., Mignani, C., Zimmermann, L., and Göldi, B.: Ice nucleating particles and ice multiplication at moderate supercooling, International Foundation HFSJG Activity Report 2019, pp. 18–19, URL https://www.hfsjg.ch/reports/2019/pdf/109_UniBasel_Conen.pdf, 2019.

Conen, F., Mignani, C., and Zimmermann, L.: Ice nucleating particles and ice multiplication at moderate supercooling, International Foundation HFSJG Activity Report 2020, p. 26, URL https://www.hfsjg.ch/reports/2020/pdf/110_UniBasel_Conen_cf.pdf, 2020.

Conen, F., Einbock, A., Mignani, C., and Hüglin, C.: Measurement report: Ice nucleating particles active $\geq -15\,^{\circ}\mathrm{C}$ in free tropospheric air over western Europe, Atmos. Chem. Phys. Discuss. [preprint], https://doi.org/10.5194/acp-2021-879, 2021.

Costa, A., Meyer, J., Afchine, A., Luebke, A., Günther, G., Dorsey, J. R., Gallagher, M. W., Ehrlich, A., Wendisch, M., Baumgardner, D., Wex, H., and Krämer, M.: Classification of Arctic, midlatitude and tropical clouds in the mixed-phase temperature regime, Atmos. Chem. Phys., 17, 12 219–12 238, https://doi.org/10.5194/acp-17-12219-2017, 2017.

Creamean, J. M., Kirpes, R. M., Pratt, K. A., Spada, N. J., Maahn, M., de Boer, G., Schnell, R. C., and China, S.: Marine and terrestrial influences on ice nucleating particles during continuous springtime measurements in an Arctic oilfield location, Atmos. Chem. Phys., 18, 18 023–18 042, https://doi.org/10.5194/acp-18-18023-2018, 2018a.

Creamean, J. M., Primm, K. M., Tolbert, M. A., Hall, E. G., Wendell, J., Jordan, A., Sheridan, P. J., Smith, J., and Schnell, R. C.: HOVERCAT: a novel aerial system for evaluation of aerosol–cloud interactions, Atm. Meas. Tech., 11, 3969–3985, https://doi.org/10.5194/amt-11-3969-2018, 2018b.

Creamean, J. M., Mignani, C., Bukowiecki, N., and Conen, F.: Using freezing spectra characteristics to identify ice-nucleating particle populations during the winter in the Alps, Atmos. Chem. Phys., 19, 8123–8140, https://doi.org/10.5194/acp-19-8123-2019, 2019.

Cziczo, D. J., Ladino, L., Boose, Y., Kanji, Z. A., Kupiszewski, P., Lance, S., Mertes, S., and Wex, H.: Measurements of ice nucleating particles and ice residuals. Ice Formation and Evolution in Clouds and Precipitation: Measurement and Modeling Challenges, Meteor. Mon., 58, 8.1–8.13, https://doi.org/10.1175/AMSMONOGRAPHS-D-16-0008.1, 2017.

David, R. O., Marcolli, C., Fahrni, J., Qiu, Y., Perez Sirkin, Y. A., Molinero, V., Mahrt, F., Brühwiler, D., Lohmann, U., and Kanji, Z. A.: Pore condensation and freezing is responsible for ice formation below water saturation for porous particles, Proceedings of the National Academy of Sciences, 116, 8184–8189, https://doi.org/10.1073/pnas.1813647116, 2019.

Delanoë, J., Protat, A., Jourdan, O., Pelon, J., Papazzoni, M., Dupuy, R., Gayet, J.-F., and Jouan, C.: Comparison of airborne in situ, airborne Radar–Lidar, and spaceborne Radar–Lidar retrievals of polar ice cloud properties sampled during the POLARCAT campaign, J. Atmos. Ocean. Technol., 30, 57 – 73, https://doi.org/10.1175/JTECH-D-11-00200.1, 2013.

DeMott, P. J.: Quantifying Ice Nucleation by Silver iodide Aerosols, Ph.D. Dissertation, Dep. Atmospheric Science, Colorado State Univ., p. 259 pp., 1990.

DeMott, P. J. and Prenni, A. J.: New Directions: Need for defining the numbers and sources of biological aerosols acting as ice nuclei, Atmospheric Environment, 44, 1944–1945, https://doi.org/10.1016/j.atmosenv.2010.02.032, 2010.

DeMott, P. J., Prenni, A. J., Liu, X., Kreidenweis, S. M., Petters, M. D., Twohy, C. H., Richardson, M. S., Eidhammer, T., and Rogers, D. C.: Predicting global atmospheric ice nuclei distributions and their impacts on climate, P. Natl. Acad. Sci. USA, 107, 11 217–11 222, https://doi.org/10.1073/pnas.0910818107, 2010.

DeMott, P. J., Prenni, A. J., McMeeking, G. R., Sullivan, R. C., Petters, M. D., Tobo, Y., Niemand, M., Möhler, O., Snider, J. R., Wang, Z., and Kreidenweis, S. M.: Integrating laboratory and field data to quantify the immersion freezing ice nucleation activity of mineral dust particles, Atmos. Chem. Phys., 15, 393–409, https://doi.org/10.5194/acp-15-393-2015, 2015.

Diehl, K., Matthias-Maser, S., Jaenicke, R., and Mitra, S. K.: The ice nucleating ability of pollen:: Part II. Laboratory studies in immersion and contact freezing modes, Atmospheric Research, 61, 125–133, https://doi.org/10.1016/S0169-8095(01)00132-6, 2002.

Eidhammer, T., DeMott, P. J., Prenni, A. J., Petters, M. D., Twohy, C. H., Rogers, D. C., Stith, J., Heymsfield, A., Wang, Z., Pratt, K. A., Prather, K. A., Murphy, S. M., Seinfeld, J. H., Subramanian, R., and Kreidenweis, S. M.: Ice initiation by aerosol particles: Measured and predicted ice nuclei concentrations versus measured ice crystal concentrations in an orographic wave cloud, J. Atmos. Sci., pp. 2417–2436, https://doi.org/10.1175/2010JAS3266.1, 2010.

Einbock, A.: Biological ice-nucleating particles during frontal passages (german title: Biologische Eiskeime beim Durchzug einer Kaltfront), Unpublished Bachelor thesis, University of Basel, 2021.

Els, N., Larose, C., Baumann-Stanzer, K., Tignat-Perrier, R., Keuschnig, C., Vogel, T. M., and Sattler, B.: Microbial composition in seasonal time series of free tropospheric air and precipitation reveals community separation, Aerobiologia, 35, 671–701, https://doi.org/10.1007/s10453-019-09606-x, 2019.

Emersic, C., Connolly, P. J., Boult, S., Campana, M., and Li, Z.: Investigating the discrepancy between wet-suspension- and dry-dispersion-derived ice nucleation efficiency of mineral particles, Atmos. Chem. Phys., 15, 11 311–11 326, https://doi.org/10.5194/acp-15-11311-2015, 2015.

Farrington, R. J., Connolly, P. J., Lloyd, G., Bower, K. N., Flynn, M. J., Gallagher, M. W., Field, P. R., Dearden, C., and Choularton, T. W.: Comparing model and measured ice crystal concentrations in orographic clouds during the INUPIAQ campaign, Atmos. Chem. Phys., 16, 4945–4966, https://doi.org/10.5194/acp-16-4945-2016, 2016.

Fick, S. E. and Hijmans, R. J.: WorldClim 2: new 1-km spatial resolution climate surfaces for global land areas, Int. J. Climatol., 37, 4302–4315, https://doi.org/10.1002/joc.5086, 2017.

Field, R. P., Lawson, R. P., Brown, P. R. A., Lloyd, G., Westbrook, C., Moisseev, D., Miltenberger, A., Nenes, A., Blyth, A., Choularton, D., Connolly, P., Buehl, J., Crosier, J., Cui, Z., Dearden, C., DeMott, P. J., Flossmann, A., Heymsfield, A., Huang, Y., Kalesse, H., Kanji, Z. A., Korolev, A., Kirchgaessner, A., Lasher-Trapp, S., Leisner, T., McFarquhar, G., Phillips, V., Stith, J., and Sullivan, S.: Secondary ice production: Current state of the science and recommendations for the future, Meteorol. Monogr., 58, 7.1–7.20, https://doi.org/10.1175/AMSMONOGRAPHS-D-16-0014.1, 2017.

Forster, P., Storelvmo, T., Armour, K., Collins, W., Dufresne, J.-L., Frame, D., Lunt, D., Mauritsen, T., Palmer, M., Watanabe, M., Wild, M., and Zhang, H.: The Earth's Energy Budget, Climate Feedbacks, and Climate Sensitivity. In Climate Change 2021: The Physical Science Basis. Contribution of Working Group I to the Sixth Assessment Report of the Intergovernmental Panel on Climate Change. [Masson-Delmotte, V., P. Zhai, A. Pirani, S.L. Connors, C. Péan, S. Berger, N. Caud, Y. Chen, L. Goldfarb, M.I. Gomis, M. Huang, K. Leitzell, E. Lonnoy, J.B.R. Matthews, T.K. Maycock, T. Waterfield, O. Yelekçi, R. Yu, and B. Zhou (eds)], Cambridge University Press, Cambridge, United Kingdom and New York, NY, USA. In Press., 2021.

Fridlind, A. M., van Diedenhoven, B., Ackerman, A. S., Avramov, A., Mrowiec, A., Morrison, H., Zuidema, P., and Shupe, M. D.: A FIRE-ACE/SHEBA case study of mixed-phase Arctic boundary layer clouds: Entrainment rate limitations on rapid primary ice nucleation processes, J. Atmos. Sci., 69, 365–389, https://doi.org/10.1175/JAS-D-11-052.1, 2012.

Fröhlich-Nowoisky, J., Hill, T. C. J., Pummer, B. G., Yordanova, P., Franc, G. D., and Pöschl, U.: Ice nucleation activity in the widespread soil fungus Mortierella alpina, Biogeosciences, 12, 1057–1071, https://doi.org/10.5194/bg-12-1057-2015, 2015.

Fröhlich-Nowoisky, J., Kampf, C. J., Weber, B., Huffman, A. J., Pöhlker, C., Andreae, M. O., Lang-Yona, N., Burrows, S. M., Gunthe, S. S., Elbert, W., Su, H., Hoor, P., Thines, E., Hoffmann, T., Després, V. R., and Pöschl, U.: Bioaerosols in the Earth system: Climate, health, and

ecosystem interactions, Atmospheric Research, 182, 346–376, https://doi.org/10.1016/j.atmosres.2016.07.018, 2016.

Fukuta, N. and Takahashi, T.: The growth of atmospheric ice crystals: A summary of findings in vertical supercooled cloud tunnel studies, J. Atmos. Sci., 56, 1963–1979, 1999.

Furukawa, Y.: Structures and formation mechanisms of snow polycrystals, J. Meteorol. Soc. Jpn., 60, 535–547, 1982.

Garrett, T., Fallgatter, C., Shkurko, K., and Howlett, D.: Fall speed measurement and high-resolution multi-angle photography of hydrometeors in free fall, Atmos. Meas. Tech., 5, 2625–2633, 2012.

Georgakaki, P., Bougiatioti, A., Wieder, J., Mignani, C., Ramelli, F., Kanji, Z. A., Henneberger, J., Hervo, M., Berne, A., Lohmann, U., and Nenes, A.: On the drivers of droplet variability in alpine mixed-phase clouds, Atmos. Chem. Phys., 21, 10 993–11 012, https://doi.org/10.5194/acp-21-10993-2021, 2021a.

Georgakaki, P., Sotiropoulou, G., Vignon, E., Billault-Roux, A.-C., Berne, A., and Nenes, A.: Secondary ice production processes in wintertime alpine mixed-phase clouds, Atmos. Chem. Phys. Discuss. [preprint], 2021, 1–46, https://doi.org/10.5194/acp-2021-760, 2021b.

Gierens, R., Kneifel, S., Shupe, M. D., Ebell, K., Maturilli, M., and Löhnert, U.: Low-level mixed-phase clouds in a complex Arctic environment, Atmos. Chem. Phys., 20, 3459–3481, https://doi.org/10.5194/acp-20-3459-2020, 2020.

Göldi, B.: Secondary ice crystal fraction at Weissfluhjoch (german title: Anteil sekundärer Schneekristalle im Niederschlag auf dem Weissfluhjoch), Unpublished Master thesis, University of Basel, 2019.

Griggs, D. J. and Choularton, T. W.: A laboratory study of secondary ice particle production by the fragmentation of rime and vapour-grown ice crystals, Q. J. Roy. Meteor. Soc., 112, 149–163, https://doi.org/10.1002/qj.49711247109, 1986.

Hall, A. and Qu, X.: Using the current seasonal cycle to constrain snow albedo feedback in future climate change, Geophys., 33, https://doi.org/10.1029/2005GL025127, 2006.

Hallett, J. and Mossop, S. C.: Production of secondary ice particles during the riming process, Nature, 249, 26–28, 1974.

Hanlon, R., Powers, C., Failor, K., Monteil, C. L., Vinatzer, B. A., and Schmale III, D. G.: Microbial ice nucleators scavenged from the atmosphere during simulated rain events, Atmos. Environ., 163, 182–189, https://doi.org/10.1016/j.atmosenv.2017.05.030, 2017.

Hanna, J. W., Schultz, D. M., and Irving, A. R.: Cloud-top temperatures for precipitating winter clouds, J. Appl. Meteorol. Climatol., 47, 351—359, https://doi.org/10.1175/2007JAMC1549.1, 2008.

Hara, K., Maki, T., Kobayashi, F., Kakikawa, M., Wada, M., and Matsuki, A.: Variations of ice nuclei concentration induced by rain and snowfall within a local forested site in Japan, Atmos. Environ., 127, 1–5, https://doi.org/10.1016/j.atmosenv.2015.12.009, 2016.

Hassett, M. O., Fischer, M. W. F., and Money, N. P.: Mushrooms as Rainmakers: How Spores Act as Nuclei for Raindrops, PLOS ONE, 10, 1–10, https://doi.org/10.1371/journal.pone.0140407, 2015.

Henneberger, J., Fugal, J. P., Stetzer, O., and Lohmann, U.: HOLIMO II: a digital holographic instrument for ground-based in situ observations of microphysical properties of mixed-phase clouds, Atm. Meas. Tech., 6, 2975–2987, https://doi.org/10.5194/amt-6-2975-2013, 2013.

Heymsfield, A. J., Schmitt, C., Chen, C.-C.-J., Bansemer, A., Gettelman, A., Field, P. R., and Liu, C.: Contributions of the liquid and ice phases to global surface precipitation: observations and global climate modeling, J. Atmos. Sci., 77, 2629–2648, https://doi.org/10.1175/JAS-D-19-0352.1, 2020.

Hill, T. C. J., Moffett, B. F., DeMott, P. J., Georgakopoulos, D. G., Stump, W. L., and Franc, G. D.: Measurement of ice nucleation-active bacteria on plants and in precipitation by quantitative PCR, Appl. Environ. Microbiol., 80, 1256–1267, https://doi.org/10.1128/AEM.02967-13, 2014.

Hill, T. C. J., DeMott, P. J., Tobo, Y., Fröhlich-Nowoisky, J., Moffett, B. F., Franc, G. D., and Kreidenweis, S. M.: Sources of organic ice nucleating particles in soils, Atmos. Chem. Phys., 16, 7195–7211, https://doi.org/10.5194/acp-16-7195-2016, 2016.

Hirsikko, A., O'Connor, E. J., Komppula, M., Korhonen, K., Pfüller, A., Giannakaki, E., Wood, C. R., Bauer-Pfundstein, M., Poikonen, A., Karppinen, T., Lonka, H., Kurri, M., Heinonen, J., Moisseev, D., Asmi, E., Aaltonen, V., Nordbo, A., Rodriguez, E., Lihavainen, H., Laaksonen, A., Lehtinen, K. E. J., Laurila, T., Petäjä, T., Kulmala, M., and Viisanen, Y.: Observing wind, aerosol particles, cloud and precipitation: Finland's new ground-based remote-sensing network, Atmos. Meas. Tech., 7, 1351–1375, https://doi.org/10.5194/amt-7-1351-2014, URL https://amt.copernicus.org/articles/7/1351/2014/, 2014.

Hobbs, P. V. and Rangno, A. L.: Ice particle concentrations in clouds, J. Atmos. Sci., 42, 2523–2549, 1985.

Hobbs, P. V., Chang, S., and Locatelli, J. D.: The dimensions and aggregation of ice crystals in natural clouds, J. Geophys. Res., 79, 2199–.2206, https://doi.org/10.1029/JC079i015p02199, 1974.

Hoffer, T. E. and Braham, R. R.: A laboratory study of atmospheric ice particles, J. Atmos. Sci., 19, 232–235, 1962.

Hogan, R. J., Mittermaier, M. P., and Illingworth, A. J.: The Retrieval of Ice Water Content from Radar Reflectivity Factor and Temperature and Its Use in Evaluating a Mesoscale Model, J. Appl. Meteorol. Climatol., 45, 301 – 317, https://doi.org/10.1175/JAM2340.1, 2006.

Hooke, R.: Micrographia, Some physiological descriptions of minute bodies made by magnifying glasses with observations and inquiries thereupon, LONDON, Printed by John Martyn, and James Allestry, Printers to the Royal Society., 1664.

Hooke, R.: Micrographia, Some physiological descriptions of minute bodies made by magnifying glasses with observations and inquiries thereupon, eBook, The Project Gutenberg, URL https://www.gutenberg.org/cache/epub/15491/, 2005.

Huang, S., Hu, W., Chen, J., Wu, Z., Zhang, D., and Fu, P.: Overview of biological ice nucleating particles in the atmosphere, Environment International, 146, 106 197, https://doi.org/10.1016/j.envint.2020.106197, 2021.

Huffman, J. A., Prenni, A. J., DeMott, P. J., Pöhlker, C., Mason, R. H., Robinson, N. H., Fröhlich-Nowoisky, J., Tobo, Y., Després, V. R., Garcia, E., Gochis, D. J., Harris, E., Müller-Germann, I., Ruzene, C., Schmer, B., Sinha, B., Day, D. A., Andreae, M. O., Jimenez, J. L., Gallagher, M., Kreidenweis, S. M., Bertram, A. K., and Pöschl, U.: High concentrations of biological aerosol particles and ice nuclei during and after rain, Atmos. Chem. Phys, 13, 6151–6164, https://doi.org/10.5194/acp-13-6151-2013, 2013.

Hyvärinen, O.: A Probabilistic Derivation of Heidke Skill Score, Weather Forecast., 29, 177 – 181, https://doi.org/10.1175/WAF-D-13-00103.1, 2014.

Jackson, R., French, J. R., Leon, D. C., Plummer, D. M., Lasher-Trapp, S., Blyth, A. M., and Korolev, A.: Observations of the microphysical evolution of convective clouds in the southwest of the United Kingdom, Atmos. Chem. Phys., 18, 15 329–15 344, https://doi.org/10.5194/acp-18-15329-2018, 2018.

James, R. L., Phillips, V. T. J., and Connolly, P. J.: Secondary ice production during the break-up of freezing water drops on impact with ice particles, Atmos. Chem. Phys., 21, 18 519–18 530, https://doi.org/10.5194/acp-21-18519-2021, 2021.

Jensen, M. P., Holdridge, D. J., Survo, P., Lehtinen, R., Baxter, S., Toto, T., and Johnson, K. L.: Comparison of Vaisala radiosondes RS41 and RS92 at the ARM Southern Great Plains site, Atmos. Meas. Tech., 9, 3115–3129, https://doi.org/10.5194/amt-9-3115-2016, 2016.

Jiusto, J. E. and Weickmann, H. K.: types of snowfall, Bull. Am. Meteorol. Soc., 54, 1148 – 1162, https://doi.org/10.1175/1520-0477(1973)054⟨1148:TOS⟩2.0.CO;2, 1973.

Joung, Y. S., Ge, Z., and Buie, C. R.: Bioaerosol generation by raindrops on soil, Nat. Commun., 8, https://doi.org/10.1038/ncomms14668, 2017.

Kanji, Z. A. and Abbatt, J. P. D.: Laboratory studies of ice formation via deposition mode nucleation onto mineral dust and n-hexane soot samples, J. Geophys., 111, https://doi.org/10.1029/2005JD006766, 2006.

Kanji, Z. A., Ladino, L. A., Wex, H., Boose, Y., Burkert-Kohn, M., Cziczo, D. J., and Krämer, M.: Overview of ice nucleating particles, Meteor. Mon., 58, 1.1–1.33, https://doi.org/10.1175/AMSMONOGRAPHS-D-16-0006.1, 2017.

Kikuchi, K., Kameda, T., Higuchi, K., and Yamashita, A.: A global classification of snow crystals, ice crystals, and solid precipitation based on observations from middle latitudes to polar regions, Atmos. Res., 132–133, 460–472, https://doi.org/10.1016/j.atmosres.2013.06.006, 2013.

Kikuchi, M., Okamoto, H., Sato, K., Suzuki, K., Cesana, G., Hagihara, Y., Takahashi, N., Hayasaka, T., and Oki, R.: Development of algorithm for discriminating hydrometeor particle types with a synergistic use of CloudSat and CALIPSO, J. Geophys., 122, 11,022–11,044, https://doi.org/10.1002/2017JD027113, 2017.

Kim, S., Park, H., Gruszewski, H. A., Schmale, D. G., and Jung, S.: Vortex-induced dispersal of a plant pathogen by raindrop impact, Proceedings of the National Academy of Sciences, 116, 4917–4922, https://doi.org/10.1073/pnas.1820318116, 2019.

Kiselev, A., Bachmann, F., Pedevilla, P., Cox, S. J., Michaelides, A., Gerthsen, D., and Leisner, T.: Active sites in heterogeneous ice nucleation—the example of K-rich feldspars, Science, 355, 367–371, https://doi.org/10.1126/science.aai8034, 2017.

Kita, K., Igarashi, Y., Kinase, T., Hayashi, N., Ishizuka, M., Adachi, K., Koitabashi, M., Sekiyama, T. T., and Onda, Y.: Rain-induced bioecological resuspension of radiocaesium in a polluted forest in Japan, Scientific Reports, 10, 15 330, https://doi.org/10.1038/s41598-020-72029-z, 2020.

Kneifel, S. and Moisseev, D.: Long-term statistics of riming in nonconvective clouds derived from ground-based Doppler cloud radar observations, J. Atmos. Sci., 77, 3495 – 3508, https://doi.org/10.1175/JAS-D-20-0007.1, 2020.

Knopf, D. A., Alpert, P. A., Wang, B., O'Brien, R. E., Kelly, S. T., Laskin, A., Gilles, M. K., and Moffet, R. C.: Microspectroscopic imaging and characterization of individually identified ice nucleating particles from a case field study, J. Geophys., 119, 10,365–10,381, https://doi.org/10.1002/2014JD021866, 2014.

Knutson, E. O., Sood, S. K., and Stockham, J. D.: Aerosol collection by snow and ice crystals, Atmos. Environ., 10, 395–402, https://doi.org/10.1016/0004-6981(76)90009-3, 1976.

Kobayashi, T.: The growth of snow crystals at low supersaturations, Philosophical Magazine, 6, 1363–1370, https://doi.org/10.1080/14786436108241231, 1961.

Kochendorfer, J., Nitu, R., Wolff, M., Mekis, E., Rasmussen, R., Baker, B., Earle, M. E., Reverdin, A., Wong, K., Smith, C. D., Yang, D., Roulet, Y.-A., Buisan, S., Laine, T., Lee, G., Aceituno, J. L. C., Alastrué, J., Isaksen, K., Meyers, T., Brækkan, R., Landolt, S., Jachcik, A., and Poikonen, A.: Analysis of single-Alter-shielded and unshielded measurements of mixed and solid precipitation from WMO-SPICE, Hydrol. Earth. Syst. Sci., 21, 3525–3542, https://doi.org/10.5194/hess-21-3525-2017, 2017.

Korolev, A.: Limitations of the Wegener–Bergeron–Findeisen mechanism in the evolution of mixed-phase clouds, J. Atmos. Sci., 64, 3372–3375, https://doi.org/10.1175/JAS4035.1, 2007.

Korolev, A. and Leisner, T.: Review of experimental studies of secondary ice production, Atmos. Chem. Phys., 20, 11 767–11 797, https://doi.org/10.5194/acp-20-11767-2020, 2020.

Korolev, A., McFarquhar, G., Field, P. R., Franklin, C., Lawson, P., Wang, Z., Williams, E., Abel, S. J., Axisa, D., Borrmann, S., Crosier, J., Fugal, J., Krämer, M., Lohmann, U., Schlenczek, O., Schnaiter, M., and Wendisch, M.: Mixed-phase clouds: Progress and challenges, Meteorological Monographs, 58, 5.1 – 5.50, https://doi.org/10.1175/AMSMONOGRAPHS-D-17-0001.1, 2017.

Korolev, A., Heckman, I., Wolde, M., Ackerman, A. S., Fridlind, A. M., Ladino, L. A., Lawson, R. P., Milbrandt, J., and Williams, E.: A new look at the environmental conditions favorable to secondary ice production, Atmos. Chem. Phys., 20, 1391–1429, https://doi.org/10.5194/acp-20-1391-2020, 2020.

Kumai, M.: Electron-microscope study of snow-crystal nuclei, J. Meteorol., 8, 151–156, 1951.

Kumai, M.: Snow crystals and the identification of the nuclei in the northern United States of America, J. Meteorol., 18, 139–150, 1961.

Kumai, M. and Francis, K. E.: Nuclei in snow and ice crystals on the Greenland ice cap under natural and artificially stimulated conditions, J. Atmos. Sci., 19, 474–481, 1962.

Kupiszewski, P., Weingartner, E., Vochezer, P., Schnaiter, M., Bigi, A., Gysel, M., Rosati, B., Toprak, E., Mertes, S., and Baltensperger, U.: The Ice Selective Inlet: a novel technique for exclusive extraction of pristine ice crystals in mixed-phase clouds, Atm. Meas. Tech., 8, 3087–3106, https://doi.org/10.5194/amt-8-3087-2015, 2015.

Lacher, L., Lohmann, U., Boose, Y., Zipori, A., Herrmann, E., Bukowiecki, N., Steinbacher, M., and Kanji, Z. A.: The Horizontal Ice Nucleation Chamber (HINC): INP measurements at conditions relevant for mixed-phase clouds at the High Altitude Research Station Jungfraujoch, Atmos. Chem. Phys., 17, 15 199–15 224, https://doi.org/10.5194/acp-17-15199-2017, 2017.

Ladino, L. A., Korolev, A., Heckman, I., Wolde, M., Fridlind, A. M., and Ackerman, A. S.: On the role of ice-nucleating aerosol in the formation of ice particles in tropical mesoscale convective systems, Geophys. Res. Lett., 44, 1574–1582, https://doi.org/10.1002/2016GL072455, 2017.

Lance, S., Shupe, M. D., Feingold, G., Brock, C. A., Cozic, J., Holloway, J. S., Moore, R. H., Nenes, A., Schwarz, J. P., Spackman, J. R., Froyd, K. D., Murphy, D. M., Brioude, J., Cooper, O. R., Stohl, A., and Burkhart, J. F.: Cloud condensation nuclei as a modulator of ice processes in Arctic mixed-phase clouds, Atmos. Chem. Phys., 11, 8003–8015, https://doi.org/10.5194/acp-11-8003-2011, 2011.

Lasher-Trapp, S., Leon, D. C., DeMott, P. J., Villanueva-Birriel, C. M., Johnson, A. V., Moser, D. H., Tully, C. S., and Wu, W.: A multisensor investigation of rime splintering in tropical maritime cumuli, J. Atmos. Sci., 73, 2547–2564, https://doi.org/10.1175/JAS-D-15-0285.1, 2016.

Lauber, A., Kiselev, A., Pander, T., Handmann, P., and Leisner, T.: Secondary ice formation during freezing of levitated droplets, J. Atmos. Sci., 75, 2815–2826, https://doi.org/10.1175/JAS-D-18-0052.1, 2018.

Lauber, A., Henneberger, J., Mignani, C., Ramelli, F., Pasquier, J. T., Wieder, J., Hervo, M., and Lohmann, U.: Continuous secondary-ice production initiated by updrafts through the melting layer in mountainous regions, Atmos. Chem. Phys., 21, 3855–3870, https://doi.org/10.5194/acp-21-3855-2021, 2021.

Libbrecht, K. G.: Physical dynamics of ice crystal growth, Annu. Rev. Mat. Res., 47, 271–295, https://doi.org/10.1146/annurevmatsci-070616-124135, 2017.

Liu, G.: Deriving snow cloud characteristics from CloudSat observations, J. Geophys., 113, https://doi.org/10.1029/2007JD009766, 2008.

Lloyd, G., Choularton, T. W., Bower, K. N., Gallagher, M. W., Connolly, P. J., Flynn, M., Farrington, R., Crosier, J., Schlenczek, O., Fugal, J., and Henneberger, J.: The origins of ice crystals measured in mixed-phase clouds at the high-alpine site Jungfraujoch, Atmos. Chem. Phys., 15, 12 953–12 969, https://doi.org/10.5194/acp-15-12953-2015, 2015.

Locatelli, J. D. and Hobbs, P. V.: Fall speeds and masses of solid precipitation particles, J. Geophys., 79, 2185–2197, 1974.

Lohmann, U.: A glaciation indirect aerosol effect caused by soot aerosols, Geophys. Res. Lett., 29, https://doi.org/10.1029/2001GL014357, 2002.

Madonna, F., Kivi, R., Dupont, J.-C., Ingleby, B., Fujiwara, M., Romanens, G., Hernandez, M., Calbet, X., Rosoldi, M., Giunta, A., Karppinen, T., Iwabuchi, M., Hoshino, S., von Rohden, C., and Thorne, P. W.: Use of automatic radiosonde launchers to measure temperature and humidity profiles from the GRUAN perspective, Atmos. Meas. Tech., 13, 3621–3649, https://doi.org/10.5194/amt-13-3621-2020, URL https://amt.copernicus.org/articles/13/3621/2020/, 2020.

Magono, C.: The temperature conditions for the growth of natural and artificial snow crystals, J. Meteorol. Soc. Jpn., 40, 185–192, 1962.

Magono, C. and Lee, C. W.: Meteorological classification of natural snow crystals, Journal of the Faculty of Science, Hokkaido University. Series 7, Geophysics, 321–335, URL http://hdl.handle.net/2115/8672, 1966.

Martens, F.: Spitzbergische oder Groenlandische Reise Beschreibung gethan im Jahr 1671, Aus eigner Erfahrunge beschrieben/die dazu erforderte Figuren nach dem Leben selbst abgerissen/(so hierbey in Kupffer zu sehen) und jetzo durch den Druck mitgetheilet, Hamburg, URL https://ia600302.us.archive.org/14/items/friderichmartens00mart/, 1675.

Mason, R. H., Si, M., Li, J., Chou, C., Dickie, R., Toom-Sauntry, D., Pöhlker, C., Yakobi-Hancock, J. D., Ladino, L. A., Jones, K., Leaitch, W. R., Schiller, C. L., Abbatt, J. P. D., Huffman, J. A., and Bertram, A. K.: Ice nucleating particles at a coastal marine boundary layer site: correlations with aerosol type and meteorological conditions, Atmos. Chem. Phys., 15, 12 547–12 566, https://doi.org/10.5194/acp-15-12547-2015, 2015.

Mason, R. H., Si, M., Chou, C., Irish, V. E., Dickie, R., Elizondo, P., Wong, R., Brintnell, M., Elsasser, M., Lassar, W. M., Pierce, K. M., Leaitch, W. R., MacDonald, A. M., Platt, A., Toom-Sauntry, D., Sarda-Estève, R., Schiller, C. L., Suski, K. J., Hill, T. C. J., Abbatt, J. P. D., Huffman, J. A., DeMott, P. J., and Bertram, A. K.: Size-resolved measurements of ice-nucleating particles at six locations in North America and one in Europe, Atmos. Chem. Phys., 16, 1637–1651, https://doi.org/10.5194/acp-16-1637-2016, 2016.

Matus, A. V. and L'Ecuyer, T. S.: The role of cloud phase in Earth's radiation budget, J. Geophys., 122, 2559–2578, https://doi.org/https://doi.org/10.1002/2016JD025951, 2017.

McCoy, D. T., Tan, I., Hartmann, D. L., Zelinka, M. D., and Storelvmo, T.: On the relationships among cloud cover, mixed-phase partitioning, and planetary albedo in GCMs, J. Adv. Model. Earth Syst., 8, 650–668, https://doi.org/https://doi.org/10.1002/2015MS000589, 2016.

Mertes, S., Verheggen, B., Walter, S., Connolly, P., Ebert, M., Schneider, J., Bower, K. N., Cozic, J., Weinbruch, S., Baltensperger, U., and E., W.: Counterflow virtual impactor based collection of small ice particles in mixed-phase clouds for the physico-chemical characterization of tropospheric ice nuclei: sampler description and first case study, Aerosol Science and Technology, 41, 848–864, https://doi.org/10.1080/02786820701501881, 2007.

Mignani, C., Creamean, J. M., Zimmermann, L., Alewell, C., and Conen, F.: New type of evidence for secondary ice formation at around −15 °C in mixed-phase clouds, Atmos. Chem. Phys., 19, 877–886, https://doi.org/10.5194/acp-19-877-2019, 2019a.

Mignani, C., Weber, D., Schrod, J., Zimmermann, L., Bingemer, H. G., Conen, F., and Alewell, A.: Analysis of Arctic ice-nucleating particles by electron microscopy [Presentation abstract], Nano Imaging User Event, Basel, Switzerland, June 13th, URL https://nanoscience.ch/wp-content/uploads/sites/8/2019/07/nano-imaging-newsletter-3-july-2019.pdf, 2019b.

Mignani, C., Wieder, J., Sprenger, M. A., Kanji, Z. A., Henneberger, J., Alewell, C., and Conen, F.: Ice nucleating particle concentrations active at −15 °C at Weissfluhjoch, EnviDat, https://doi.org/10.16904/envidat.193, 2020.

Mignani, C., Wieder, J., Sprenger, M. A., Kanji, Z. A., Henneberger, J., Alewell, C., and Conen, F.: Towards parameterising atmospheric concentrations of ice-nucleating particles active at moderate supercooling, Atmos. Chem. Phys., 21, 657–664, https://doi.org/10.5194/acp-21-657-2021, 2021.

Mignani, C., Zimmermann, L., Kivi, R., Berne, A., and Conen, F.: Snowfall in Northern Finland derives mostly from ice clouds, in prep.

Miller, A. J., Brennan, K. P., Mignani, C., Wieder, J., David, R. O., and Borduas-Dedekind, N.: Development of the drop Freezing Ice Nuclei Counter (FINC), intercomparison of droplet freezing techniques, and use of soluble lignin as an atmospheric ice nucleation standard, Atm. Meas. Tech., 14, 3131–3151, https://doi.org/10.5194/amt-14-3131-2021, 2021.

Mioche, G., Jourdan, O., Delanoë, J., Gourbeyre, C., Febvre, G., Dupuy, R., Monier, M., Szczap, F., Schwarzenboeck, A., and Gayet, J.-F.: Vertical distribution of microphysical properties of Arctic springtime low-level mixed-phase clouds over the Greenland and Norwegian seas, Atmos. Chem. Phys., 17, 12 845–12 869, https://doi.org/10.5194/acp-17-12845-2017, 2017.

Mora-Valentín, E., Ortiz-de Urbina-Criado, M., and Nájera-Sánchez, J.: Mapping the conceptual structure of science and technology parks, J. Tech. Tran., 43, 1410–1435, https://doi.org/10.1007/s10961-018-9654-8, 2018.

Morris, C. E., Conen, F., Alex Huffman, J., Phillips, V., Pöschl, U., and Sands, D. C.: Bioprecipitation: a feedback cycle linking Earth history, ecosystem dynamics and land use through biological ice nucleators in the atmosphere, Global Change Biology, 20, 341–351, https://doi.org/10.1111/gcb.12447, 2014.

Morrison, H., Zuidema, P., McFarquhar, G. M., Bansemer, A., and Heymsfield, A. J.: Snow microphysical observations in shallow mixed-phase and deep frontal Arctic cloud systems, Q. J. R. Meteorol. Soc., 137, 1589–1601, https://doi.org/10.1002/qj.840, 2011.

Mosimann, L., Weingartner, E., and Waldvogel, A.: An Analysis of Accreted Drop Sizes and Mass on Rimed Snow Crystals, J. Atmos. Sci., 51, 1548 – 1558, https://doi.org/10.1175/1520-0469(1994)051⟨1548:AAOADS⟩2.0.CO;2, 1994.

Mossop, S. C.: The influence of drop size distribution on the production of secondary ice particles during graupel growth, Q. J. Roy. Meteor. Soc., 104, 323–330, https://doi.org/10.1002/qj.49710444007, 1978.

Murray, B. J., Broadley, S. L., Wilson, T. W., Bull, S. J., Wills, R. H., Christenson, H. K., and Murray, E. J.: Kinetics of the homogeneous freezing of water, Phys. Chem. Chem. Phys., 12, 10 380–10 387, https://doi.org/10.1039/c003297b, 2010.

Murray, B. J., O'Sullivan, D., Atkinson, J., and Webb, M. E.: Ice nucleation by particles immersed in supercooled cloud droplets, Chem. Soc. Rev., 41, 6519–6554, https://doi.org/10.1039/C2CS35200A, 2012.

Murray, B. J., Carslaw, K. S., and Field, P. R.: Opinion: Cloud-phase climate feedback and the importance of ice-nucleating particles, Atmos. Chem. Phys., 21, 665–679, https://doi.org/10.5194/acp-21-665-2021, 2021.

Mülmenstädt, J., Sourdeval, O., Delanoë, J., and Quaas, J.: Frequency of occurrence of rain from liquid-, mixed-, and ice-phase clouds derived from A-Train satellite retrievals, Geophys. Res. Lett., 42, 6502–6509, https://doi.org/10.1002/2015GL064604, 2015.

Nakaya, U.: Snow crystals: Natural and artificial, Harvard University Press, Cambridge, UK, 510 pp., 1954.

Nakaya, U. and Terada, T.: Simultaneous observations of the mass, falling velocity and form of individual snow crystals, Journal of the Faculty of Science, Hokkaido Imperial University, Ser. 2, Physics, 1, 191–200, URL http://eprints.lib.hokudai.ac.jp/dspace/handle/2115/34452, 1935.

Nath, S., Ahmadi, S. F., Gruszewski, H. A., Budhiraja, S., Bisbano, C. E., Jung, S., Schmale, D. G., and Boreyko, J. B.: "Sneezing" plants: pathogen transport via jumping-droplet condensation, Journal of The Royal Society Interface, 16, 20190 243, https://doi.org/10.1098/rsif.2019.0243, 2019.

Nelson, J. T. and Baker, M. B.: New theoretical framework for studies of vapor growth and sublimation of small ice crystals in the atmosphere, J. Geophys. Res., 101, 7033–7047, https://doi.org/10.1029/95JD03162, 1996.

Nitu, R., Roulet, Y.-A., Wolff, M., Earle, M., Reverdin, A., Smith, C., Kochendorfer, J., Morin, S., Rasmussen, R., Wong, K., Alastrué, J., Arnold, L., Baker, B., Buisán, S., Collado, J., Colli, M., Collins, B., Gaydos, A., Hannula, H.-R., Hoover, J., Joe, P., Kontu, A., Laine, T., Lanza,

L., Lanzinger, E., Lee, G., Lejeune, Y., Leppänen, L., Mekis, E., Panel, J.-M., Poikonen, A., Ryu, S., Sabatini, F., Theriault, J., Yang, D., Genthon, C. van den Heuvel, F., Hirasawa, N., Konishi, H., Motoyoshi, H., Nakai, S., Nishimura, K., Senese, A., and Yamashita, K.: WMO Solid Precipitation Intercomparison Experiment (SPICE) (2012–2015), IOM Report No. 131, URL https://library.wmo.int/index.php?lvl=notice_display&id=20742, 2018.

O'Gorman, P. A.: Precipitation extremes under climate change, Current Climate Change Reports, 1, 49–59, https://doi.org/10.1007/s40641-015-0009-3, 2015.

Pasquier, J.: Ice nucleation in different parts of the flower bud of Rhododendron and Castanea (german title: Eis-Nukleation in verschiedenen Teilen der Blütenknospe von Rhododendron und Kastanie), Unpublished Bachelor thesis, University of Basel, 2021.

Patade, S., Phillips, V. T. J., Amato, P., Bingemer, H. G., Burrows, S. M., DeMott, P. J., Goncalves, F. L. T., Knopf, D. A., Morris, C. E., Alwmark, C., Artaxo, P., Pöhlker, C., Schrod, J., and Weber, B.: Empirical formulation for multiple groups of primary biological ice nucleating particles from field observations over Amazonia, J. Amos. Sci., 78, 2195–2220, https://doi.org/10.1175/JAS-D-20-0096.1, 2021.

Petters, M. D. and Wright, T. P.: Revisiting ice nucleation from precipitation samples, Geophys. Res. Lett., 42, 8758–8766, https://doi.org/10.1002/2015GL065733, 2015.

Phillips, V. T. J., Choularton, T. W., Illingworth, A. J., Hogan, R. J., and Field, P. R.: Simulations of the glaciation of a frontal mixed-phase cloud with the Explicit Microphysics Model, Q. J. R. Meteorol. Soc., 129, 1351–1371, https://doi.org/10.1256/qj.02.100, 2003.

Phillips, V. T. J., DeMott, P. J., Andronache, C., Pratt, K. A., Prather, K. A., Subramanian, R., and Twohy, C.: Improvements to an Empirical Parameterization of Heterogeneous Ice Nucleation and Its Comparison with Observations, J. Atmos. Sci., 70, 378–409, https://doi.org/10.1175/JAS-D-12-080.1, 2013.

Phillips, V. T. J., Yano, J.-I., and Khain, A.: Ice multiplication by breakup in ice-ice collisions. Part I: Theoretical formulation, J. Atmos. Sci., 74, 1705–1719, https://doi.org/10.1175/JAS-D-16-0224.1, 2017.

Polen, M., Lawlis, E., and Sullivan, R. C.: The unstable ice nucleation properties of Snomax®bacterial particles, J. Geophys. Res.-Atmos., 121, 11 666–11 678, https://doi.org/10.1002/2016JD025251, 2016.

Polen, M., Brubaker, T., Somers, J., and Sullivan, R. C.: Cleaning up our water: reducing interferences from nonhomogeneous freezing of "pure" water in droplet freezing assays of ice-nucleating particles, Atm. Meas. Tech., 11, 5315–5334, https://doi.org/10.5194/amt-11-5315-2018, 2018.

Poltera, Y., Martucci, G., Collaud Coen, M., Hervo, M., Emmenegger, L., Henne, S., Brunner, D., and Haefele, A.: PathfinderTURB: an automatic boundary layer algorithm. Development, validation and application to study the impact on in situ measurements at the Jungfraujoch, Atmos. Chem. Phys., 17, 10 051–10 070, https://doi.org/10.5194/acp-17-10051-2017, 2017.

Pouleur, S., Richard, C., Martin, J. G., and Antoun, H.: Ice nucleation activity in *Fusarium acuminatum* and *Fusarium avenaceum*, Appl. Environ. Microbiol., 59, 2960–2964, 1992.

Power, B. A., Summers, P. W., and D'Avignon, J.: Snow crystal forms and riming effects as related to snowfall density and general storm conditions, J. Atmos. Sci., 21, 300 – 305, https://doi.org/10.1175/1520-0469(1964)021⟨0300:SCFARE⟩2.0.CO;2, 1964.

Praz, C., Roulet, Y.-A., and Berne, A.: Solid hydrometeor classification and riming degree estimation from pictures collected with a Multi-Angle Snowflake Camera, Atm. Meas. Tech., 10, 1335–1357, https://doi.org/10.5194/amt-10-1335-2017, 2017.

Proske, U., Bessenbacher, V., Dedekind, Z., Lohmann, U., and Neubauer, D.: How frequent is natural cloud seeding from ice cloud layers ($< -35\,^{\circ}\mathrm{C}$) over Switzerland?, Atmos. Chem. Phys., 21, 5195–5216, https://doi.org/10.5194/acp-21-5195-2021, 2021.

Pruppacher, H. R. and Klett, J. D.: Microphysics of clouds and precipitation. Second revised and expanded edition with an introduction to cloud chemistry and cloud electricity, Springer Dordrecht Heidelberg London New York, https://doi.org/10.1007/978-0-306-48100-0, 2010.

Raabe, O. G.: Aerosol aerodynamic size conventions for inertia! Sampler calibration, J. Air Pollut. Control Assoc., 26, 856–860, https://doi.org/10.1080/00022470.1976.10470329, 1976.

Ramelli, F., Henneberger, J., David, R. O., Bühl, J., Radenz, M., Seifert, P., Wieder, J., Lauber, A., Pasquier, J. T., Engelmann, R., Mignani, C., Hervo, M., and Lohmann, U.: Microphysical investigation of the seeder and feeder region of an Alpine mixed-phase cloud, Atmos. Chem. Phys., 21, 6681–6706, https://doi.org/10.5194/acp-21-6681-2021, 2021.

Rangno, A. L. and Hobbs, P. V.: Ice particles in stratiform clouds in the Arctic and possible mechanisms for the production of high ice concentrations, J. Geophys. Res., 106, 15 065–15 075, https://doi.org/10.1029/2000JD900286, 2001.

Rauber, R. M.: Characteristics of cloud ice and precipitation during wintertime storms over the mountains of Northern Colorado, J. Clim. Appl. Meteor., 26, 488–524, https://doi.org/10.1175/1520-0450(1987)026⟨0488:COCIAP⟩2.0.CO;2, 1987.

Rogers, D. C. and Vali, G.: Ice crystal production by mountain surfaces, J. Clim. Appl. Meteorol., 26, 1152–1168, https://doi.org/10.1175/1520-0450(1987)026⟨1152:ICPBMS⟩2.0.CO;2, 1987.

Rogers, R. R. and Yau, M. K.: A short course in cloud physics, Oxford, New York: Pergamon Press, 293 pp., 1989.

Rueden, C. T., Schindelin, J., Hiner, M. C., DeZonia, B. E., Walter, A. E., Arena, E. T., and Eliceiri, K. W.: ImageJ2: ImageJ for the next generation of scientific image data, BMC Bioinformatics, 18, https://doi.org/10.1186/s12859-017-1934-z, 2017.

Saleeby, S. M., Cotton, W. R., Lowenthal, D., and Messina, J.: Aerosol impacts on the microphysical growth processes of orographic snowfall, J. Appl. Meteorol. Climatol., 52, 834–852, https://doi.org/10.1175/JAMC-D-12-0193.1, 2013.

Sanchez-Marroquin, A., West, J. S., Burke, I. T., McQuaid, J. B., and Murray, B. J.: Mineral and biological ice-nucleating particles above the South East of the British Isles, Environ. Sci.: Atmos., 1, 176 – 191, https://doi.org/10.1039/D1EA00003A, 2021.

Sands, D. C., Langhans, V. E., Scharen, A. L., and de Smet, G.: The association between bacteria and rain and possible resultant meteorological implications, Journal of the Hungarian Meteorological Service, 86, 148–152, 1982.

Schindelin, J., Arganda-Carreras, I., Frise, E., Kaynig, V., Longair, M., Pietzsch, T., Preibisch, S., Rueden, C., Saalfeld, S., Schmid, B., Tinevez, J., White, D. J., Hartenstein, V., Eliceiri, K., Tomancak, P., and Cardona, A.: Fiji: An open-source platform for biological-image analysis, Nat. Methods, 9, 676–682, 2012.

Schneider, J., Höhler, K., Heikkilä, P., Keskinen, J., Bertozzi, B., Bogert, P., Schorr, T., Umo, N. S., Vogel, F., Brasseur, Z., Wu, Y., Hakala, S., Duplissy, J., Moisseev, D., Kulmala, M., Adams, M. P., Murray, B. J., Korhonen, K., Hao, L., Thomson, E. S., Castarède, D., Leisner, T., Petäjä, T., and Möhler, O.: The seasonal cycle of ice-nucleating particles linked to the abundance of biogenic aerosol in boreal forests, Atmos. Chem. Phys., 21, 3899–3918, https://doi.org/10.5194/acp-21-3899-2021, 2021.

Schrod, J., Danielczok, A., Weber, D., Ebert, M., Thomson, E. S., and Bingemer, H. G.: Re-evaluating the Frankfurt isothermal static diffusion chamber for ice nucleation, Atmos. Meas. Tech., 9, 1313–1324, https://doi.org/10.5194/amt-9-1313-2016, 2016.

Schrod, J., Weber, D., Drücke, J., Keleshis, C., Pikridas, M., Ebert, M., Cvetković, B., Nickovic, S., Marinou, E., Baars, H., Ansmann, A., Vrekoussis, M., Mihalopoulos, N., Sciare, J., Curtius, J., and Bingemer, H. G.: Ice nucleating particles over the Eastern Mediterranean measured by unmanned aircraft systems, Atmos. Chem. Phys., 17, 4817–4835, https://doi.org/10.5194/acp-17-4817-2017, 2017.

Schrod, J., Thomson, E. S., Weber, D., Kossmann, J., Pöhlker, C., Saturno, J., Ditas, F., Artaxo, P., Clouard, V., Saurel, J.-M., Ebert, M., Curtius, J., and Bingemer, H. G.: Long-term deposition and condensation ice-nucleating particle measurements from four stations across the globe, Atmos. Chem. Phys., 20, 15 983–16 006, https://doi.org/10.5194/acp-20-15983-2020, 2020.

Schwarzenboeck, A., Shcherbakov, V., Lefevre, R., Gayet, J.-F., Pointin, Y., and Duroure, C.: Indications for stellar-crystal fragmentation in Arctic clouds, Atmos. Res., 92, 220–228, https://doi.org/10.1016/j.atmosres.2008.10.002, 2009.

Seo, W.-S., Eun, S.-H., Kim, B.-G., Ko, A.-R., Seong, D.-K., Lee, K.-M., Jeon, H.-R., Han, S.-O., and Park, Y.-S.: Study on characteristics of snowfall and snow crystal habits in the ESSAY (Experiment on Snow Storms At Yeongdong) campaign in 2014, Atmosphere, 25, 261–270, https://doi.org/10.14191/Atmos.2015.25.2.261, 2015.

Shupe, M. D. and Intrieri, J. M.: Cloud radiative forcing of the Arctic surface: The influence of cloud properties, surface albedo, and solar zenith angle, J. Clim., 17, 616 – 628, https://doi.org/10.1175/1520-0442(2004)017⟨0616:CRFOTA⟩2.0.CO;2, 2004.

Si, M., Irish, V. E., Mason, R. H., Vergara-Temprado, J., Hanna, S. J., Ladino, L. A., Yakobi-Hancock, J. D., Schiller, C. L., Wentzell, J. J. B., Abbatt, J. P. D., Carslaw, K. S., Murray, B. J., and Bertram, A. K.: Ice-nucleating ability of aerosol particles and possible sources at three coastal marine sites, Atmos. Chem. Phys., 18, 15 669–15 685, https://doi.org/10.5194/acp-18-15669-2018, 2018.

Silber, I., Fridlind, A. M., Verlinde, J., Ackerman, A. S., Cesana, G. V., and Knopf, D. A.: The prevalence of precipitation from polar supercooled clouds, Atmos. Chem. Phys., 21, 3949–3971, https://doi.org/10.5194/acp-21-3949-2021, 2021.

Sprenger, M.: Backward Trajectories, EnviDat, https://doi.org/10.16904/envidat.120, 2019.

Sprenger, M. and Wernli, H.: The LAGRANTO Lagrangian analysis tool – version 2.0, Geosci. Model Dev., 8, 2569–2586, https://doi.org/10.5194/gmd-8-2569-2015, 2015.

Stopelli, E., Conen, F., Zimmermann, L., Alewell, C., and Morris, C. E.: Freezing nucleation apparatus puts new slant on study of biological ice nucleators in precipitation, Atmos. Meas. Tech., 7, 129–134, https://doi.org/10.5194/amt-7-129-2014, 2014.

Stopelli, E., Conen, F., Guilbaud, C., Zopfi, J., Alewell, C., and Morris, C. E.: Ice nucleators, bacterial cells and *Pseudomonas syringae* in precipitation at Jungfraujoch, Biogeosciences, 14, 1189–1196, https://doi.org/10.5194/bg-14-1189-2017, 2017.

Sullivan, S. C., Barthlott, C., Crosier, J., Zhukov, I., Nenes, A., and Hoose, C.: The effect of secondary ice production parameterization on the simulation of a cold frontal rainband, Atmos. Chem. Phys., 18, 16 461–16 480, https://doi.org/10.5194/acp-18-16461-2018, 2018a.

Sullivan, S. C., Hoose, C., Kiselev, A., Leisner, T., and Nenes, A.: Initiation of secondary ice production in clouds, Atmos. Chem. Phys., 18, 1593–1610, https://doi.org/10.5194/acp-18-1593-2018, 2018b.

Takahashi, C. and Yamashita, A.: Shattering of frozen water drops in a supercooled cloud, J. Meteorol. Soc. Jpn., 48, 373–376, 1970.

Takahashi, T.: Influence of liquid water content and temperature on the form and growth of branched planar snow crystals in a cloud, J. Atmos. Sci., 71, 4127–4142, https://doi.org/10.1175/JAS-D-14-0043.1, 2014.

Takahashi, T., Endoh, T., Wakahama, G., and Fukuta, N.: Vapour diffusional growth of free-falling snow crystals between −3 and −23 °C, J. Meteorol. Soc. Jpn., 69, 15–30, 1991.

Takahashi, T., Nagao, Y., and Kushiyama, Y.: Possible high ice particle production during graupel-graupel collisions, J. Atmos. Sci., 52, 4523–4527, 1995.

Tan, I. and Storelvmo, T.: Evidence of strong contributions from mixed-phase clouds to Arctic climate change, Geophys. Res. Lett., 46, 2894–2902, https://doi.org/10.1029/2018GL081871, 2019.

Tarn, M. D., Sikora, S. N. F., Porter, G. C. E., Wyld, B. V., Alayof, M., Reicher, N., Harrison, A. D., Rudich, Y., Shim, J.-u., and Murray, B. J.: On-chip analysis of atmospheric ice-nucleating particles in continuous flow, Lab Chip, 20, 2889–2910, https://doi.org/10.1039/D0LC00251H, 2020.

Tesson, S. V. M. and Šantl-Temkiv, T.: Ice nucleation activity and aeolian dispersal success in airborne and aquatic microalgae, Frontiers in Microbiology, 9, 2681, https://doi.org/10.3389/fmicb.2018.02681, 2018.

Tobo, Y.: An improved approach for measuring immersion freezing in large droplets over a wide temperature range, Sci. Rep., 6, https://doi.org/10.1038/srep32930, 2016.

Vali, G.: Quantitative evaluation of experimental results on the heterogeneous freezing nucleation of supercooled liquids, J. Atmos. Sci., 28, 402–409, https://doi.org/10.1175/1520-0469(1971)028⟨0402:QEOERA⟩2.0.CO;2, 1971a.

Vali, G.: Supercooling of water and nucleation of ice (drop freezer), Am. J. Phys., 39, 1125–1128, https://doi.org/10.1119/1.1976585, 1971b.

Vali, G.: Nucleation terminology, B. Am. Meteorol. Soc., 66, 1426–1427, 1985.

Vali, G.: Repeatability and randomness in heterogeneous freezing nucleation, Atmos. Chem. Phys., 8, 5017–5031, https://doi.org/10.5194/acp-8-5017-2008, 2008.

Vali, G., Leon, D., and Snider, J. R.: Ground-layer snow clouds, Q. J. R. Meteorol. Soc., 138, 1507–1525, https://doi.org/10.1002/qj.1882, 2012.

Vali, G., DeMott, P. J., Möhler, O., and Whale, T. F.: Technical Note: A proposal for ice nucleation terminology, Atmos. Chem. Phys., 15, 10 263–10 270, https://doi.org/10.5194/acp-15-10263-2015, 2015.

van Eck, N. J. and Waltman, L.: Software survey: VOSviewer, a computer program for bibliometric mapping, J. Tech. Tran., 84, 523–538, https://doi.org/10.1007/s11192-009-0146-3, 2010.

Vardiman, L.: The generation of secondary ice particles in clouds by crystal—crystal collisions, J. Atmos. Sci., 35, 2168–2180, https://doi.org/10.1175/1520-0469(1978)035⟨2168:TGOSIP⟩2.0.CO;2, 1978.

Vassel, M., Ickes, L., Maturilli, M., and Hoose, C.: Classification of Arctic multilayer clouds using radiosonde and radar data in Svalbard, Atmos. Chem. Phys., 19, 5111–5126, https://doi.org/10.5194/acp-19-5111-2019, 2019.

Weber, L.: Investigation of ice germs in foliage and blades of grass of arctic plants (german title: Untersuchung von Eiskeimen in Laub und Grashalmen arktischer Pflanzen), Unpublished Master thesis, University of Basel, 2018.

Weingartner, E., Nyeki, S., and Baltensperger, U.: Seasonal and diurnal variation of aerosol size distributions ($10 < D < 750$ nm) at a high-alpine site (Jungfraujoch 3580 m asl), J. Geophys. Res., 104, 26 809–26 820, https://doi.org/10.1029/1999JD900170, 1999.

Westbrook, C. D. and Illingworth, A. J.: Evidence that ice forms primarily in supercooled liquid clouds at temperatures $> -27\,^{\circ}$C, Geophys. Res. Lett., 38, https://doi.org/10.1029/2011GL048021, 2011.

Westbrook, C. D. and Illingworth, A. J.: The formation of ice in a long-lived supercooled cloud, Q. J. Roy. Meteor. Soc., 139, 2209–2221, https://doi.org/10.1002/qj.2096, 2013.

Wieder, J., Mignani, C., Schär, M., Roth, L., Sprenger, M., Henneberger, J., Lohmann, U., Brunner, C., and Kanji, Z. A.: Unveiling atmospheric transport and mixing mechanisms of ice nucleating particles over the Alps, Atmos. Chem. Phys. Discuss. [preprint], https://doi.org/10.5194/acp-2021-718, 2021.

Wieder, J., Ihn, N., Mignani, C., Haarig, M., Bühl, J., Seifert, P., Engelmann, R., Ramelli, F., Kanji, Z. A., Lohmann, U., and Henneberger, J.: Retrieving ice nucleating particle concentration and ice multiplication factors using active remote sensing validated by in situ observations, Atmos. Chem. Phys. Discuss. [preprint], https://doi.org/10.5194/acp-2022-67, 2022.

Wilson, T. W., Ladino, L. A., Alpert, P. A., Breckels, M. N., Brooks, I. M., Browse, J., Burrows, S. M., Carslaw, K. S., Huffman, J. A., Judd, C., Kilthau, W. P., Mason, R. H., McFiggans, G., Miller, L. A., Najera, J. J., Polishchuk, E., Rae, S., Schiller, C. L., Si, M., Temprado, J. V., Whale, T. F., Wong, J. P. S., Wurl, O., Yakobi-Hancock, J. D., Abbatt, J. P. D., Aller, J. Y., Bertram, A. K., Knopf, D. A., and Murray, B. J.: A marine biogenic source of atmospheric ice-nucleating particles, Nature, 42, 234–238, https://doi.org/10.1038/nature14986, 2015.

Wright, T. P., Petters, M. D., Hader, J. D., Morton, T., and Holder, A. L.: Minimal cooling rate dependence of ice nuclei activity in the immersion mode, J. Geophys. Res.-Atmos., 118, 10 535–10 543, https://doi.org/10.1002/jgrd.50810, 2013.

Wyss, M.: Dynamics of organic ice nuclei in soils of Alpine chronological sequences (german title: Dynamik organischer Eiskeime in Böden alpiner Chronosequenzen), Unpublished Bachelor thesis, University of Basel, 2018.

Mountain in clouds at sunset

Photo: Claudia Mignani

Acknowledgements

The completion of this PhD thesis would not have been possible without the support of numerous individuals. I would like to take this opportunity to express my deep gratitude to them all. Very special thanks to my supervisors Franz Conen, Christine Alewell and Markus Kalberer for guiding me through this journey. I am deeply grateful to:

- **Franz Conen** for the continuous intellectual guidance, for the unparallel support in so many aspects, for creating the perfect conditions to learn new things and for giving me the opportunity to take responsibilities. Franz, your support went beyond what I could ever imagine. You inspire me for your extensive and in-depth knowledge about nature, your generous patience and time, and you straightforward way of giving constructive feedback, which has been a great privilege all these years. Thank you for being an excellent scientific advisor. It has been a joy to learn from you.
- **Christine Alewell** for giving me the change to work on this project, for creating such an interdisciplinary working environment and for the trust.
- **Markus Kalberer** for the interest about my research, for participating in my semester seminars, and for the opportunity to assist a lecture lesson.
- My committee members **Paul J. DeMott** and **Tina Šantl-Temkiv** for accepting to read my thesis and for their flexibility in terms of timing.
- **Lukas Zimmermann** for manufacturing instruments and for his technical assistance transferring and processing data, which were key in this research.
- Each co-author as well as reviewer for the help in writing the manuscripts.
- **Stefan Reimann** for introducing me to field work at Jungfraujoch and making me aware of the open PhD position at University of Basel.
- All the generous people who helped in the snowy field or the cosy laboratories. **Jessie M. Creamean** for sharing her valuable experience at the beginning of this project during a stay at Jungfraujoch. **Heinz Bingemer** and his group, who introduced me to their isostatic diffusion chamber and helped me with the measurements in the harsh weather conditions in northern Norway. The whole Nano Imaging Lab Team, led by **Markus Dürrenberger**, who taught me a lot about microscopy. **Judith Kobler Waldis** and **Annika Einbock** for measuring INPs. Much of the INP concentrations shown in Fig. 6.2 are a result of their large commitments.
- The entire RACLETS team who organised the intensive campaign in the Davos region. Very special thanks to **Jörg**, **Jan**, **Annika**, **Fabiola**, **Julie**, **Bettina**, **Mario**, and **Lucie** for the numerous discussions about the field data as well as the fun raclette evenings.

- All the lovely colleagues who made my time at Bernoullianum unforgettable. In particular, to **Pedro**, for inspiring me, for his valuable help in processing data and creating figures, for reading through the work and for his mental support in the final stages. Special thanks to **Daniela** for all the hours of administrative support. Many thanks to **Judith**, **Thomas** and **Axel** for their support in the lab. **Martin** for keeping me company during numerous train journeys. **Stefan** for giving advise with grant applications. **Lauren**, **Miriam**, **Lena**, **Pranav**, **Terry**, **Pasquale**, **Jen-How**, **Sonja**, **Simon**, **Marlène** and all the members of the biogeochemistry group for the conversations about this and that, for turning the Bernoullianum into a little green oasis and for the fun times during the breaks. I have fond memories of playing table tennis, swimming in the Rhine and eating or barbecuing on the beautiful roof terrace.
- **Moritz Lehmann** for chairing my defense and for his great commitment to the university.
- The undergraduate and graduate students **Lea**, **Mirjam**, **Bettina**, **Joëlle**, and **Annika**, who did their research thesis on ice formation. I am grateful for their interest, critical thinking and patience with me as a co-supervisor.
- The Swiss National Science Foundation for supporting this research. The Department of Environmental Sciences for funding the snowflake camera and two months of my salary.
- **Ulrike Lohmann** and the colleagues of her group for giving me the amazing opportunity to participate not only in their group meetings and paper discussions, but also in the RACLETS campaign. A nice side effect of this was that it allowed me to return to ETH Zurich from time to time, a place that shaped me during my studies. Here, I would also like to mention **Thomas Peter**, who gave such exciting lectures on atmospheric chemistry and who was a great inspiration to follow my own path.
- **Tina Šantl-Temkiv** and **Heinz Bingemer** for the warm welcomes during my stays in Aarhus and Frankfurt, respectively.
- All the people that brought the community together to discuss and exchange. **Hinrich Grothe** for organising many conference sessions and workshops. **Cyril** and **Ellen** for setting up and moderating the virtual INP colloquium. **Tina Šantl-Temkiv** for an exciting summer school on Aerobiology. **Cindy Morris** for a stimulating workshop. Attending such meetings always motivated me.
- Dear colleagues, friends and family members who have given me feedback on my work.
- My friends, for their endurance in listening to stories about ice crystals and snowfall all year round, and the leisure hours when we laughed, danced and hiked together.
- My family for their love and efforts for so many years. Especially my sister, parents, and grandparents for giving me the opportunity to continue my studies and pursue my dreams. Also, my nephew, who gives me so much hope.
- The love of my life and partner for the immeasurable help, cooking delicious food and for always believing in me.

Thank you! Danke! Merci!